UNIVERSITY OF SOUTHAMPTON

institute of sound and vibration research

ON THE PREDICTION OF OIL LAYER DAMPING ON PLATES

ISVR Technical Report No: 137

May 1986

L C Chow & R J Pinnington

ON THE PREDICTION OF OIL LAYER DAMPING ON PLATES

L C CHOW & R J PINNINGTON

ISVR Technical Report No 137

May 1986

(Author)

(Author)

(Group Chairman)

University of Southampton
Institute of Sound and Vibration Research

ON THE PREDICTION OF OIL LAYER DAMPING ON PLATES

by

L C CHOW AND R J PINNINGTON

ISVR TECHNICAL REPORT NO: 137

May 1986

Acknowledgements

The authors would like to express their gratitude to the Science and Engineering Research Council for the support of this research. The assistance with the flow resistance measurement of Mr Jin XiaoXiong is also greatly acknowledged.

SUMMARY

High damping of machinery panels can be achieved using a sandwich construction consisting of an attached plate sandwiching a layer of fluid filled porous material. The vibration of the plate pumps the fluid laterally at high velocities, resulting in energy loss due to the fluid viscosity. Loss factors greater than 0.1 can be achieved with this layered configuration. However, if the gap is filled with the high viscosity fluid alone, the losses are very low. The ratio of the fluid dynamic viscosity and its density is the controlling parameter on the level of the losses. High loss factors are possible only if the fluid viscosity can be increased by many orders of magnitude for liquids.

The damping over the whole frequency range above and below the excited plate critical frequency is measured and compared with prediction. The agreement in results is good. The layered configurations are so strongly coupled that the loss factor measured on both the excited and the attached plates are the same.

Page

CONTENTS

Page

NOMENCLATURE

a	radius of holes in the perforated plate
A	a constant $(= 12\mu/d^2 + i\omega\rho)$
b	length of each slot
B	flexural rigidity of a plate
C, C_1, C_2, C_3, C_4	constants
$C_{X_1}, C_{2_{X_1}}, C_{3_{X_1}}$	constants in element 1
$C_{X_2}, C_{2_{X_2}}, C_{3_{X_2}}$	constants in element 2
d	gap between two plates
f	frequency in Hertz
g	porosity of the porous material
G_o	shear modulus of the porous material
h	attached plate thickness
$H(x)$	gap between the plate and the wall at position x
i	complex value ($= \sqrt{-1}$)
k	flexural rigidity of the excited plate including the loading from the fluid and the attached plate
k_p	free flexural wavenumber of the excited plate
ℓ	distance between the centre of holes or slots
m	total mass per unit area of the system
m_1, m_2	mass per unit area of the excited and attached plate respectively
M	mobility
N	Nth element under consideration
P	pressure of fluid in the gap
P_a	fluid pressure in pores
P_f	pressure force in the gap with solid material alone
P_m	frame pressure in the gap
P_1	the total force applied to the frame per unit cross-sectional area of the bulk material
P_2	the total force acting on the fluid component
Q	fluid mass discharge rate
r	radius of the element in the hole

s, T	constants
t	time in seconds
u, u_z	fluid velocity in x and z direction respectively
$\bar{U}$, $\bar{U}_z$	fluid mean flow velocity in x and z direction respectively
$\bar{U}_p$	fluid mean flow velocity in the pores
V, $V(x)$	velcoity of the excited plate (at position x)
$\bar{V}_1$	mean frame velocity in x-direction corresponding to the fluid velocity $\bar{V}_2$
$\bar{V}_2$	mean fluid velocity in x-direction in the pores
$\bar{V}_f$	mean flow velocity in the gap with solid material alone
W, $\bar{W}$	fluid velocity and mean flow velocity in y direction respectively
W_o	maximum velocity at the centre axis of the hole
$Y_1,\ldots Y_4$	constants
Z	impedance per unit area at y=0
Z_b, Z_3	average blocked impedance per unit area
Z_h	impedance per unit area of a hole at y=0
Z_t	treatment impedance per unit area
z_1, z_2, z_3	dimension of the perspex tube for flow resistance measurement
σ_p	the flow resistance coefficient
μ	fluid dynamic viscosity
ρ	fluid density
ρ_m	material density of the frame
ρ_1	bulk density of the frame
ρ_2	bulk density of the fluid
ω	frequency in radians
η	loss factor
η_s	shear loss factor of the porous material
τ	shear stress
ξ	distance along the pore axis
θ	angle of the pore to x-axis
ϵ	structure factor of the porous material
α, α_1, α_2, β	constants

LIST OF FIGURES

1.0 INTRODUCTION

It is well known that increasing the damping of machinery components can reduce the noise radiation due to the ringing vibrations. Various damping treatments such as viscoelastic materials, frictional damping etc are available. However, the choice of a particular damping treatment for a particular machinery component depends on many factors such as its effectiveness, the cost and the hospitality of the surrounding environment. For industrial machinery such as gear boxes, pipes or tanks which contain high viscosity fluid, it is possible to increase the loss factor by utilizing the damping capacity of these fluids. This report examines the feasibility of this kind of damping mechanism both theoretically and experimentally.

Trochidis [1] developed a theoretical model to predict the loss factor of double plates separated by a fluid gap. The model assumes the fluid to be incompressible and the plates are infinitely long. He carried out an experiment on a 1 mm thick aluminium plate which was parallel to a rigid wall. The gap between the wall and this excited plate was filled with water and the loss factor was measured. Good agreement between the measured and the estimated values is claimed to be obtained. No other references of published work have been found in this area.

Industrial machinery is made of plates, shells and beams attached together either by welding or by bolting, it is therefore sensible to carry out the investigation on one of these shapes. The present investigation will be concentrated on the plate-like structures.

In this study, the damping on plates due to the squeeze-film motion on the fluid is predicted using an impedance approach, in which the response of infinite coupled layers may be predicted by assigning an impedance per unit area to each layer. The excited plate, however, is assumed to have a bending stiffness higher than that of the attached plate. Such an approach has proved to be successful in predicting the loss factor when air is trapped between two vibrating plates [2].

The theoretical model allows the attached plate to be perforated or a plate with slots of equally spaced by a distance ℓ. The investigation is

concentrated on heavy fluids with high dynamic viscosity which is modelled as an incompressible fluid with a parabolic velocity flow profile. The model also assumes the attached plate to satisfy $k\ell << 1$, the condition which is normally observed for a closely spaced holes practical perforated plate. k is the bending wavelength of the coupled systems.

From the theoretical model it is found that the ratio of the fluid dynamic viscosity and its density controls the level of the loss factor. Various experiments are carried out to verify the theory and the above verdict. The relationship between this ratio and the loss factor cannot be simply expressed.

The viscosity of the fluid is increased artifically by inserting porous materials into the fluid (oil) gap. Theoretical modelling of damping with porous material in layered configurations using the impedance approach is presented. The effects of the material properties, the mass of the plates and the size of the gap on the loss factor are also discussed. Various experiments are carried out to verify the theory.

2.0 OIL LAYER DAMPING MODELLING AND ESTIMATION

This chapter describes the theories to obtain the blocked impedance of the attached plate, which is either a perforated plate with circular holes or a plate with slots equally spaced by a distance ℓ, or just another flexible plate. Based on the estimated blocked impedance values, the actual modelling of the system is presented. For the blocked impedance estimation and the subsequent experiments, the fluid used to fill the gap between the plates is Essolube hdxplus 20W/50 diesel engine lubricating oil. It has fluid density 891 kg/m^3 and dynamic viscosity 0.423 Ns/m^2 at 20^{o}C (data supplied by the manufacturer).

2.1 The Calculation of the Blocked Impedance for a Plate with Equally Spaced Slots

Consider the two plates which are assumed to be of infinite extent and are separated by an oil layer. For simplicity, the analysis is carried out for the two dimensional case. (diagram 2.1) It is assumed that the flexural stiffness of the attached plate is much smaller than that of the thick excited plate. This means that the impedance per unit area of the attached plate is mass controlled when it is being excited. [2]

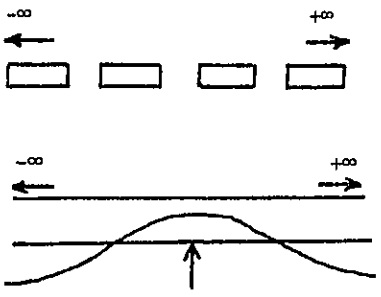

diagram 2.1

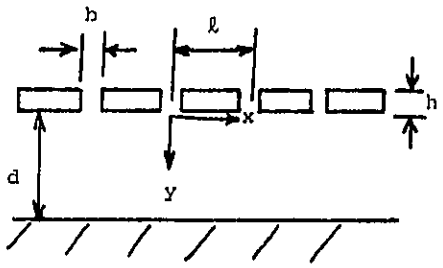

diagram 2.2

To calculate the blocked impedance, we consider a plate which has many equally spaced slots of length ℓ and size b, is infinitely long and is placed a distance d above a rigid wall. (diagram 2.2). Assume the slots each of size b is very small compared with ℓ, therefore the velocity of each small element in ℓ can be assumed to have a constant velocity gradient. The coordinate of the system is chosen such that at the beginning of each small element ℓ, x is zero (diagram 2.3a). The subscripts, 1, 2 and 3 correspond to element 1, 2, 3 respectively and the pressure in $x_1 = 0$ to ℓ is p_1, in $x_2 = 0$ to ℓ is p_2 and so on. The velocity in y-direction at the Nth element ($x_N = 0$) can be written as

$$V_N = [|V|e^{-ik(N-1)\ell} + \frac{|V|}{\ell} e^{-ik(N-1)\ell} \cdot (e^{-ik\ell} - 1)x_N]e^{i\omega t} \qquad (2.1)$$

This equation is obtained from the finite element approach in which the variables of each element between slots are a velocity with a constant velocity gradient.

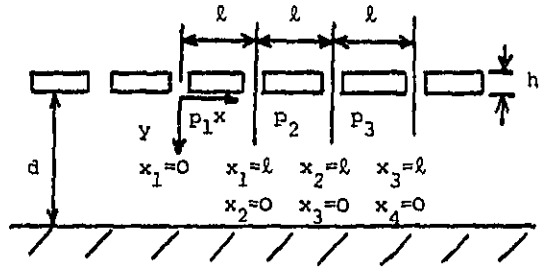

diagram 2.3a

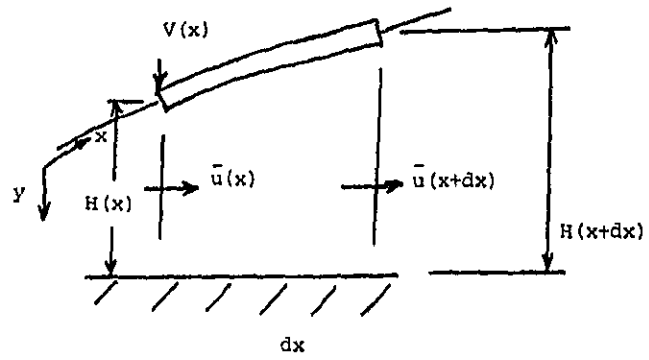

diagram 2.3b

Consider a small element of the oscillating plate between two slots (diagram 2.3b), to satisfy the equation of continuity, we have [2]

$$V(x) = H(x)\frac{d\bar{u}(x)}{dx} + \bar{u}(x)\frac{dH(x)}{dx} \qquad (2.2)$$

where $H(x)$ is the gap between the plate and the wall at position x, $\bar{u}(x)$ is the average horizontal flow velocity at position x. Assuming the velocity profile of the gap is of parabolic shape together with the equation of motion

$$\mu\frac{d^2u}{dy^2} = \frac{dp}{dx} + \rho\frac{du}{dt}$$

it can be shown that

$$\frac{dp}{dx} = -\left(\frac{12\mu}{d^2} + i\omega\rho\right)\bar{u} \qquad (2.3)$$

where μ and ρ are the fluid dynamic viscosity and its density. Using equations (2.1), (2.2) and (2.3), it can be shown that

$$P_1 = -\frac{A}{d}\left[|V|\frac{x_1^2}{2} + C_{x_1}\frac{x_1^3}{6} + C_{2_{x_1}}x_1 + C_{3_{x_1}}\right]e^{iwt} \qquad (2.4)$$

$$P_2 = -\frac{A}{d}\left[V_2\frac{x_2^2}{2} + C_{x_2}\frac{x_2^3}{6} + C_{2_{x_2}}x_2 + C_{3_{x_2}}\right]e^{iwt} \qquad (2.5)$$

where C_{x_1}, $C_{2_{x_1}}$, $C_{3_{x_1}}$ are the constants in element 1,

C_{x_2}, $C_{2_{x_2}}$, $C_{3_{x_2}}$ are the constants in element 2,

$$A = \left(\frac{12\mu}{d^2} + i\omega\rho\right) \text{ and } V_2 = |V|\, e^{-ik\ell}$$

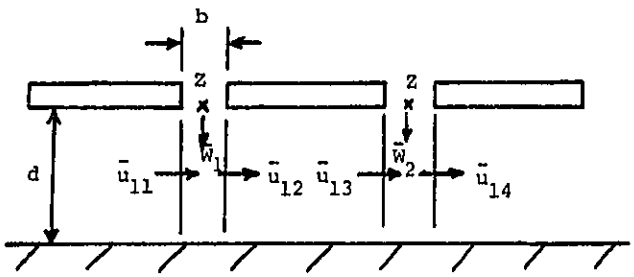

diagram 2.4

Since the elements are symmetrical and periodic, therefore

$$P_{N+1} = P_N\, e^{-ik\ell} \tag{2.6}$$

$$\bar{U}_{N+1} = \bar{U}_N\, e^{-ik\ell} \tag{2.7}$$

$$\text{and } Z = \frac{p_1 b}{-w_1 d} = \frac{-p_1(x_1 = \ell)}{(\bar{u}_{12}-\bar{u}_{11})\frac{d}{b}} = \frac{-p_2(x_2 = 0)}{(\bar{u}_{12}-\bar{u}_{11})\frac{d}{b}} = \frac{-p_2(x_2=\ell)}{(\bar{u}_{14}-\bar{u}_{13})\frac{d}{b}} \tag{2.8}$$

where Z is the impedance per unit area of the slot at y=0 (see diagram 2.4), the constants can be found. The constants are

$$C_{x_N} = C_{x_1}\, e^{-i(N-1)k\ell}$$

$$C_{2_{x_N}} = C_{2_{x_1}}\, e^{-i(N-1)k\ell}$$

$$C_{3_{x_N}} = C_{3_{x_1}} e^{-i(N-1)k\ell}$$

$$C_{x_1} = \frac{|V|}{\ell}\left(e^{ik\ell} - 1\right)$$

$$C_{2_{x_1}} = \frac{1}{\left[\frac{Z}{b}(e^{-ik\ell}-1) - \frac{A\ell e^{-ik\ell}}{d(e^{-ik\ell}-1)}\right]} \cdot \left\{ |V| \left[\frac{Z\ell}{b} + \frac{\frac{A\ell^2}{2d}e^{-ik\ell}}{(e^{-ik\ell}-1)} \right] + C_{x_1}\left[\frac{Z\ell^2}{2b} + \frac{\frac{A\ell^3}{6d}e^{-ik\ell}}{(e^{-ik\ell}-1)} \right] \right\}$$

$$C_{3_{x_1}} = \frac{1}{(e^{-ik\ell}-1)} \left[|V| \frac{\ell^2}{2} + C_{x_1} \frac{\ell^3}{6} + C_{2_{x_1}} \ell \right] \qquad (2.9)$$

Substituting the constants in equation (2.9) back to equation (2.4) and rearranging gives

$$P_1 = -\frac{A}{d}\left\{ \left[|V| \left\{ \frac{x_1^2}{2} + \frac{\ell^2}{2(e^{-ik\ell}-1)} + \frac{\left[x_1 + \frac{\ell}{(e^{-ik\ell}-1)}\right]\left[\frac{Z\ell}{b} + \frac{A\ell^2 e^{-ik\ell}}{2d(e^{-ik\ell}-1)}\right]}{\left[\frac{Z}{b}(e^{-ik\ell}-1) - \frac{A\ell e^{-ik\ell}}{d(e^{-ik\ell}-1)}\right]} \right\} + \frac{|V|(e^{-ik\ell}-1)}{\ell} \left\{ \frac{x_1^3}{6} + \frac{\ell^3}{6(e^{-ik\ell}-1)} + \frac{\left[x_1 + \frac{\ell}{(e^{-ik\ell}-1)}\right]\left[\frac{Z\ell^2}{2b} + \frac{A\ell^3 e^{-ik\ell}}{6d(e^{-ik\ell}-1)}\right]}{\left[\frac{Z}{b}(e^{-ik\ell}-1) - \frac{A\ell e^{-ik\ell}}{d(e^{-ik\ell}-1)}\right]} \right\} \right] \right\} \cdot e^{i\omega t} \qquad (2.10)$$

Assuming $k\ell<<1$ it can be shown that the average blocked impedance per unit area is

$$Z_b = \frac{\frac{1}{\ell}\int_0^{\ell} P_1 dx_1}{\frac{1}{\ell}\int_0^{\ell} V_1 dx_1} = \frac{A\ell^2}{d}\left[\frac{1}{12} + \frac{Zd}{A\ell b}\right] \qquad (2.11)$$

This average blocked impedance is the same everywhere in each small element and it is independent of the bending wavenumber k of the coupled system. Detailed derivation of this equation is shown in Appendix I. The unknown that remains to be found in this equation is the impedance per unit area Z at the slot.

2.2 The calculation of the impedance at the slots

The same method to calculate the mean flow velocity $\bar{u}$ in x-direction can be used to calculate the mean flow velocity $\bar{w}$ in y-direction. Assuming the flow through the slot is also of parabolic velocity profile and from.

$$\mu \frac{d^2w}{dx^2} = \frac{dP}{dy} + \rho \frac{dw}{dt}$$

it can be shown that as with equation (2.3)

$$\frac{dP}{dy} = -\bar{w}\left(\frac{12\mu}{b^2} + i\omega\rho\right) \qquad (2.12)$$

and $$p = -\bar{w}\left(\frac{12\mu}{b^2} + i\omega\rho\right)y + C_1 \qquad (2.13)$$

where C_1 is a constant.

If the fluid is filled to the top level of the slots, that is to y = -h, then $d\bar{w}/dy = 0$ and p = 0 at y = -h. Equation (2.13) with y=0 is

$$p(y=0) = -\bar{w}\left(\frac{12\mu}{b^2} + i\omega\rho\right)h \qquad (2.14)$$

Therefore the impedance per unit area at each slot is

$$Z = \left(\frac{12\mu}{b^2} + i\omega\rho\right)h \qquad (2.15)$$

The negative sign in equation (2.15) disappear because pressure and the flow direction oppose each other.

2.3 The calculation of the blocked impedance for a perforated plate with equally spaced circular holes.

A similar approach to that for the slotted beam can be used in calculating the blocked impedance for a plate with slots. However, several equations have to be modified and the analysis is extended to three-dimensional case. The fundamental change is in equation (2.8). (see diagram 2.5). Again the holes with radius a are assumed to be small compared with ℓ, the distance between the hole centres.

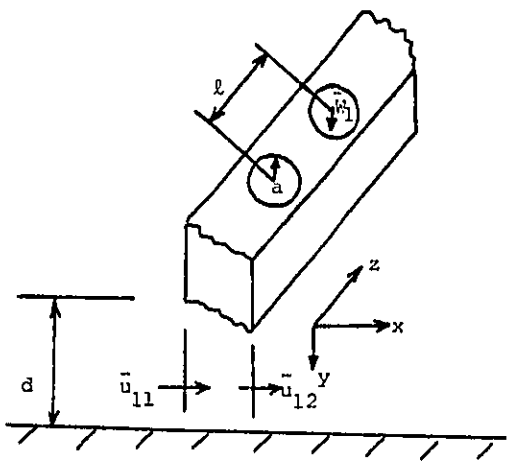

diagram 2.5

It is assumed that the plate waves travel perpendicular to a line of holes. By continuity

$$\bar{w}_1 \pi a^2 + \bar{u}_{11} \ell d = \bar{u}_{12} \ell d$$

$$\bar{w}_1 = (\bar{u}_{12} - \bar{u}_{11}) \frac{\ell d}{\pi a^2}$$

$$\text{therefore} \quad Z = \frac{-P_1(x_1=\ell)}{(\bar{u}_{12}-\bar{u}_{11})\frac{\ell d}{\pi a^2}} = \frac{-P_2(x_2=0)}{(\bar{u}_{12}-\bar{u}_{11})\frac{\ell d}{\pi a^2}} \tag{2.16}$$

This changes the constants $C_{2_{x_1}}$ hence $C_{3_{x_1}}$. The constant $C_{2_{x_1}}$ becomes

$$C_{2_{x_1}} = \frac{1}{\left[\frac{Z\ell}{\pi a^2}(e^{-ik\ell}-1) - \frac{A\ell e^{-ik\ell}}{d(e^{-ik\ell}-1)}\right]} \cdot \left\{ |V| \left[\frac{Z\ell^2}{\pi a^2} + \frac{A\ell^2 e^{-ik\ell}}{2d(e^{-ik\ell}-1)} \right] + \frac{|V|(e^{-ik\ell}-1)}{\ell} \left[\frac{Z\ell^3}{2\pi a^2} + \frac{A\ell^3 e^{-ik\ell}}{6d(e^{-ik\ell}-1)} \right] \right\} \tag{2.17}$$

and equation (2.10) becomes

$$P_1 = -\frac{A}{d} \left\{ \left[|V| \left\{ \frac{x_1^2}{2} + \frac{\ell^2}{2(e^{-ik\ell}-1)} + \frac{\left[x_1 + \frac{\ell}{(e^{-ik\ell}-1)}\right]\left[\frac{Z\ell^2}{\pi a^2} + \frac{A\ell^2 e^{-ik\ell}}{2d(e^{-ik\ell}-1)}\right]}{\left[\frac{Z\ell}{\pi a^2}(e^{-ik\ell}-1) - \frac{A\ell e^{-ik\ell}}{d(e^{-ik\ell}-1)}\right]} \right\} + \frac{|V|(e^{-ik\ell}-1)}{\ell} \left\{ \frac{x_1^3}{6} + \frac{\ell^3}{6(e^{-ik\ell}-1)} + \frac{\left[x_1 + \frac{\ell}{(e^{-ik\ell}-1)}\right]\left[\frac{Z\ell^3}{2\pi a^2} + \frac{A\ell^3 e^{-ik\ell}}{6d(e^{-ik\ell}-1)}\right]}{\left[\frac{Z\ell}{\pi a^2}(e^{-ik\ell}-1) - \frac{A\ell e^{-ik\ell}}{d(e^{-ik\ell}-1)}\right]} \right\} \right] \right\} e^{i\omega t} \tag{2.18}$$

The average blocked impedance per unit area can be shown as

$$Z_b = \frac{A\ell^2}{d}\left[\frac{1}{12} + \frac{Zd}{\pi a^2 A}\right] \qquad (2.19)$$

2.4 The calculation of the impedance for a circular hole and the impedance in the z-direction

To calculate the impedance per unit area Z for a perforated plate with circular holes, we have to extend the analysis to three dimensions. First the impedance per unit area of a circular hole is calculated, then this impedance is used to determine the impedance in z-direction. For simplicity, the movement of the plate is assumed to have a constant velocity in z-direction.

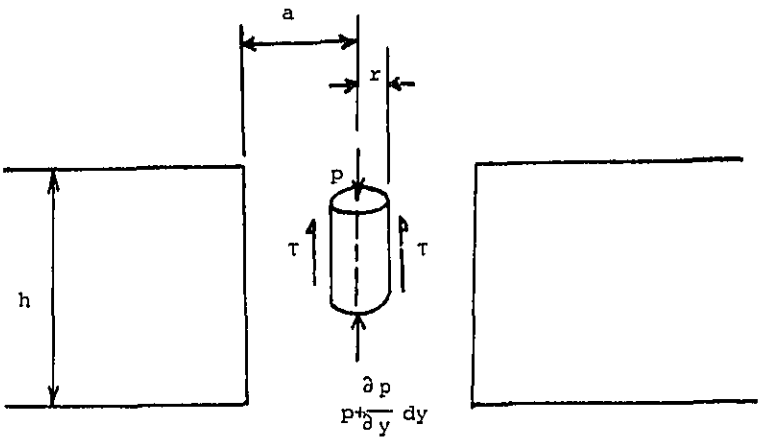

diagram 2.6

The impedance per unit area of a hole Z_h at y=0 can be shown equal to (diagram 2.6)

$$Z_h = \left(\frac{8\mu}{a^2} + i\omega\rho \right) h \qquad (2.20)$$

where a is the radius of the hole and h is the depth of the hole. Full derivation of this equation is given in Appendix II.

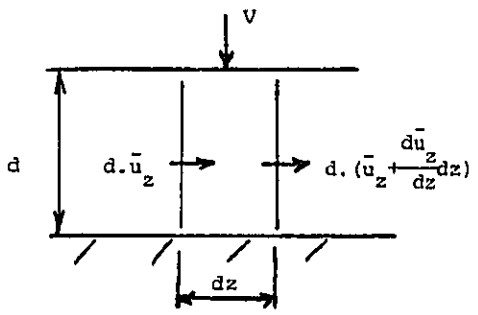

diagram 2.7

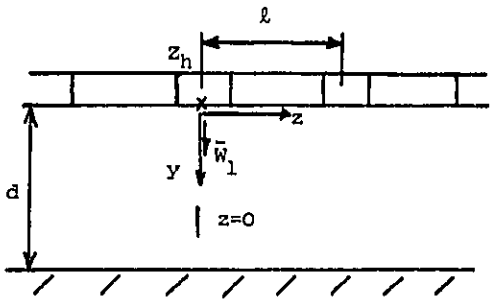

diagram 2.8

The average impedance per unit area in z-direction (diagrams 2.7 and 2.8) can be equated as

$$Z = \frac{\frac{1}{\ell}\int_0^{\ell} p(z)dz}{V} = \left(\frac{12\mu}{d^2} + i\omega\rho\right)\left[\frac{\ell^2}{12d} + \frac{1}{\left(\frac{12\mu}{d^2}+i\omega\rho\right)}\frac{2\ell}{\pi a} Z_h\right] \qquad (2.21)$$

Substituting equation (2.21) into equation (2.19), the blocked impedance per unit area for a perforated plate with circular holes can be estimated. The derivation of the equation (2.21) can be seen in Appendix III.

2.5 The estimated blocked impedance of a perforated plate with circular holes

Figures 2.1(a) to 2.1(c) show the real and imaginary part of the estimated blocked impedance for a perforated plate with circular holes of varying distance away from a rigid wall. In the computation, the diameter of each hole in the perforated plate of 3.25 mm thickness is assumed equal to 2.28 mm (= 90/1000 in.). The distance between the holes centre is 7.0 mm. This is the dimensions of one of the perforated plate (PVC perforated plate) used later in the experiment. The gap between the perforated plate and the wall is filled with the Essolube hdxplus 20W/50 lubricating oil ($20^{o}C$).

The real part is constant with frequency as for a simple dashpot whereas the imaginary part is positive and increases proportional to $(\text{frequency})^{1/2}$ indicating mass like behaviour dependent on the wavelength in the plates for squeeze film damping [2]. Both the real and imaginary parts decrease with increasing gap again as with unperforated plates [2]. The real part of the blocked impedance decreases sharply with increasing gap, however, as the gap continues to increase this decrement slows down. The imaginary part also decreases with increasing gap but the decrement is small compared with that of the real part.

2.6 The actual modelling of the system

Since the estimated blocked impedance shows that the oil in the gap has the inertia and viscosity controlled behaviour, therefore a model with the appropriate behaviour is shown in the diagram 2.9.

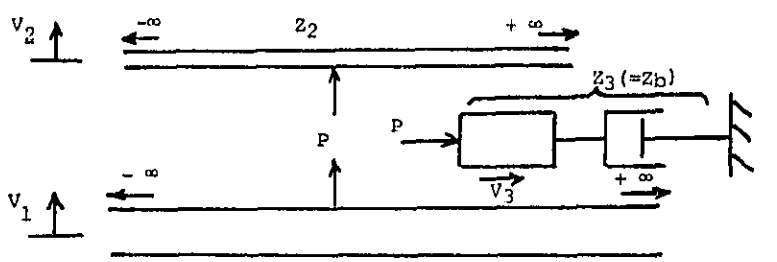

diagram 2.9

The oil is modelled as a mass-dashpot system. The mass and dashpot account for the inertia and viscosity of the oil for incompressible flow model with uniform pressure across the gap.

The loss factor of the system is

$$\eta = \frac{\text{Energy dissipated/radian}}{\text{Energy stored in (excited plate + oil + attached plate)}} \qquad (2.22)$$

The power absorbed in the system

$$= \frac{1}{2} |P|^2 R_e\{M_b\} = \frac{1}{2} |P|^2 R_e\{M_3\} = \frac{1}{2} |V_3|^2 R_e\{Z_3\} \qquad (2.23)$$

where M is the mobility of the element of concern ($M = \frac{1}{Z}$).

$$\text{The energy stored} = \frac{1}{2} m_1 |V_1|^2 + \frac{1}{2} (m_2+\rho d) |V_2|^2 + \frac{1}{2} \frac{I_m\{Z_3\}}{\omega} |V_3|^2 \qquad (2.24)$$

$$\text{Since } \frac{p}{V_1} = \frac{Z_3 Z_2}{Z_3+Z_2} = Z_t \qquad (2.25)$$

where Z_t is the treatment impedance per unit area,

$$\frac{p}{V_2} = Z_2 \qquad (2.26)$$

and

$$\frac{p}{V_3} = Z_3 \qquad (2.27)$$

in terms of V_1, $$V_3 = \frac{Z_2}{Z_3+Z_2} V_1 \text{ or } \frac{V_3}{V_1} = \frac{Z_t}{Z_3} \qquad (2.28)$$

and $$V_2 = \frac{Z_3}{Z_3+Z_2} V_1 \text{ or } \frac{V_2}{V_1} = \frac{Z_t}{Z_2} \qquad (2.29)$$

Therefore the loss factor can be equated as

$$\eta = \frac{R_e\{Z_t\}}{\omega m_1 + \omega(m_2+\rho d)\left|\frac{Z_t}{Z_2}\right|^2 + Im(Z_3)\left|\frac{Z_t}{Z_3}\right|^2} \qquad (2.30)$$

where m_1, m_2 are the mass per unit area of the excited and the attached plate respectively.

Figures 2.2a to 2.2c show the estimated treatment impedance when a photographic glass plate (500x500x6.35 mm) is coupled to a PVC perforated plate with an oil layer of different gaps. The PVC perforated plate has equally spaced holes of 7.0 mm and diameter 2.28 mm. The size of this perforated plate is 495x495x3.25 mm and its material density is 1400 kg/m^3. At low frequencies the real part of the estimated treatment impedance increases with increasing gap whereas at high frequencies it decreases with increasing gap. The imaginary part, however, remains constant with increasing gap. This imaginary impedance increases with frequency at 10 dB/decade.

3.0 EXPERIMENTAL VERIFICATION OF THE THEORY

The experiments were carried out using a thick photographic glass plate (500x500x6.35mm) as the excited plate. The attached plate was either a PVC perforated plate (495x495x3.25mm) or a perspex perforated plate (490x490x3.0 mm) or a photographic glass plate (492x492x3.175mm). The surfaces of these experimental plates were flat and therefore the gap between the plates can be constant all over the surface. By putting shims or washers of different thickness in between the two plates, the gap thickness can be controlled.

The diameter of the holes in both the perforated plates was 2.28 mm. The distance between the holes centre, however, was 7.0 mm and 4.67 mm for the PVC and the perspex perforated plate respectively. The edges of the excited glass plate was sealed with perspex strips using Araldite. This glass plate was suspended horizontally with four wires from the four plate corners and the glass was excited via a coil and magnet system underneath the plate (see figures 3.1a and 3.1b).

The loss factor was measured using the time decay method. The tested structure was excited via an electromagnetic coil to which a third octave bandpass white noise was applied. The vibrational signal was monitored by an accelerometer (B&K 4344) attached onto the excited plate. When the applied power was cut off, the energy time decay in each third octave band was measured and analysed using the Hewlett Packard 5420A digital signal analyser. The loss factor was calculated using the following formula

$$\eta = \frac{2.2}{fT_{60}} \qquad (3.1)$$

where T_{60} is the reverberation time, the duration while the signal decays by 60 dB, f is the centre frequency of the band under consideration.

3.1 Comparison of the measured and predicted loss factor on the glass-PVC plates

Figure 3.2 shows the measured loss factor when the plates are separated with different oil gaps. The loss factor at low frequencies is of the order of 10^{-3} and it reaches 10^{-2} at high frequencies. The measured results also indicate that at low frequencies, the loss factor is higher for larger gaps whereas at high frequencies it is smaller for larger gaps.

Figure 3.3 displays the estimated loss factor calculated using equation (2.30). The loss factor increases until a maximum is reached and then decreases. The level of this maximum increases with increasing gap. However, the frequency at which this maximum occurs decreases with increasing gap. This gives an overall picture that the loss factor for larger gaps is higher at low frequencies and lower at high frequencies. This trend agrees with the measured result as shown in figure 3.2.

The predicted value, however, is much smaller than the measured loss factor. Figure 3.4a shows the measured loss factor of the excited plate with four perspex strips glued onto the plate edges using Araldite. Figure 3.4b gives the estimated total loss factor when this measured losses of the excited plate (due to radiation, material losses and the losses from the edges) are included. Figures 3.5a to 3.5c compare the measured and the estimated total loss factor with varying gaps. The agreement is good. The losses from the squeezing of oil is small and the measured loss factor is mainly from the losses of the excited plate.

3.2 The effect of the dimensions of perforated plate on the predicted loss factor

Figure 3.6a displays the predicted loss factor versus frequency by varying the distance between the holes centre ℓ and keeping the other parameters constant. The result shows that the smaller the hole spacing ℓ, the higher is the loss factor. The result also indicates that the loss factor decreases by more than 10 dB for doubling the distance ℓ. Figure 3.6b shows the predicted total loss factor, and again, the change of the loss factor with ℓ can be seen very clearly.

Figures 3.7a and 3.7b show the predicted loss factor by varying the attached plate thickenss h (i.e. mass) and keeping the other parameters constant. This indicates that the heavier the attached plate, the higher is the loss factor. However, the increment of the loss factor per doubling the mass is much less than that of doubling ℓ.

Figures 3.8a and 3.8b give the predicted loss factor by varying the hole diameter in the perforated plate. The result shows that the larger the holes, the higher is the loss factor. The result also indicates that there is an optimum size of the holes for a constant ℓ, h and d to give the highest losses. The increment of the loss factor, however, is much less than 10 dB for doubling the holes diameter.

Since the impedance per unit area of the attached perforated plate is mass controlled, the larger the size of the holes for a constant plate thickness means a lighter mass. On the one hand, the light attached mass results in a low loss factor; on the other hand, the larger holes size gives higher losses. Therefore there is an optimum size of the holes for constant ℓ, h and d to give the highest loss factor. However, if the mass of the attached plate can be kept constant by varying the plate thickness, the larger the holes size results higher loss factor.

The variation of the predicted loss factor with the gap d are already shown in figures 3.3 and 3.4b. The influence of loss factor by varying the gap is very significant. Therefore the above results suggest that among the four parameters discussed, the distance between the holes centre and the oil gap are the more important parameters in affecting the loss factor. The results also suggest to use a perforated plate with large holes and small ℓ for high losses.

3.3 Comparison of the measured and predicted loss factor on the glass-perspex plates.

Figure 3.9 gives the measured loss factor when the attached plate is a perspex perforated plate (650gm). The measured result again indicates that for larger gap, the loss factor is higher at low frequencies and lower at higher frequencies. However, the measured loss factor is again very small. Figure 3.10 shows the predicted loss factor whereas figures 3.11a and 3.11b

display the comparison of the measured and the predicted total loss factor of different gaps. The agreement for 0.25 mm gap is good while the difference between the measured and the predicted value becomes larger for the 1.34 mm gap. This is probably due to the slight bending of the perspex plate, which is the consequence of the drilling of holes on the plate, which in effect alter the gap. The agreement, however, is still within 3 dB.

3.4 Comparison of the measured and predicted loss factor on the glass-glass plates

Figure 3.12 gives the measured loss factor when the two glass plates (non-perforated) are separated by an oil layer. This loss factor is significantly lower than that when the gap is filled with air [2]. In order to find out the reasons behind these low losses, it is necessary to examine the terms in equation (2.30) properly.

The blocked impedance per unit area of a plate a distance d from a rigid wall is [2]

$$Z_b = \frac{1}{k^2 d} \left(\frac{12\mu}{d^2} + i\omega\rho \right) \qquad (3.2)$$

The flow in the gap is assumed incompressible and of parabolic profile. If the fluid is air, the wavenumber k in this equation can be assumed equal to the free flexural wavenumber of the excited plate. However, if the fluid is oil (heavy fluid) the mass effect of the oil and the attached plate should be included in evaluating k. This k can be approximately calculated as

$$k^4 = \frac{\omega^2 (m_1 + m_2 + \rho d)}{B} \qquad (3.3)$$

where m_1, m_2 are the mass per unit area of the excited and the attached plate, ρ is the fluid density and B is the flexural rigidity of the excited plate. The validity of this equation was justified in chapter 5.

Substituting equations (3.2) and (3.3) into (2.30) and simplifying gives

$$\eta = \frac{1}{\frac{\sqrt{B(m_1+m_2+\rho d)}}{\omega^2(m_2+\rho d)^2 d}\left[\frac{12\mu}{d^2}+\frac{\omega^2\rho^2 d^2}{12\mu}\right]+\frac{\omega\rho d^3}{12\mu}\frac{(2m_1+m_2+\rho d)}{(m_2+\rho d)}+\frac{\omega^2 m_1 d^3}{12\mu}\sqrt{\frac{m_1+m_2+\rho d}{B}}} \qquad (3.4)$$

The only parameters changed to predict the loss factor when oil is used instead of air are the fluid density and its dynamic viscosity. As can be seen from this equation, the relation between these two parameters and the loss factor is very complicated.

Figure 3.13a shows the predicted loss factor versus the gap calculated using equation (3.4). By keeping the frequency (800 Hz) and the fluid dynamic viscosity (air viscosity) constant, the fluid density increases from 1.21 kg/m^3 (air density) to 50 and 100 times of this value. The results indicate that as the fluid density increases, the loss factor drops sharply. A similar trend is observed in figure 3.13b. In this figure, the frequency (800 Hz) and the fluid dynamic viscosity is again kept constant (oil viscosity). The fluid density (oil density), however, decreases from 891 kg/m^3 by 50 and 100 times of its value.

Figure 3.14a again gives the predicted loss factor versus the fluid gap. In this case, the frequency (800 Hz) and the fluid density are kept constant (air density). The dynamic viscosity increases from 1.81×10^{-5} N s/m^2 (air viscosity) to 5 and 20 times of this value. The results show that the loss factor rises significantly as the fluid dynamic viscosity increases. A similar trend is observed in figure 3.14b. In this figure, the loss factor is computed at constant frequency (800 Hz) and fluid density (oil density). The dynamic viscosity, however, increases from 0.423 Ns/m^2 (oil viscosity at 20^{o}C) to 5 and 20 times of this value. The predicted results indicate that for a particular gap, fluid density and its dynamic viscosity, a maximum loss factor can be obtained at a particular

frequency. The value of the gap for maximum losses increases with increasing viscosity. Above this peak, the trend is similar to that shown in figure 3.14a; that is, the loss factor increases with the increasing viscosity.

The above computation results (figures 3.13 and 3.14) demonstrate a very important point. It is the ratio of the fluid dynamic viscosity and its density which is the dominant factor in controlling the value of the loss factor. If the fluid density is high, high loss factor can still be possible provided that the fluid dynamic viscosity can also be increased significantly. However, as can be seen from equation (3.4), the dependence of the loss factor on this ratio is not a simple and straightforward one.

Figures 3.15a to 3.15c display the comparison between the measured and the predicted total loss factor using glass plates. The agreement is good. The cause for the low loss factor is now very clearly understood.

3.5 The effect on the loss factor due to the drastic increase of the fluid viscosity

Some experiments were carried out to verify the verdict that as the fluid density increases, high loss factors are still possible provided that the fluid dynamic viscosity can be increased significantly too. The initial experiment was carried out on the glass-PVC plates with a 1.34 mm oil gap. The oil was then filled up to 7.0 mm above the top surface of the PVC perforated plate. Figure 3.16 gives the measured loss factor for these two conditions. By filling in more oil, the total mass was increased. The result shows that the loss factor increment at low frequencies is infinitely small, however, the increment becomes obvious at high frequencies.

Figure 3.17 displays the measured loss factor for which the perspex perforated plate is inserted between the two glass plates and the gaps between the plates are filled with oil. The total mass is increased which results an increase in the value k. Therefore it is expected to see that the larger the oil gap, the higher the loss factor. The viscosity is also increased as a result of the insertion of the perspex perforated plate and therefore the measured loss factor is increased. This can be clearly

demonstrated when the measured loss factor in this figure, at which the sandwich plates with gaps 1.34 mm, giving the total gap of 5.68 mm between the two glass plates, is compared to that in figure 3.15c (6 mm oil gap). The loss factor has increased significantly.

To further increase the viscosity, a 490x490x7 mm DCMEAD polyester foam was inserted into the oil layer. Four washers of the same thickness were put at the four plate corners to support the attached plate. Figure 3.18 gives the measured loss factor and as can be seen, the loss factor increases to nearly 0.1. The insertion of the foam has increased the total mass and the fluid density slightly. However, the viscosity is increased by many times. Fifteen Nylon scouring pads (150x98x7mm) were also used to insert into the oil layer. Again, as shown in figure 3.18, high loss factor was obtained.

The above experiments confirm that it is the ratio of the fluid dynamic viscosity and its density which controls the loss factor. In the light of the high loss factor being achieved by inserting materials like foam and scouring pads, efforts were put into developing model to predict the loss factor of this kind. The following chapters will show the developed theory and its experimental verification.

4.0 THEORETICAL MODELLING OF DAMPING WITH POROUS MATERIALS IN LAYERED CONFIGURATIONS USING IMPEDANCE APPROACH

There are many available theories describing sound propagation in porous materials. The classic work in this field is that of Zwikker and Kosten, described at length in reference [3]. In this book they have tried to give the design of absorbing materials a more scientific basis. The principles underlying the wave propagation through porous or non-porous media are described. The theory developed is essentially phenomenological in that its parameters are related to macroscopically measurable properties: e.g. flow resistance, porosity, bulk stiffness etc. It has since been pointed out that the Zwikker and Kosten frame continuity equation is non-physical and under some conditions leads to paradoxical results [4].

Reference [5] gives a more comprehensive review on the main features of work in this area. Several recent theories are also assessed in some details. In the theoretical analysis that follows, the Rosin's approach is adopted [4]. It is a phenomenological model in which the minimum number of assumptions are made regarding microstructure. No limitation is placed on the structure factor and only two-dimensional motion is considered.

4.1 The equations of motion of the fluid and the frame excluding the frame shear stiffness

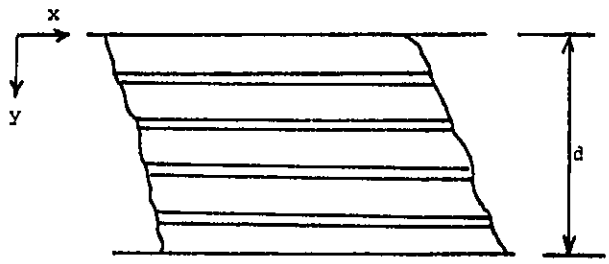

diagram 4.1

It is assumed that the material structure considered is similar to the Rayleigh model [6] in which parallel pores are embedded in a solid material (diagram 4.1). The pores are cylindrical with radius a, the pressure drop along the pores with mean flow velocity $\bar{U}_p$ is

$$-\frac{dP_a}{dx} = \frac{8\mu}{a^2}\bar{U}_p = \sigma_p \bar{U}_p \qquad (4.1)$$

where x is the distance along the pore axis, P_a is the fluid pressure, μ is the fluid dynamic viscosity and σ_p is the flow resistance coefficient. The derivation of this equation is described in Appendix II. At any surface of constant x within the material, the total force per unit area acting on the fluid component is P_2, which is equal to $P_a g$ with g the material porosity. The above equation can be written as

$$-\frac{dP_2}{dx} = \sigma_p g \bar{U}_p \qquad (4.2)$$

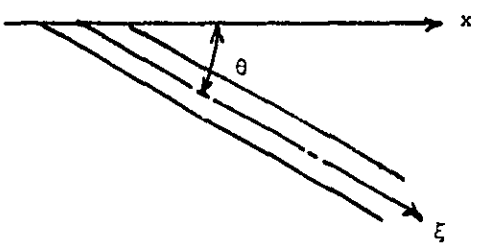

diagram 4.2

If a pore whose axis is inclined at an angle θ to the x-axis (diagram 4.2), equation (4.2) should be written as

$$\frac{-dP_2}{d\ell} = \sigma_p \, g \, \bar{U}_p$$

where ℓ is the distance along the pore axis. Denoting $\bar{V}_2$ the fluid velocity in x-direction, ie. $\bar{V}_2 = \bar{U}_p \cos\theta$, the above equation can be rewritten as

$$\frac{-dP_2}{dx} = \frac{\sigma_p g}{\cos^2\theta} \bar{V}_2 \qquad (4.3)$$

The $1/\cos^2\theta$ accounts for the pore orientation and is called the structure factor ϵ. By defining $\sigma = \epsilon\sigma_p/g$, the macroscopic flow resistance, equation (4.3) can be rewritten purely in terms of the macroscopically measurable properties, ie,

$$\frac{-dP_2}{dx} = \sigma \, g^2 \, \bar{V}_2 \qquad (4.4)$$

This relation will be used to describe the viscous force developed per unit volume between the fluid and the material solid frame when they are in relative motion. That is, $\bar{V}_2$ will be replaced by the difference between fluid and frame velocity.

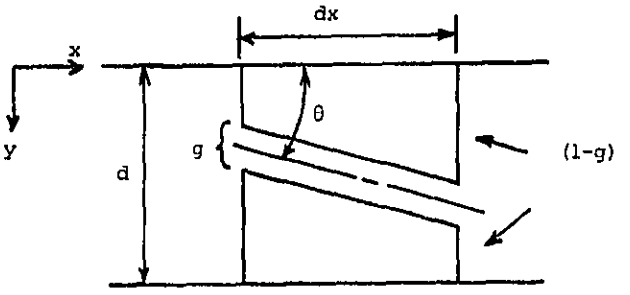

diagram 4.3

The total inertia forces associated with the motion of a unit cube of fluid and solid frame remain unchanged if the pores at a given cross-section are combined into a large pore. Therefore the Rayleigh model can be replaced by a simple structure as shown in diagram 4.3 for developing the inertia terms. Assume the pressure P_m is constant across the whole gap d at any x, the total force applied to the frame per unit cross-sectional area of the bulk material is $p_1 = p_m(1-g)$. As defined above, the total force acting on the fluid component is $P_2 = p_a g$. Let $\bar{V}_1$ be the frame velocity in the x-direction corresponding to the fluid velocity $\bar{V}_2$. The bulk density of the frame is $\rho_1 = \rho_m(1-g)$, where ρ_m is the frame material density. Similarly, $\rho_2 = \rho g$, where ρ is the fluid density.

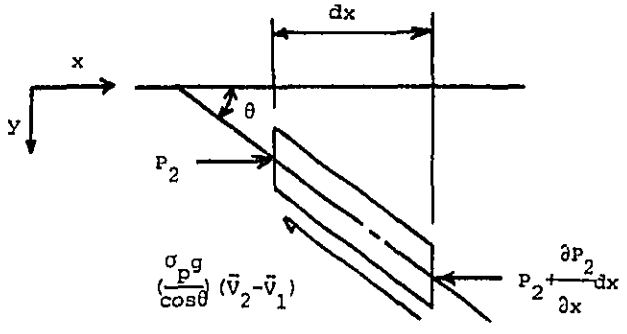

diagram 4.4

Considering the fluid element alone (diagram 4.4), the fluid experiences two simultaneous motions with a translational motion in the x-direction with frame velocity $\bar{V}_1$ and a relative motion along the pore with velocity $\bar{U}_p = (\bar{V}_2-\bar{V}_1)/\cos\theta$. With all forces projected onto the pore axis, the force balance for the fluid element can be written as

$$\frac{-\partial P_2}{\partial x} \cos\theta = \rho_2 \cos\theta \frac{\partial \bar{V}_1}{\partial t} + \frac{\rho_2}{\cos\theta} \frac{\partial(\bar{V}_2-\bar{V}_1)}{\partial t} + \frac{\sigma_p g}{\cos\theta} (\bar{V}_2-\bar{V}_1)$$

Dividing this equation by cos θ and in terms of the structure factor and macroscopic flow resistance, the equation can be rewritten as

$$\frac{-\partial P_2}{\partial x} = \rho_2 \frac{\partial \bar{V}_2}{\partial t} + \rho_2 (\epsilon-1) \frac{\partial(\bar{V}_2-\bar{V}_1)}{\partial t} + \sigma g^2(\bar{V}_2-\bar{V}_1) \qquad (4.5)$$

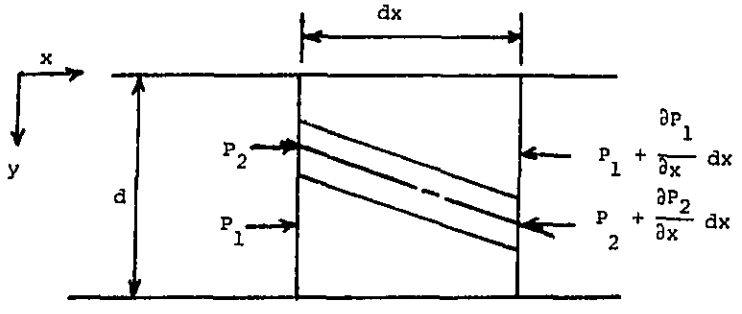

diagram 4.5

The equation of motion of the whole element (diagram 4.5) is

$$\frac{-\partial P_1}{\partial x} - \frac{\partial P_2}{\partial x} = \rho_1 \frac{\partial \bar{V}_1}{\partial t} + \rho_2 \frac{\partial \bar{V}_2}{\partial t} \qquad (4.6)$$

Therefore the equation of motion of the frame can be obtained by subtracting equation (4.5) from (4.6), that is

$$-\frac{\partial P_1}{\partial x} = \rho_1 \frac{\partial \bar{V}_1}{\partial t} + \rho_2 (\epsilon-1) \frac{\partial(\bar{V}_1-\bar{V}_2)}{\partial t} + \sigma g^2 (\bar{V}_1-\bar{V}_2) \qquad (4.7)$$

The equations (4.5) and (4.7) are the same with those presented by Zwikker and Kosten [3]. This approach and results are also the same as Rosin's [4]. These equations are coupled by an inertia term (which goes to zero when the structure factor is unity) and a viscous term (which becomes zero when the flow resistance is zero).

Since P_m is assumed constant across the gap d at any x, the fluid pressure P_a must also equal to P_m, which gives

$$\frac{(1-g)}{g}\frac{dP_2}{dx} = \frac{dP_1}{dx} \tag{4.8}$$

The mean flow velocity U across the gap can be calculated from

$$\bar{U} = \bar{V}_1 (1-g) + \bar{V}_2 g \tag{4.9}$$

Combining equations (4.5), (4.7) and (4.8),

$$\bar{V}_1 = \frac{i\omega\rho(\epsilon-g)\bar{V}_2}{\sigma_p\epsilon - i\omega[\rho_m(1-g) + \rho(\epsilon-1)]} \tag{4.10}$$

Grouping equations (4.5), (4.9) and (4.10) gives

$$\frac{-dP_a}{dx} = \frac{(\sigma_p\epsilon)^2-\omega^2\rho\rho_m\epsilon(1-g)-\omega^2\rho^2 g(\epsilon-1)+i\omega\sigma_p\epsilon[\rho\epsilon+\rho(g-1)+\rho_m(1-g)]}{\sigma_p\epsilon+i\omega(1-g)(\rho_m-\rho)} \cdot \bar{U}$$

$$= \frac{1}{s} \cdot \bar{U} \tag{4.11}$$

Utilizing the equation of continuity for the whole system [2], the blocked impedance per unit area can be calculated as

$$Z_b = \frac{1}{k^2 d} \cdot \frac{1}{s} \qquad (4.12)$$

Referring back to equation (4.10), if $\bar{V}_2 >> \bar{V}_1$, the frame can be assumed rigid, i.e. $V_1 = 0$. The equations (4.5) and (4.9) can be combined to give a very simple equation as

$$-\frac{dP_a}{dx} = \frac{\epsilon(\sigma_p - i\omega\rho)}{g} \cdot \bar{U} \qquad (4.13)$$

This in turn gives the blocked impedance per unit area as

$$Z_b = \frac{1}{k^2 d} \frac{\epsilon(\sigma_p + i\omega\rho)}{g} \qquad (4.14)$$

4.2 The equations of motion of the fluid and the frame including the frame shear stiffness

If the porous material is glued onto the plates, it is necessary to include the shearing motion of the frame. By assuming the motion of the frame across the gap has a parabolic flow profile, it can be shown that the relation between the pressure P_f and the mean flow velocity $\bar{V}_f$ is

$$-\frac{dP_f}{dx} = \left[\frac{12G_o\eta_s}{\omega d^2} + i(\omega\rho_m - \frac{12G_o}{\omega d^2})\right] \bar{V}_f \qquad (4.15)$$

where G_o and η_s are the shear modulus and the shear loss factor of the frame respectively. The derivation of this equation is shown in Appendix IV.

The fact that the velocity of a linearly viscoelastic frame material takes up a parabolic profile when the upper boundary is moved towards the lower boundary is well documented [7]. When a small oscillatory compression is applied to the upper surface of the frame, it is deformed in compression and the fluid is forced to flow in the lateral x-direction. However, as the frame (polymer foams) will exhibit non-linear behaviour in compression, this deformed shape is valid only for small oscillatory force. In addition when $\omega\rho_m > 12G_o/\omega d^2$ in equation (4.15) the flow becomes inertia dominated and the flow profile departs from a parabolic to a flatter form. However it is thought that this makes little difference to the overall behaviour.

As the frequency of the excitation is increased the energy loss due to the viscous flow increases. However, at high frequencies the viscous interaction between the flowing fluid and the frame is so large that the frame is forced to move with the fluid resulting zero net flow giving no flow losses. Therefore, it is expected that the loss factor to increase with increasing frequency, pass through a maximum and then decrease as the frequency is increased further.

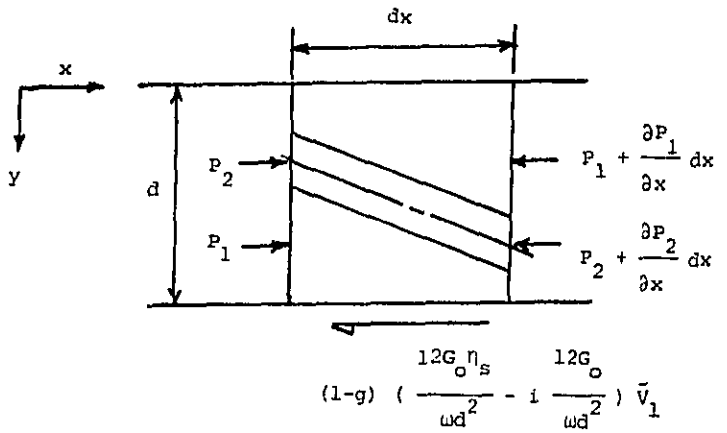

diagram 4.6

The equation of motion for the whole element including the frame shear stiffness is (diagram 4.6)

$$-\frac{\partial p_1}{\partial x} - \frac{\partial p_2}{\partial x} = \rho_1 \frac{\partial \bar{V}_1}{dt} + \rho_2 \frac{\partial \bar{V}_2}{dt} + (1-g)\left[\frac{12G_o\eta_s}{\omega d^2} - i\frac{12G_o}{\omega d^2}\right]\bar{V}_1 \tag{4.16}$$

The equation of motion of the fluid element alone (equation (4.5)) remains the same. Using these two equations and equations (4.8), (4.9) gives

$$\bar{V}_1 = \frac{[\sigma_p\epsilon + i\omega\rho(\epsilon-g)]\bar{V}_2}{[\sigma_p\epsilon + (1-g)\frac{12G_o\eta_s}{\omega d^2}] + i[\omega\rho_m(1-g) + \omega\rho(\epsilon-1) - (1-g)\frac{12G_o}{\omega d^2}]} \tag{4.17}$$

and

$$-\frac{dp_a}{dx} = \frac{Y_1 + iY_2}{Y_3 + iY_4} \cdot \bar{U} \tag{4.18}$$

where

$$Y_1 = -\omega\rho[\omega\rho_m(1-g) + \omega\rho(\epsilon-1) - (1-g)\frac{12G_o}{\omega d^2}] + \sigma_p\epsilon(1-g)\frac{12G_o\eta_s}{\omega d^2}$$
$$- \omega\rho(\epsilon-1)(1-g)(\omega\rho_m - \omega\rho - \frac{12G_o}{\omega d^2})$$

$$Y_2 = \omega\rho[\sigma_p\epsilon + (1-g)\frac{12G_o\eta_s}{\omega d^2}] + \omega\rho(\epsilon-1)(1-g)\frac{12G_o\eta_s}{\omega d^2}$$
$$+ \sigma_p\epsilon(1-g)(\omega\rho_m - \omega\rho - \frac{12G_o}{\omega d^2})$$

$$Y_3 = (1-g)\sigma_p\epsilon + g[\sigma_p\epsilon + (1-g)\frac{12G_o\eta_s}{\omega d^2}]$$

and $$Y_4 = \omega\rho(1-g)(\epsilon-g) - g[\omega\rho_m(1-g) + \omega\rho(\epsilon-1) - (1-g)\frac{12G_o}{\omega d^2}]$$

4.3 The calculation of the loss factor

If the porosity of the structural material is high, equation (2.30) is still valid for calculating the loss factor of the system. If the material is not glued onto the plates and if the frame displacement is much smaller than the fluid displacement, the frame can be assumed to be rigid and G→∞. The loss factor of the system can then be shown equal to (combining equations (2.30) and (4.14)).

$$\eta = \frac{\alpha_1\omega^2(m_2+\rho d)^2k^2d}{\omega m_1(\alpha_1^2+[\alpha_2+k^2d\omega(m_2+\rho d)]^2) + \omega(m_2+\rho d)(\alpha_1^2+\alpha_2^2) + \alpha_2k^2d\omega^2(m_2+\rho d)^2} \qquad (4.19)$$

where $\alpha_1 = \frac{\epsilon(\frac{8\mu}{a^2})}{g}$ and $\alpha_2 = \frac{\epsilon\omega\rho}{g}$

The above equation is very complicated. It is necessary to simplify this equation in order to gain some physical insight how the parameters affect the loss factor. At very low frequencies, the loss factor can be appoximated as

$$\eta \approx \frac{\omega(m_2+\rho d)^2k^2d}{\alpha_1(m_1+m_2+\rho d)} \qquad (4.20)$$

The k is the bending wavelength of the coupled system and is defined in equation (3.3). This is proved to be correct experimentally in chapter 5.

At very high frequencies, equation (4.19) is approximated as

$$\eta \approx \frac{\alpha_1}{\omega m_1k^2d} \qquad (4.21)$$

Equating equations (4.20) and (4.21) roughly gives the frequency at which maximum loss factor will occur. This is equal to

$$\omega_{max}^2 = \frac{\alpha_1}{d(m_2+\rho d)}\sqrt{\frac{B}{m_1}} = \frac{\frac{\epsilon}{2}\left[\frac{8\mu}{g}\right]}{d(m_2+\rho d)}\sqrt{\frac{B}{m_1}} \qquad (4.22)$$

Substituting this equation back to equation (4.21) gives

$$\eta_{max} = \sqrt{\frac{(m_2+\rho d)^2}{m_1(m_1+m_2+\rho d)}} \qquad (4.23)$$

In non-dimensional form, it can be written as

$$\eta_{max} = \frac{T}{\sqrt{1+T}} \qquad (4.24)$$

whwere $T = \alpha+\beta$, $\alpha = \frac{m_2}{m_1}$ and $\beta = \frac{\rho d}{m_1}$.

The above equation indicates that by increasing the attached plate mass, the loss factor will increase. However, if the gap is large (ie. $\beta>>\alpha$), the increment of α will be insignificant and the loss factor will remain the same. The equation also indicates that by increasing the gap d (ie. increase β), the loss factor will increase. The frequency at which the maximum loss occurs, however, depends on many parameters (equation (4.22)). If the gap is small, this peak will occur at higher frequency. Similarly, by increasing the material macroscopic flow resistance, this peak will also occur at higher frequency.

Figure 4.1 gives the estimated values of the maximum loss factor versus α ($\alpha = m_2/m_1$). Increasing the α increases the maximum losses. However, if β is large ($\beta>>\alpha$), the maximum losses become a constant. Figure 4.2 shows the estimated maximum loss factor versus β ($\beta=\rho d/m_1$) and a similar trend is observed. Although equation (4.24) is an oversimplified expression, it thus indicates the general trend how the maximum losses depends on various

parameters, which is otherwise impossible to identify from the complicated equation (4.19).

5.0 EXPERIMENTAL VERIFICATION OF THE THEORY WITH POROUS MATERIALS IN LAYERED CONFIGURATIONS

The experiments were again carried out using the photographic glass plates. The porous materials used in the experiments were; 7mm thick DCMEAD polyester foam, 6mm and 18mm thick reticulated (Retic 20 PPI FR3) polyurethane foam and a 9 mm thick felt (wool). The size of these materials are 0.495 x 0.495m. Essolube hdxplus 20W/50 diesel engine lubricating oil (temperature of 20^{o}C) was used as the fluid and also water was used.

5.1 The point inertance measurement

The excitation method was described in section 3.0. Figure 5.1 shows the measured point inertance curve when 7 mm thick DCMEAD polyester foam, which is filled with the lubricating oil, is immersed in the gap of the same thickness. The average inertance for an infinite plate can be found as [8].

$$I_{infinite} = \frac{\omega}{8\sqrt{Bm}} \qquad (5.1)$$

where m, B are the mass per unit area and the flexural rigidity of the plate. In this case, this m is the total mass per unit area of the whole system. The mean response curve is drawn on the same graph and it roughly agrees with the measured inertance curve. This demonstrates that the approximation of the flexural wavenumber k of the excited plate with fluid loading (equation (3.3)) is correct.

5.2 The porous materials macroscopic flow resistance measurement

Although the theoretical modelling of damping with porous materials in layered configurations using impedance approach is described in the previous chapter, it is not possible to estimate the loss factor of the system without knowing the properties of the porous material used in the experiment. The unknown parameters of each porous material are the structure factor and the pore size. However, it is possible to measure the

macroscopic flow resistance which in turn enables the parameter ϵ/a^2 to be calculated.

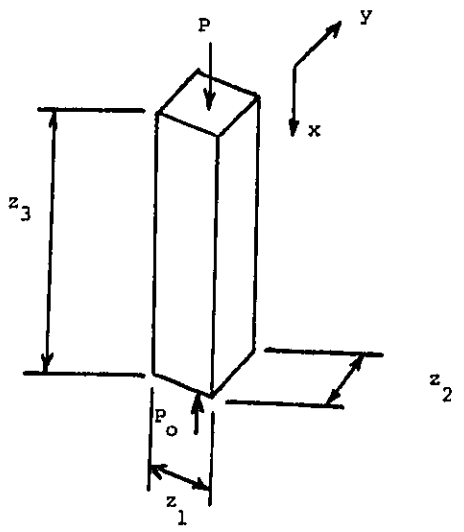

diagram 5.1

Considering the fluid which passes through a porous material of length z_3 with cross sectional area $z_1 z_2$ (diagram 5.1), the mass of the fluid discharged per unit time can be equated as

$$Q = \rho \, \bar{U} \, z_1 z_2 \qquad (5.2)$$

where $\bar{U}$ is the mean flow velocity at any x and ρ is the fluid density. This mean flow velocity is related to the pressure P_a at any x as (the real part of equation (4.13)).

$$-\frac{dP_a}{dx} = \frac{\epsilon \sigma}{g} \cdot \bar{U} = \frac{\epsilon \left[\frac{8\mu}{a^2}\right]}{g} \cdot \bar{U} \qquad (5.3)$$

Substituting equation (5.3) into (5.2) gives

$$Q = - \rho \frac{dP_a}{dx} \frac{g}{\epsilon\left[\frac{8\mu}{a^2}\right]} z_1 z_2 \qquad (5.4)$$

By measuring the discharge rate Q, the ϵ/a^2 can be calculated.

Figure 5.2 displays the apparatus used for this flow resistance measurement. A 12x12x325 mm perspex tube is made to accommodate the porous material for testing. Perspex is chosen so that if any air bubbles remain in the porous material when fluid has filled the tube, they can be clearly seen. They were removed by suction on top of the tube . A valve was attached immediately below the tube to control the flow. The level of the fluid on top of the tube was kept constant (height = 290 mm) during the experiment to give a constant pressure level. The temperature of the fluid was monitored.

For the Essolube hdxplus 20W/50 lubricating oil, the average measured ϵ/a^2 for different porous materials were:

POROUS MATERIAL	ϵ/a^2
DCMEAD polyester foam	7.62×10^6
DCMCC polyether foam	8.93×10^6
20PPI reticulated polyurethane foam	7.51×10^5

The experiments were repeated using Olive oil giving measured ϵ/a^2 values close to the above. However, there was a marked difference in the measured ϵ/a^2 when water was used. It is later found that because of the viscosity of water is comparatively small and hence the flow was very fast, the limited size of the valve restricted the flow. By removing the valve, the measured ϵ/a^2 were closer to the above values. The apparatus used for the experiments was therefore only suitable for use with high viscosity fluids.

5.3 Comparison of the measured and the estimated total loss factor with foam layer

Since the foam was not glued onto the plates, the shearing motion of the frame was not considered. Substituting the measured ϵ/a^2 values into the equation (4.10), it is found that $\overline{V}_2 >> \overline{V}_1$ which means that the frame can be assumed rigid. Therefore equation (4.19) can be used to estimate the loss factor of the system.

However, in the actual experiments, as the foam is filled with fluid, the frame will deform slightly. The frame is certainly not absolutely rigid. It is therefore difficult to justify ignoring the shearing effect of the frame. However, the experimental and theoretical results, which will be discussed in the following sections, which agree with each other demonstrate that the error for assuming the frame to be rigid is small.

As can be seen from equation (4.14), although the measured ϵ/a^2 enables the real part of this blocked impedance to be estimated, the value of the structure factor in the imaginary part remains to be assigned. The imaginary component of the structure factor controls the fluid inertia effect; an increase causes the loss factor to decrease. This effect is significant at high frequencies.

Figure 5.3 shows the measured loss factor when the gap is filled with the lubricating oil together with the 7mm thick DCMEAD polyester foam. Even by varying the structure factor, the agreement between the estimated total loss factor (including the excited plate radiation and material losses) and the measured value is not very satisfactorily. There is more than 3 dB difference between 800 Hz and 2000 Hz frequency range. Figure 5.4 gives the estimated total loss factor by varying the ϵ/a^2 value and keeping the structure factor unity. The estimated values indicate that the higher the ϵ/a^2, the smaller the loss factor at low frequencies and higher at high frequencies.

Figure 5.5 gives the best fit of the estimated values to the measured loss factor. The ϵ/a^2 for this best fit curve is about half the measured value. One of the causes for the discrepancies is probably due to the fact

that this polyester foam has irregular pores, and the portion of the foam for the viscosity testing may not represent the average ϵ/a^2 value of the big foam used for the loss factor measurement. Secondly, the cutting of the porous material (for this flow resistance testing) to the exact dimensions as the perspex tube is difficult. Any discrepancies in the dimensions will certainly change the fluid discharge rate.

Figure 5.6 displays the comparison between the measured and the estimated total loss factor (using structure factor = 1.8) with the 6 mm thick DCMCC polyether foam in the gap. The agreement is very good. Figure 5.7 gives the estimated result using the 18 mm thick polyether foam. By increasing the structure factor, the fluid inertia increases and the loss factor decreases. Figure 5.8 shows the comparison between the measured and this estimated total loss factor. Again, the structure factor of 1.8 gives the best fit result. The result also indicates that with a thicker foam, the loss factor increases. This agrees with the trend observed from equation (4.24).

Figures 5.9 and 5.10 show the comparison of the measured and the estimated total loss factor (using structure factor = 1.8) with the 6 mm and 18 mm thick 20PPI reticulated polyurethane foam in the gap respectively. The agreement is again very good. However, the pores of this foam are much larger than those in the polyester and polyether foams and as expected, the loss factor is smaller. Figure 5.11 gives the measured loss factor both at the excited and the attached plates. The results indicate that the plates are strongly coupled and therefore the measured loss factors are the same.

5.4 The influence of the attached mass and the gap on the loss factor

Figure 5.12 displays the measured loss factor with and without the attached glass plate on top of the 7 mm thick DCMEAD polyester foam. The results show that with the attached plate, the loss factor is higher. This is expected as the squeezing effect in the gap will decrease if it is without the attached plate. Figure 5.13 gives the estimated total loss factor versus the gap by varying the attached plate thickness (at a constant frequency). Increasing the attached mass increases the loss

factor for small gap, however, if the gap is large the increase in m_2 will not affect the loss factor. This agrees with the trend suggested in equation (4.24).

Figures 5.14 and 5.15 show the estimated loss factor (excluding excited plate radiation and material losses) using steel plates. The plate mass ratio α (equation (4.24)) remains unchanged, however, the individual plate mass increases. The loss factor increases at low frequencies. If the gap is large, this increment is insignificant. At high frequencies, the loss factor decreases with increasing mass.

5.5 Comparison of the measured and the estimated total loss factor with the felt layer

In order to demonstrate that the above theory can be applied to other materials other than foam, a 9 mm thick felt with 1314 kg/m^3 material density and porosity 0.827 was chosen for experiment. The structure factor of the felt was unity due to the nature of the felt. The measured average ϵ/a^2 is 2.123 x 10^7 m^{-2}. Figure 5.16 shows the comparison of the measured and the estimated total loss factor. The agreement is encouraging. However, a very close fit result can be obtained by varying the ϵ/a^2 in the estimation of the loss factor. Figure 5.17 gives this estimated values and figure 5.18 displays the best fit curve. As mentioned in section 5.3, the cutting of the material to the exact dimensions as the perspex tube for flow resistance testing is difficult and this will give an inaccurate ϵ/a^2 value. However, the estimated and the measured loss factor display a similar trend suggesting that the simple theory developed in chapter 4 is generally correct.

To complete this series of tests, the 9 mm thick felt was also immersed in water and the loss factor measured. As expected, the loss factor is small because the water has a very low dynamic viscosity. Figure 5.19 gives the measured and the estimated loss factor and the agreement is good. However, the result clearly demonstrates that it is necessary to use a high viscosity fluid in conjunction with the material to achieve the high loss factor.

6.0 CONCLUSIONS

(a) Oil layer damping with perforated or non-perforated attached plate

(i) The blocked impedance of the incompressible fluid model with the parabolic velocity flow profile indicates an inertia and viscosity controlled behaviour. For the perforated plate with $k\ell << 1$, the blocked impedance is independent of k (the flexural wavenumber of the excited plate including the loading of fluid and the attached mass). The perforations behave as independent dashpots.

(ii) The computed results suggest that for a high loss factor, the size of the holes in the perforated plate should be large. However, the distance between the holes centres should be small. For a perforated plate with constant thickness, there is an optimum combination of these parameters to give the highest losses.

(iii) The loss factor obtained with oil layer is generally low. It was found that the loss factor is controlled by the ratio of the fluid dynamic viscosity and its density. A high loss factor can still be possible provided that the fluid dynamic viscosity can be increased by many folds as its density increases. This ratio was favourable with air. This ratio is not favourable with oil. But if viscosity is increased by an infill, high loss factors can be achieved.

(b) Loss factor of plates with porous material and oil layer

(i) The loss factor can be increased to above 0.1 if a material of high porosity is immersed into the high viscosity oil layer.

(ii) The excited and the attached plates are strongly coupled and the measured loss factor on both the excited and the attached plates are the same.

(iii) The structure factor ($\epsilon \propto 1/a^2$) of the porous material should be chosen to be as small as possible to give a high loss factor.

(iv) The fluid inertia is important at high frequencies. High inertia reduces the flow speed thus giving smaller viscous losses. Therefore the porous material with a small structure factor ($\epsilon=1/\cos^2\theta$) is preferred for high losses.

(v) Increasing both the excited and the attached plate masses and keeping their mass ratio constant increases the loss factor at low frequencies. However, if the gap is already very large (ie $\beta>>\alpha$), the loss factor will not be affected by the changing α. At high frequencies, fluid inertia is the controlling parameter, and the loss factor decreases with increasing gap.

(vi) The frequency at which the maximum loss factor occurs depends on the properties of the porous material, the gap and the mass of the plates. For larger gaps or heavier attached plate, this frequency occurs at lower values. For heavier excited plate or larger porous material structure factor, this frequency will occur at higher values.

REFERENCES

[1] **TROCHIDIS, A.** Vibration damping due to air or liquid layers. Acustica 51, 4, 201-212, 1982.

[2] **CHOW, L.C. AND PINNINGTON, R.J.** On the prediction of loss factors due to squeeze film damping mechanisms. ISVR Technical Report No 130, October 1985 University of Southampton.

[3] **ZWIKKER C. AND KOSTEN, C.W.** Sound Absorbing Materials. Amsterdam: Elsevier Press 1949.

[4] **ROSIN, G.S.** Oscillations induced in porous materials with an elastic matrix by sound waves at normal incidence. Soviet Physics - Acoustics 19, 60-64, 1973.

[5] **BOLTON, J.S.** Cepstral techniques in the measurement of acoustic reflection coefficients, with applications to the determination of acoustic properties of elastic porous materials. PhD thesis, 1984 University of Southampton.

[6] **RAYLEIGH, L.** The Theory of Sound (volume II). New York: Dover Publications, second edition, 1945, re-issue.

[7] **GENT, A.N. AND KUSCH, K.C.** Permeability of Open-cell Foamed Materials. Journal of Cellular Plastics, 2, 46-51, 1966.

[8] **CREMER, L. AND HECKL, M.** Structure-borne Sound. Springer-Verlag, 1973.

APPENDIX I The Calculation of the Average Blocked Impedance of a Plate with Slots

Consider a plate, which has many equally spaced slots ℓ, and is assumed to be infinitely long and is placed a distance d above a rigid wall. Assume the slots each of length b is small compared with ℓ. Assume each small element is excited with a constant velocity gradient and for

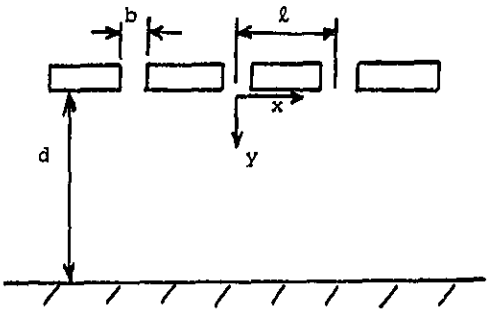

diagram I.1

simplicity, the analysis is carried out in the two dimensions. The coordinate of the system is chosen such that at the beginning of each small element, the x value is zero (see diagram I.2). The subscripts 1, 2, 3 correspond to element 1, 2, 3 respectively and the pressure in $x_1 = 0$ to ℓ is P_1, in $x_2 = 0$ to ℓ is P_2 and so on.

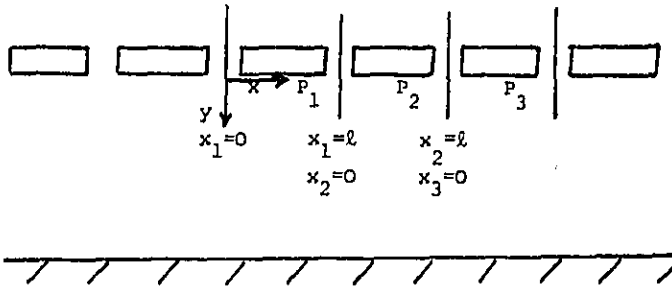

diagram I.2

The velocity at the N^{th} element in y-direction can be written as

$$V_N = [\ |V|e^{-ik(N-1)\ell} + \frac{|V|}{\ell}.e^{-ik(N-1)\ell}.(e^{-ik\ell_{-1}x_N}]e^{i\omega t} \qquad (I.1)$$

That is
$V_1 = |V|e^{i\omega t}$ at $x_1 = 0$
$V_2 = |V|e^{-ik\ell}e^{i\omega t}$ at $x_1 = \ell$ or $x_2 = 0$
$V_3 = |V|e^{-ik2\ell}e^{i\omega t}$ at $x_2 = \ell$ or $x_3 = 0$ and so on.

This is obtained from the finite element approach at which the velocity in a small slot is assumed to have a velocity with a constant velocity gradient.

Consider a small element of the oscillatory plate, for which the simplified equation of continuity is [2].

$$V(x) = H(x)\frac{d\bar{u}(x)}{dx} + \bar{u}(x)\frac{dH(x)}{dx} \qquad (I.2)$$

where $H(x)$ is the gap between the plate and the wall at position x, $\bar{u}(x)$ is the average horizontal flow velocity at position x.

Assuming the velocity profile of the gap is of parabolic shape, it can be shown that

$$\frac{dP}{dx} = -A\,\bar{u} \qquad (I.3)$$

where $A = (12\mu/d^2 + i\omega\rho)$ with μ and ρ the dynamic viscosity and the density of the fluid in the gap.

Substituting equations (I.1) and (I.3) into (I.2), the expressions for the pressure gradient and its pressure for element 1 say can be obtained. They are

$$\frac{dP_1}{dx_1} = -\frac{A}{d}\left(|V|x_1 + C_{x_1}\frac{x_1^2}{2} + C_{2_{x_1}}\right)e^{i\omega t} \qquad (I.4)$$

$$P_1 = -\frac{A}{d}\left(|V|\frac{x_1^2}{2} + \frac{C_{x_1}x_1^3}{6} + C_{2_{x_1}}x_1 + C_{3_{x_1}}\right)e^{i\omega t} \qquad (I.5)$$

Similarly, $P_2 = \frac{-A}{d}\left(V_2\frac{x_2^2}{2} + \frac{C_{x_2}x_2^3}{6} + C_{2_{x_2}}x_2 + C_{3_{x_2}}\right)e^{i\omega t}$ (I.6)

and so on with $V_2 = |V|e^{-ik\ell}$.

The C_{x_1}, $C_{2_{x_1}}$, $C_{3_{x_1}}$ are the constants for element 1.

C_{x_2}, $C_{2_{x_2}}$, $C_{3_{x_2}}$ are the constants for element 2.

Condition 1 $\qquad P_{N+1} = P_N e^{-ik\ell}$

That is $\qquad P_2(x_2=0) = P_1(x_1=0)e^{-ik\ell}$

and $\qquad P_3(x_3=0) = P_2(x_2=0)e^{-ik\ell}$

Therefore a general $C_{3_{x_N}}$ can be written as

$$C_{3_{x_N}} = C_{3_{x_1}} e^{-i(N-1)k\ell} \qquad (I.7)$$

Condition 2 $\qquad \bar{u}_{N+1} = \bar{u}_N e^{-ik\ell}$

That is $\qquad \bar{u}_2(x_2=0) = \bar{u}_1(x_1=0)e^{-ik\ell}$

Therefore a general $C_{2_{x_N}}$ can be written as

$$C_{2_{x_N}} = C_{2_{x_1}} e^{-i(N-1)k\ell} \qquad (I.8)$$

Also $\bar{u}_2(x_2=\ell) = \bar{u}_1(x_1=\ell)e^{-ik\ell}$

therefore a general C_{x_N} can be written as

$$C_{x_N} = C_{x_1} e^{-i(N-1)k\ell} \qquad (I.9)$$

From equation (I.1), $C_{x_1} = \frac{|V|}{\ell}(e^{-ik\ell}-1)$. (I.10)

Also as $P_1(x_1=\ell) = P_2(x_2=0)$

the $C_{3_{x_1}}$ can be found. It is

$$C_{3_{x_1}} = \frac{1}{(e^{-ik\ell}-1)}\left(|V|\frac{\ell^2}{2} + C_{x_1}\frac{\ell^3}{6} + C_{2_{x_1}}\ell\right) \qquad (I.11)$$

To find $C_{2_{x_1}}$ we have to equate the impedance at the slots, Z, (diagram I.3) as

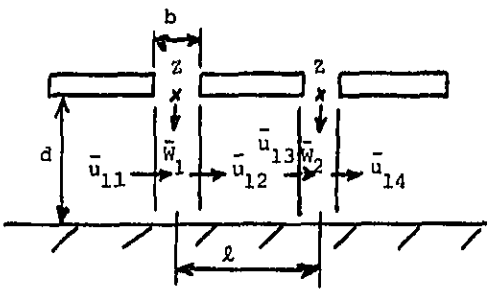

diagram I.3

$$Z = \frac{-P_1(x_1=\ell)}{(\bar{u}_{12}-\bar{u}_{11})\frac{d}{b}} = \frac{-P_2(x_2=0)}{(\bar{u}_{12}-\bar{u}_{11})\frac{d}{b}} = \frac{-P_2(x_2=\ell)}{(\bar{u}_{14}-\bar{u}_{13})\frac{d}{b}} \qquad (I.12)$$

From $Z(\bar{u}_{12}-\bar{u}_{11})\frac{d}{b} = - P_2(x_2=0)$ it can be shown that

$$C_{2_{x_1}} = \frac{1}{\left[\frac{Z}{b}(e^{-ik\ell}-1) - \frac{\frac{A\ell}{d}e^{-ik\ell}}{(e^{-ik\ell}-1)}\right]} \cdot \left\{ |V| \left[\frac{Z\ell}{b} + \frac{\frac{A\ell^2}{2d}e^{-ik\ell}}{(e^{-ik\ell}-1)}\right] + C_{x_1}\left[\frac{Z\ell^2}{2b} + \frac{\frac{A\ell^3}{6d}e^{-ik\ell}}{(e^{-ik\ell}-1)}\right]\right\} \tag{I.13}$$

Substituting all these constants into equation (I.5) gives

$$P_1 = -\frac{A}{d}\left[\left[|V| \left\{ \frac{x_1^2}{2} + \frac{\ell^2}{2(e^{-ik\ell}-1)} + \frac{\left[x_1 + \frac{\ell}{(e^{-ik\ell}-1)}\right]\left[\frac{Z\ell}{b} + \frac{A\ell^2 e^{-ik\ell}}{2d(e^{-ik\ell}-1)}\right]}{\left[\frac{Z}{b}(e^{-ik\ell}-1) - \frac{A\ell e^{-ik\ell}}{d(e^{-ik\ell}-1)}\right]} \right\} + \frac{|V|(e^{-ik\ell}-1)}{\ell}\left\{ \frac{x_1^3}{6} + \frac{\ell^3}{6(e^{-ik\ell}-1)} + \frac{\left[x_1 + \frac{\ell}{(e^{-ik\ell}-1)}\right]\left[\frac{Z\ell^2}{2b} + \frac{A\ell^3 e^{-ik\ell}}{6d(e^{-ik\ell}-1)}\right]}{\left[\frac{Z}{b}(e^{-ik\ell}-1) - \frac{A\ell e^{-ik\ell}}{d(e^{-ik\ell}-1)}\right]} \right\}\right]\right] \cdot e^{i\omega t} \tag{I.14}$$

The average blocked impedance per unit area is

$$Z_b = \frac{\frac{1}{\ell}\int_0^{\ell} P_1 dx_1}{\frac{1}{\ell}\int_0^{\ell} V_1\, dx_1}$$

$$= \frac{-A}{d}\left[\left[\frac{\ell^2}{6} + \frac{\ell^2}{2C} + \frac{(\frac{\ell}{2} + \frac{\ell}{C})(\frac{Z\ell}{b} + \frac{A\ell^2 e^{-ik\ell}}{2dC})}{\left[\frac{ZC}{b} - \frac{A\ell e^{-ik\ell}}{dC}\right]}\right]\right.$$

$$+\frac{C}{\ell}\left[\frac{\ell^3}{24}+\frac{\ell^3}{6C}+\frac{\left[\frac{\ell}{2}+\frac{\ell}{C}\right]\left[\frac{Z\ell^2}{2b}+\frac{A\ell^3 e^{-ik\ell}}{6dC}\right]}{\left[\frac{ZC}{b}-\frac{A\ell e^{-ik\ell}}{dC}\right]}\right]\Bigg]\cdot\frac{1}{(1+\frac{C}{2})}$$

where $C = (e^{-ik\ell}-1)$ (I.15)

By grouping the terms in equation (I.15) and simplifying and assuming $k\ell \ll 1$, it can be shown that the block impedance per unit area can be simplified as

$$Z_b = \frac{A\ell^2}{d}\left[\frac{1}{12}+\frac{Zd}{A\ell b}\right] \qquad (I.16)$$

This average blocked impedance is the same everywhere in each small element and it is independent of the wavenumber k. Since the real and imaginary part of A are positive, this is also true for Z (the impedance per unit area at the slot at y=0). The real and imaginary part of this blocked impedance per unit area should be positive.

APPENDIX II The Calculation of the Impedance for a Circular Hole

To calculate the impedance per unit area Z for a perforated plate with circular holes, we have to extend the analysis to 3-dimensions. First of all we have to calculate the impedance per unit area of a circular hole, then we have to use this impedance to calculate the impedance in z-direction. For simplicity, the movement of the plate is assumed to have a constant velocity in z-direction.

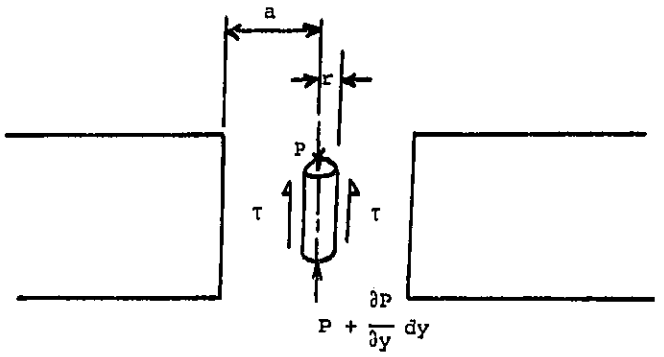

diagram II.1

To calculate the impedance per unit area of a circular hole, we have to consider a fluid element in the hole. (diagram II.1). This fluid is neither gaining nor losing momentum, therefore the forces on it must balance. That is,

$$\pi r^2 \left(\frac{dP}{dy}\, dy\right) + \tau \cdot 2\pi r dy = 0$$

where $$\tau = -\mu \frac{dW}{dr}$$

then $$\frac{dW}{dr} = \frac{r}{2\mu} \frac{dP}{dy}$$

As $\int_{W_o}^{0} dW = \frac{1}{2\mu}\frac{dP}{dy}\int_{o}^{a} r\,dr$

therefore $W_o = -\frac{a^2}{4\mu}\frac{dP}{dy}$.

This is the maximum velocity at the centre axis.

Since W = 0 at r = a, this gives

$$W = \frac{1}{4\mu}\frac{dP}{dy}(r^2 - a^2) \qquad \text{(II.1)}$$

The total volume flow $= \int_{o}^{a} 2\pi r W dr = 2\pi \int_{o}^{a} \frac{r}{4\mu}\frac{dP}{dy}(r^2-a^2)dr$

$$= -\frac{\pi a^4}{8\mu}\frac{dP}{dy}$$

The mean velocity $\bar{W} = \left(-\frac{\pi a^4}{8\mu}\frac{dP}{dy}\right)/\pi a^2$

$$= -\frac{a^2}{8\mu}\frac{dP}{dy} = \frac{W_o}{2} \qquad \text{(II.2)}$$

or $$\frac{1}{4\mu}\frac{dP}{dy} = -\frac{2\bar{W}}{a^2} \qquad \text{(II.3)}$$

Now $$-2\pi r dy\left(-\mu\frac{dW}{dr}\right) - \frac{dP}{dy}dy\pi r^2 = \frac{dW}{dt}\pi r^2 dy\rho$$

simplifying gives $$-\frac{2}{r}\mu\frac{dW}{dr} - \frac{dP}{dy} = \rho\frac{dW}{dt} \qquad \text{(II.4)}$$

Substituting equation (II.3) into (II.4) and in terms of $\bar{W}$ gives

$$P = -\bar{W}\left(\frac{8\mu}{a^2} + i\omega\rho\right)y + C_2$$

where C_2 is a constant. If the fluid is filled to the top level of the hole, then P = 0 at y = -h which gives

$$P = -\bar{W}\left(\frac{8\mu}{a^2} + i\omega\rho\right)(y+h)$$

$$\text{or } P(y=0) = -\bar{W}\left(\frac{8\mu}{a^2} + i\omega\rho\right)h$$

The impedance per unit area of a hole Z_h at y=0 is

$$Z_h = \left(\frac{8\mu}{a^2} + i\omega\rho\right)h \qquad \text{(II.5)}$$

The negative sign disappears because pressure and the flow direction oppose each other.

APPENDIX III The Calculation of the Impedance in the z-direction

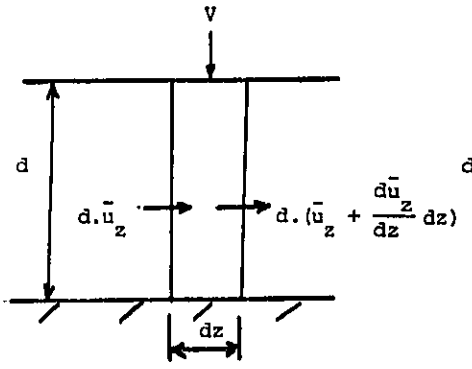

diagram III.1

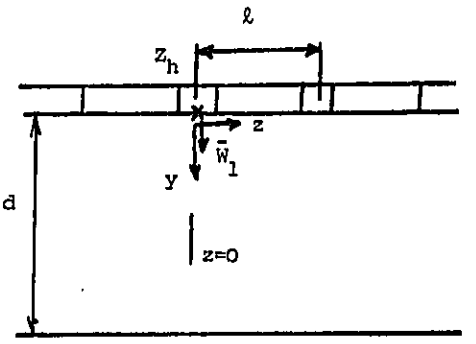

diagram III.2

For simplicity, it is assumed that the plate has a constant velcoity V in z-direction. Considering a fluid element dz at any position z (diagram III.1),

$$d \cdot \frac{d\bar{U}_z}{dz} dz = V\, dz$$

or $$\bar{U}_z = \frac{V}{d} z + C_3 \qquad \text{(III.1)}$$

where C_3 is a constant. If the flow in the gap in z-direction is also of parabolic shape, then

$$\bar{U}_z = - \frac{1}{(\frac{12\mu}{d^2} + i\omega\rho)} \frac{dP}{dz} \qquad \text{(III.2)}$$

Substituting equation (III.1) into (III.2) gives

$$\frac{dP}{dz} = -\left[\frac{12\mu}{d^2} + i\omega\rho\right)\left(\frac{Vz}{d} + C_3\right)$$

$$\text{or } P = -\left(\frac{12\mu}{d^2} + i\omega\rho\right)\left(\frac{Vz^2}{2d} + C_3 z + C_4\right) \qquad \text{(III.3)}$$

As $P(z) = P(\ell-z)$ by symmetry, this gives

$$\frac{Vz^2}{2d} + C_3 z + C_4 = = \frac{V}{2d}(\ell-z)^2 + C_3(\ell-z) + C_4$$

$$\text{or} \qquad C_3 = -\frac{V\ell}{2d}$$

$$\text{therefore} \quad \bar{U}_z = \frac{V}{d}\cdot z - \frac{V\ell}{2d} \qquad \text{(III.4)}$$

Since $P(z=0) = -\bar{W}_1 \cdot Z_h$ (see diagram (III.2) (III.5a)

and $2\bar{U}_z(z=0) \cdot 2ad = \bar{W}_1 \cdot \pi a^2$ (III.5b)

it can be shown that

$$\bar{W}_1 = \frac{4\bar{U}_z d}{\pi a} \quad , \quad P(z=0) = -\frac{4\bar{U}_z d}{\pi a} Z_h \quad ,$$

$$C_4 = -\frac{1}{\left(\frac{12\mu}{d^2} + i\omega\rho\right)} \frac{2V\ell}{\pi a} Z_h$$

$$\text{and } P(z) = -\left(\frac{12\mu}{d^2} + i\omega\rho\right)\left[\frac{Vz^2}{2d} - \frac{V\ell}{2d} z - \frac{1}{\left(\frac{12\mu}{d^2} + i\omega\rho\right)} \frac{2V\ell}{\pi a} Z_h\right] \qquad \text{(III.6)}$$

Therefore the average impedance per unit area in z-direction is

$$Z = \frac{\frac{1}{\ell}\int_0^{\ell} p(z)dz}{V} = \left(\frac{12\mu}{d^2} + i\omega\rho\right)\left[\frac{\ell^2}{12d} + \frac{1}{\left(\frac{12\mu}{d^2}+i\omega\rho\right)}\frac{2\ell}{\pi a} Z_h\right] \quad \text{(III.7)}$$

APPENDIX IV The Relationship between the Pressure and the Mean Flow Velocity with a Rubber Layer

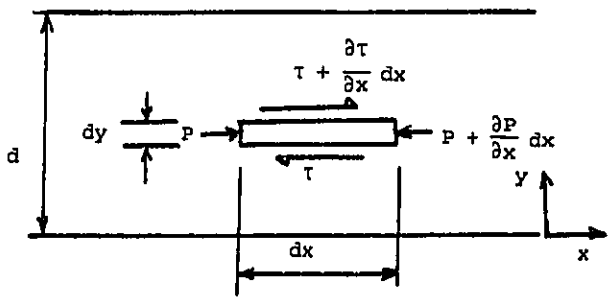

diagram IV.1

Consider the force balance of the small element in the layer with only x-direction motion, it is equal to

$$-\frac{dP}{dx} + G\frac{d^2\xi_1}{dy^2} = \rho_m \frac{d\dot{\xi}_1}{dt} \qquad \text{(IV.1)}$$

Where G is the complex shear modulus of the layer, ξ_1 is the displacement in x-direction and ρ_m is the layer material density. Assume the pressure is constant across the gap and the displacement in the gap is of parabolic shape, that is

$$\xi_1(x,y) = \xi_o + A_1 (y - \frac{d}{2})^2$$

At y=0, ξ_1=0 which gives $A_1 = -\xi_o \frac{4}{d^2}$

This gives $\varepsilon_1(x,y) \simeq \varepsilon_o\left(\frac{4y}{d} - \frac{4y^2}{d^2}\right)$ (IV.2)

and $\dot{\varepsilon}_1(x,y) \simeq \dot{\varepsilon}_o\left(\frac{4y}{d} - \frac{4y^2}{d^2}\right)$ (IV.3)

The mean flow velocity across the gap d is

$$\bar{U} = -\int_o^d \dot{\varepsilon}_1 \, dy = \frac{2}{3} \dot{\varepsilon}_o \qquad \text{(IV.4)}$$

Combining equations (IV.1) to (IV.4) gives

$$-\frac{dP}{dx} = \left(-i\frac{12G}{\omega d^2} + i\,\omega\,\rho_m\right)\bar{U} \qquad \text{(IV.5)}$$

If $G = G_o(1 + i\,\eta_s)$ where G_o and η_s are the shear modulus and shear loss factor of the material in the layer, equation (IV.5) becomes

$$-\frac{dP}{dx} = \left[\frac{12G_o\eta_s}{\omega d^2} + i\left(\omega\rho_m - \frac{12G_o}{\omega d^2}\right)\right]\bar{U} \qquad \text{(IV.6)}$$

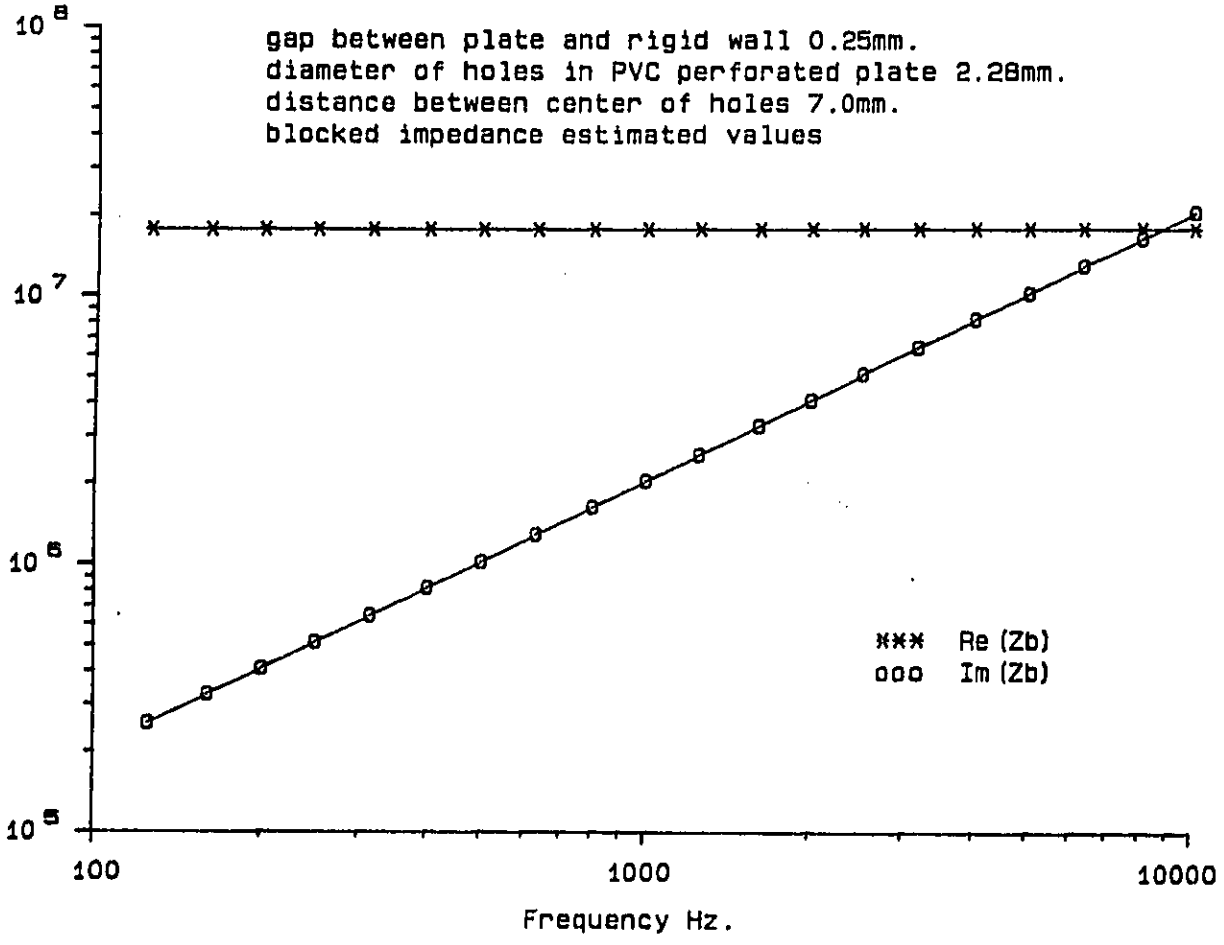

URE 2.1a Estimated blocked impedance for a perforated plate with circular holes.

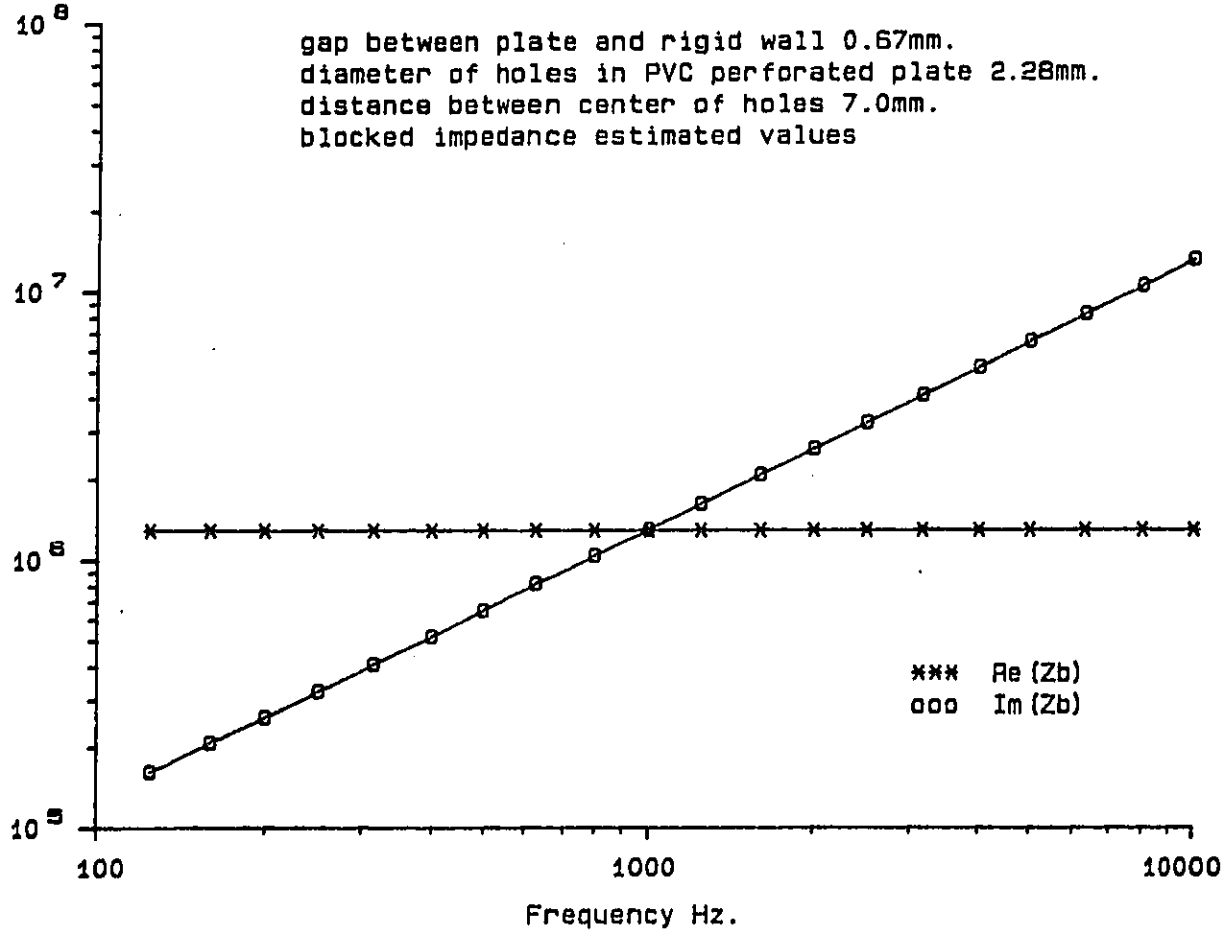

RE 2.1b Estimated blocked impedance for a perforated plate with circular holes

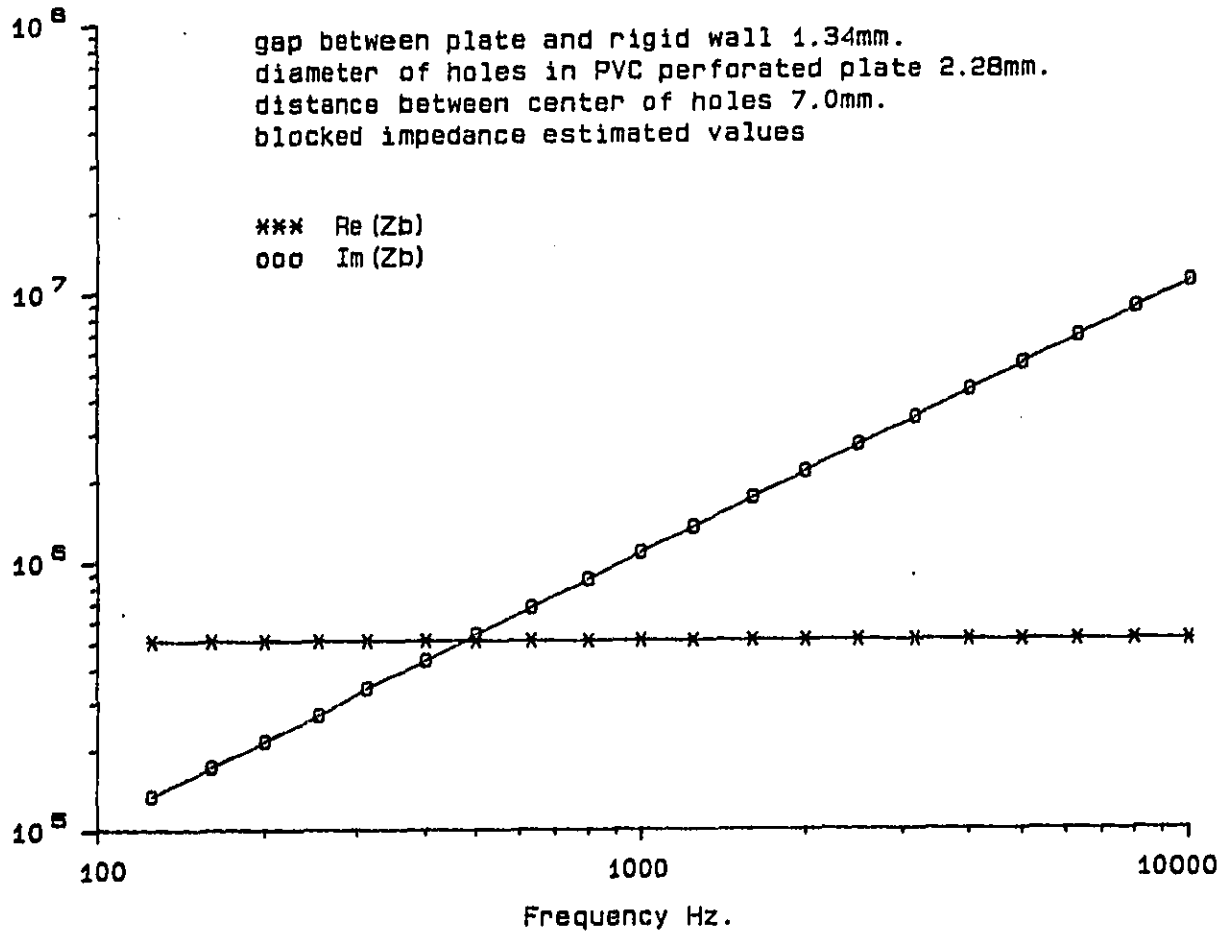

)RE 2.1c Estimated blocked impedance for a perforated plate with circular holes.

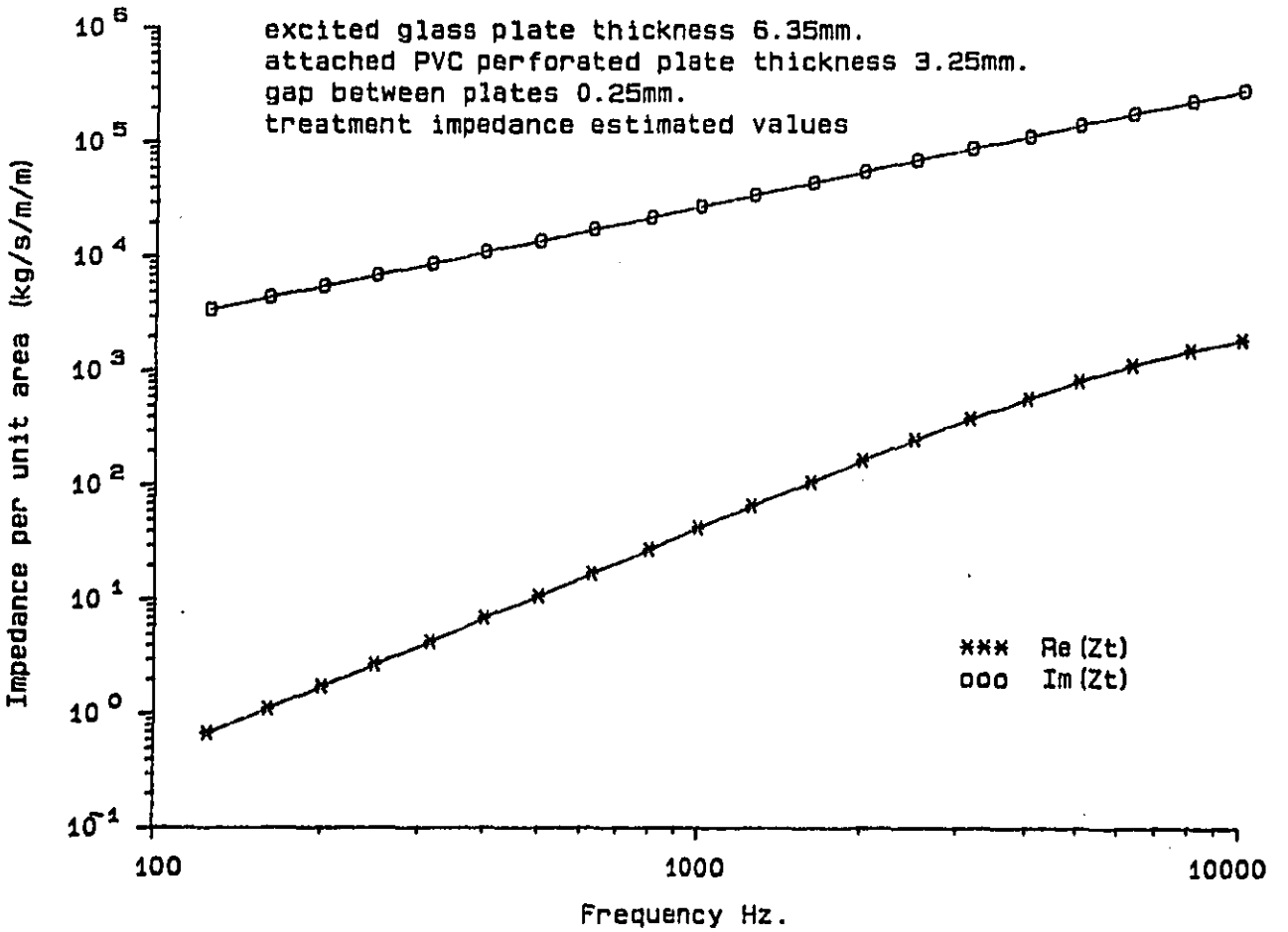

FIGURE 2.2a Estimated blocked impedance for glass-PVC plates.

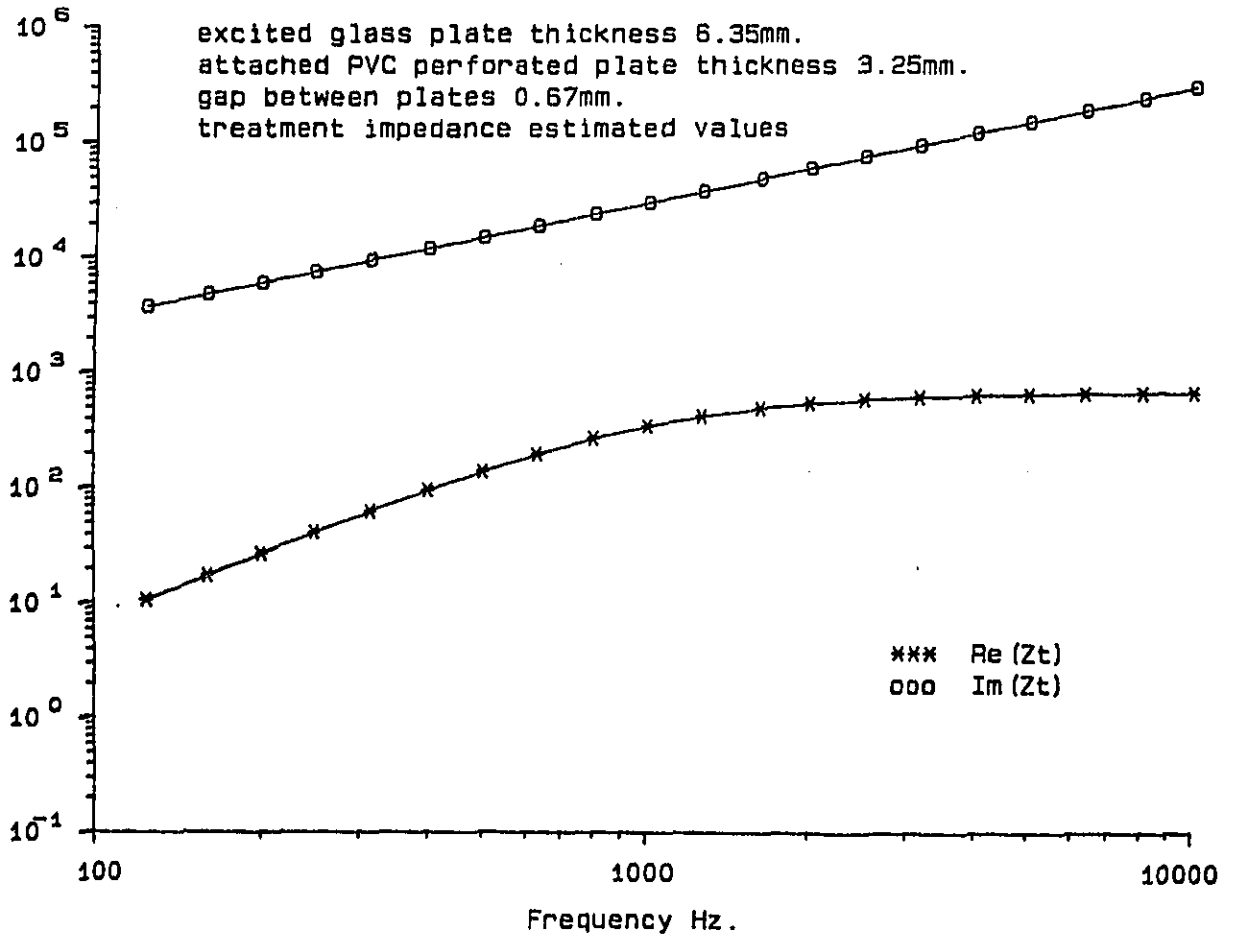

RE 2.2b Estimated blocked impedance for glass-PVC plates.

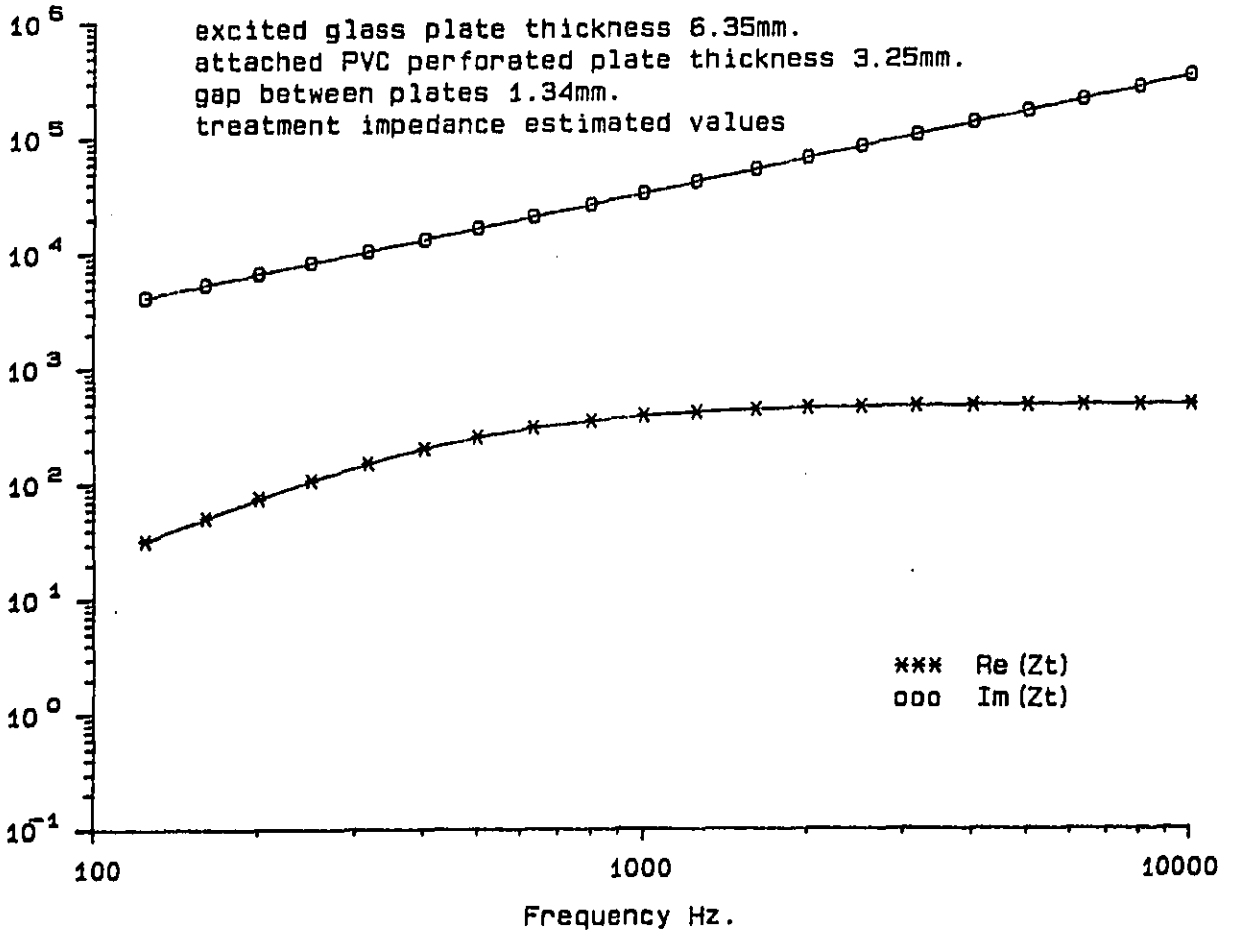

JRE 2.2c Estimated blocked impedance for glass-PVC plates.

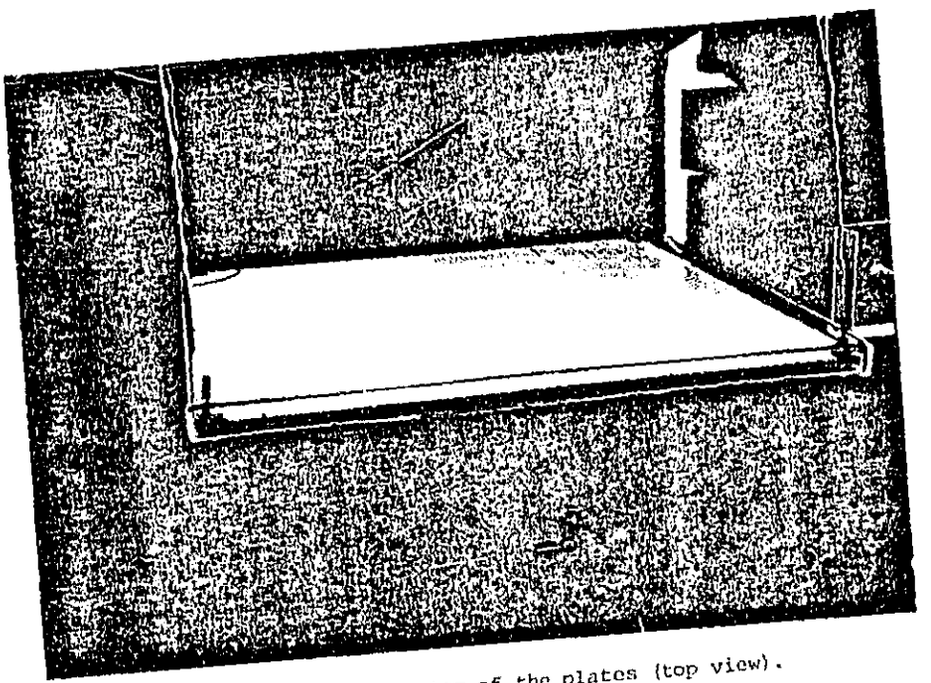

FIGURE 3.1a The suspension system of the plates (top view).

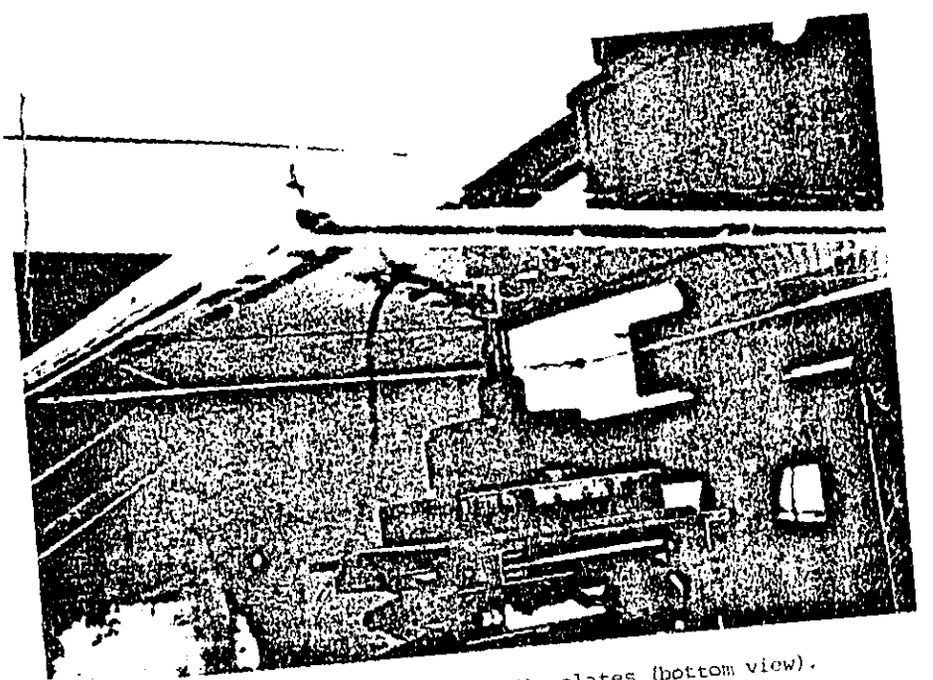

FIGURE 3.1b The suspension system of the plates (bottom view).

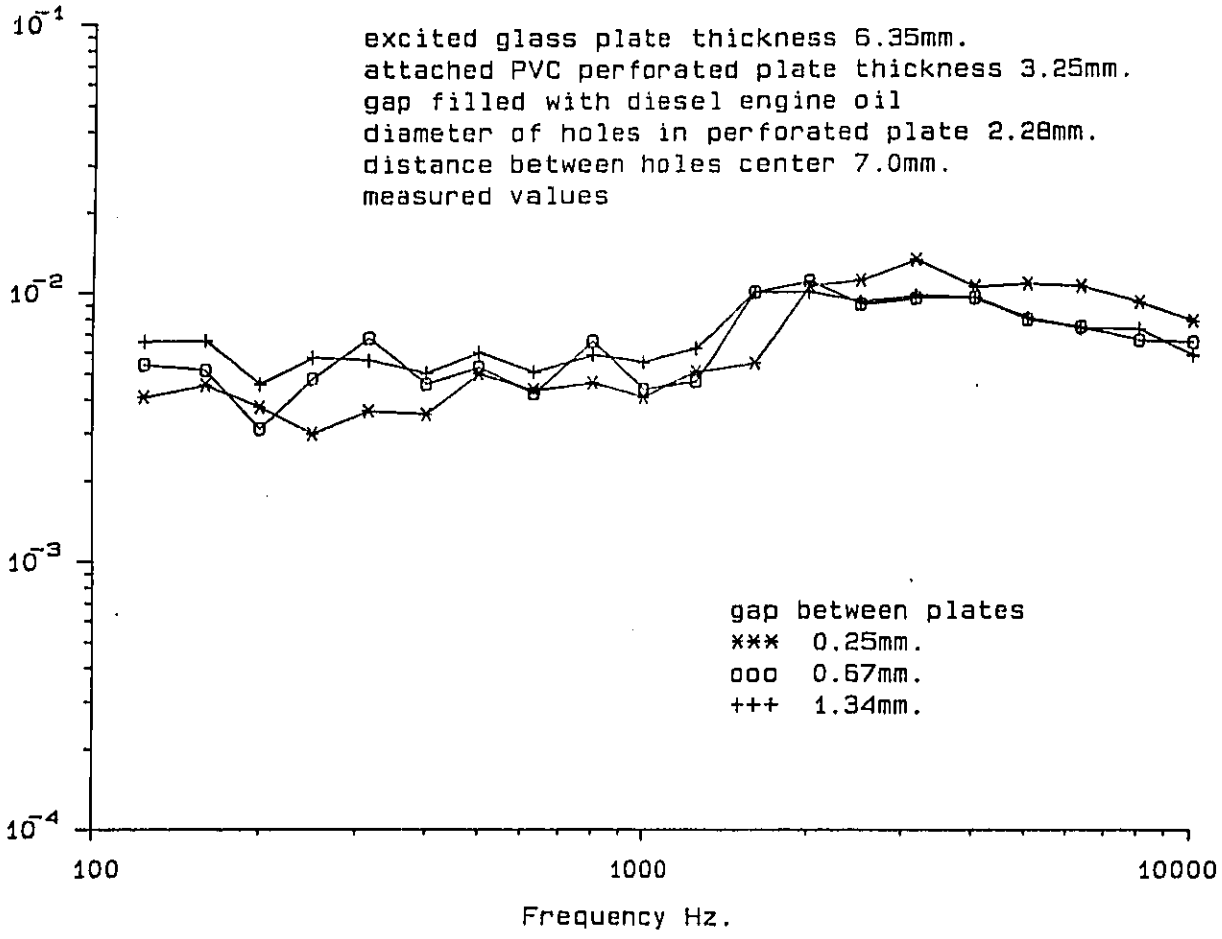

GURE 3.2 The measured loss factor on glass-PVC plates.

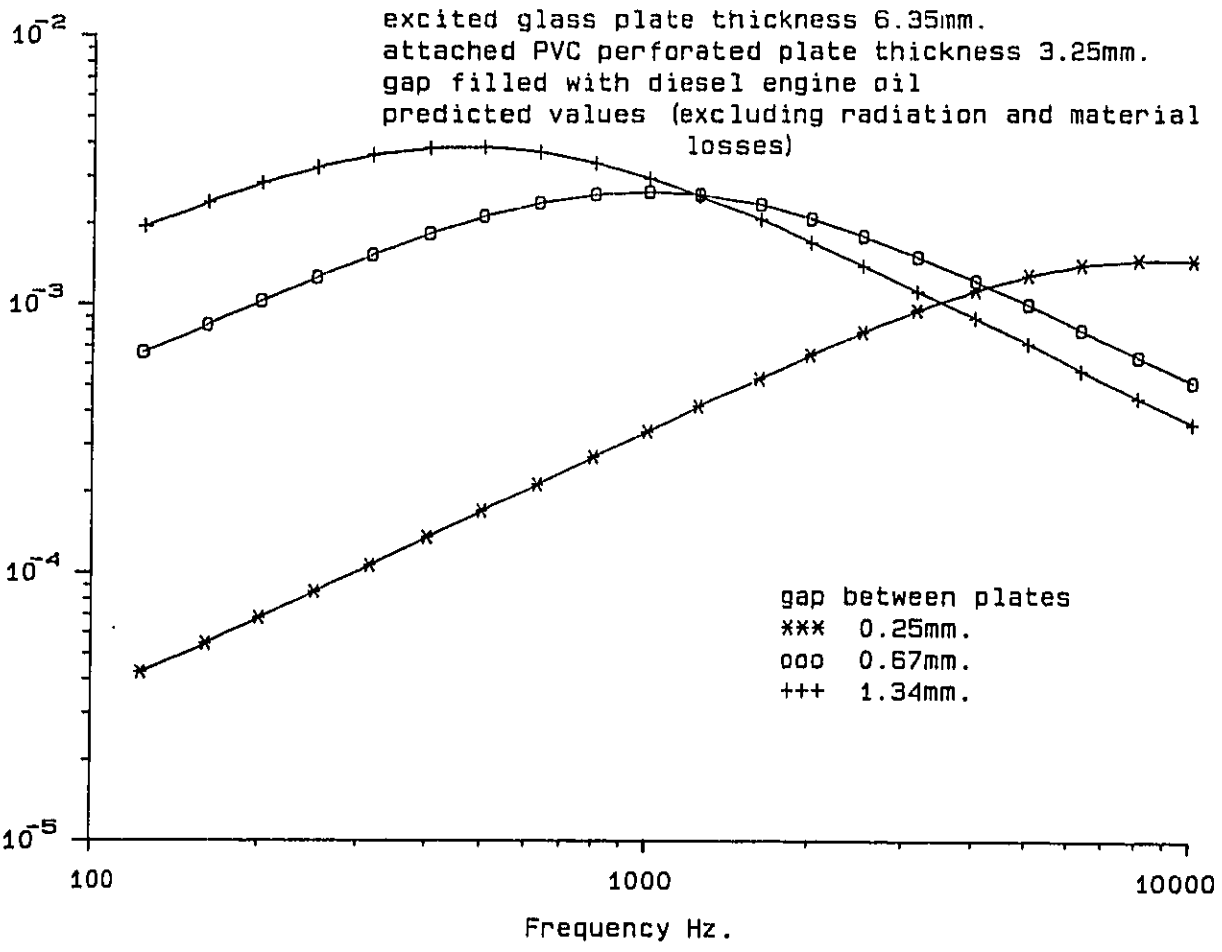

RE 3.3 The estimated loss factor on glass-PVC plates.

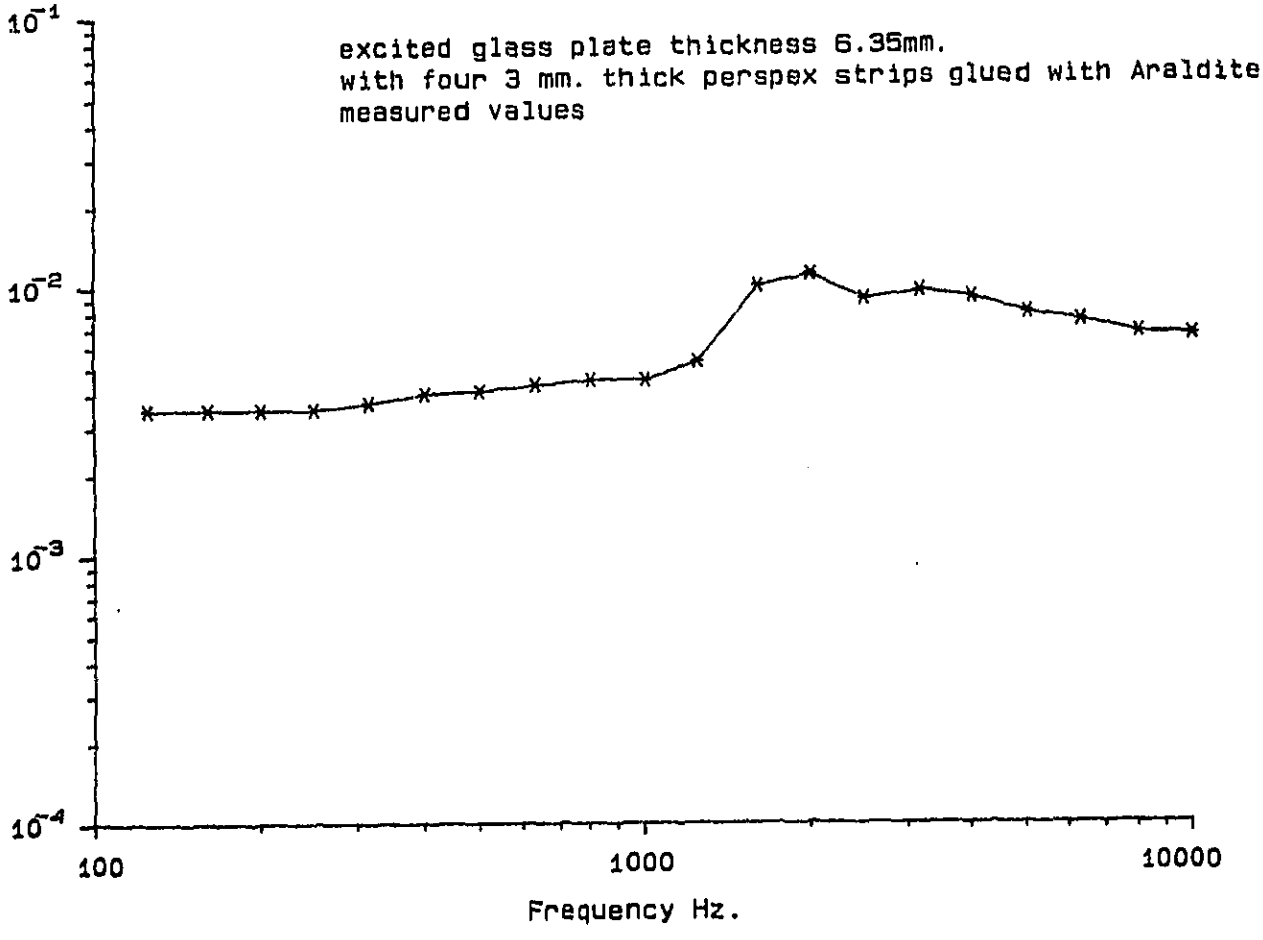

GURE 3.4a The measured excited glass plate loss factor.

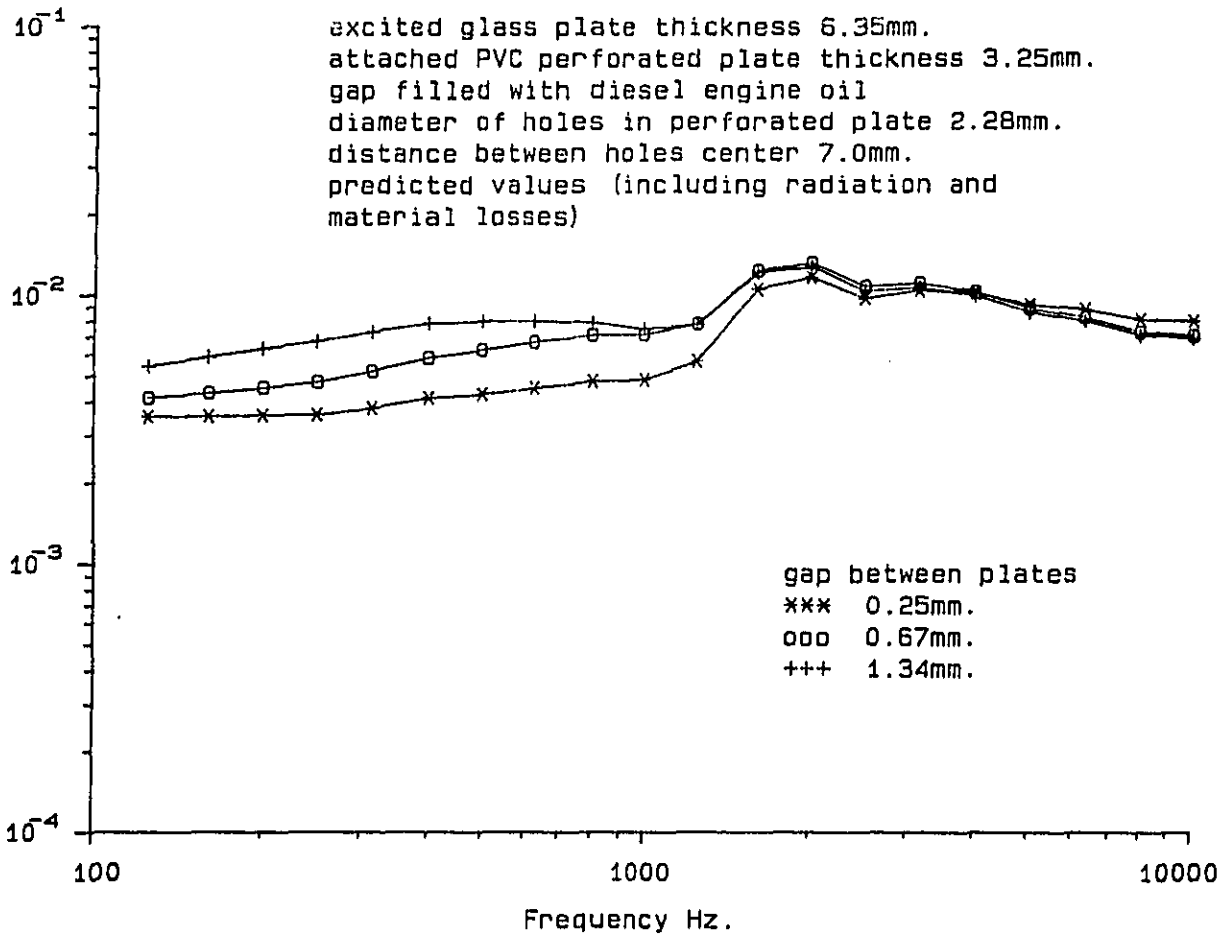

ɪE 3.4b The estimated total loss factor on glass-PVC plates.

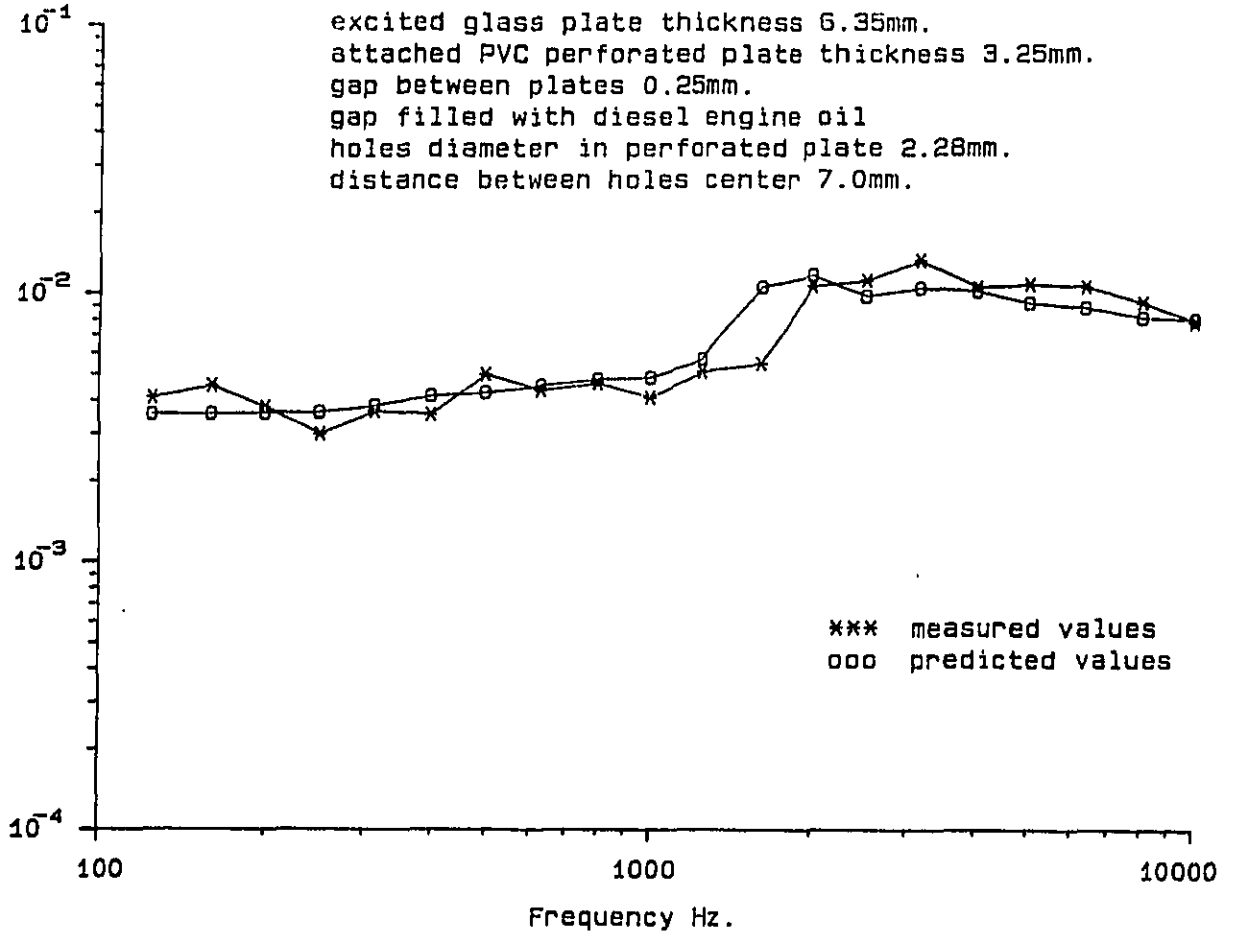

Ξ 3.5a Comparison of the measured and predicted total loss factor on the glass-PVC plates.

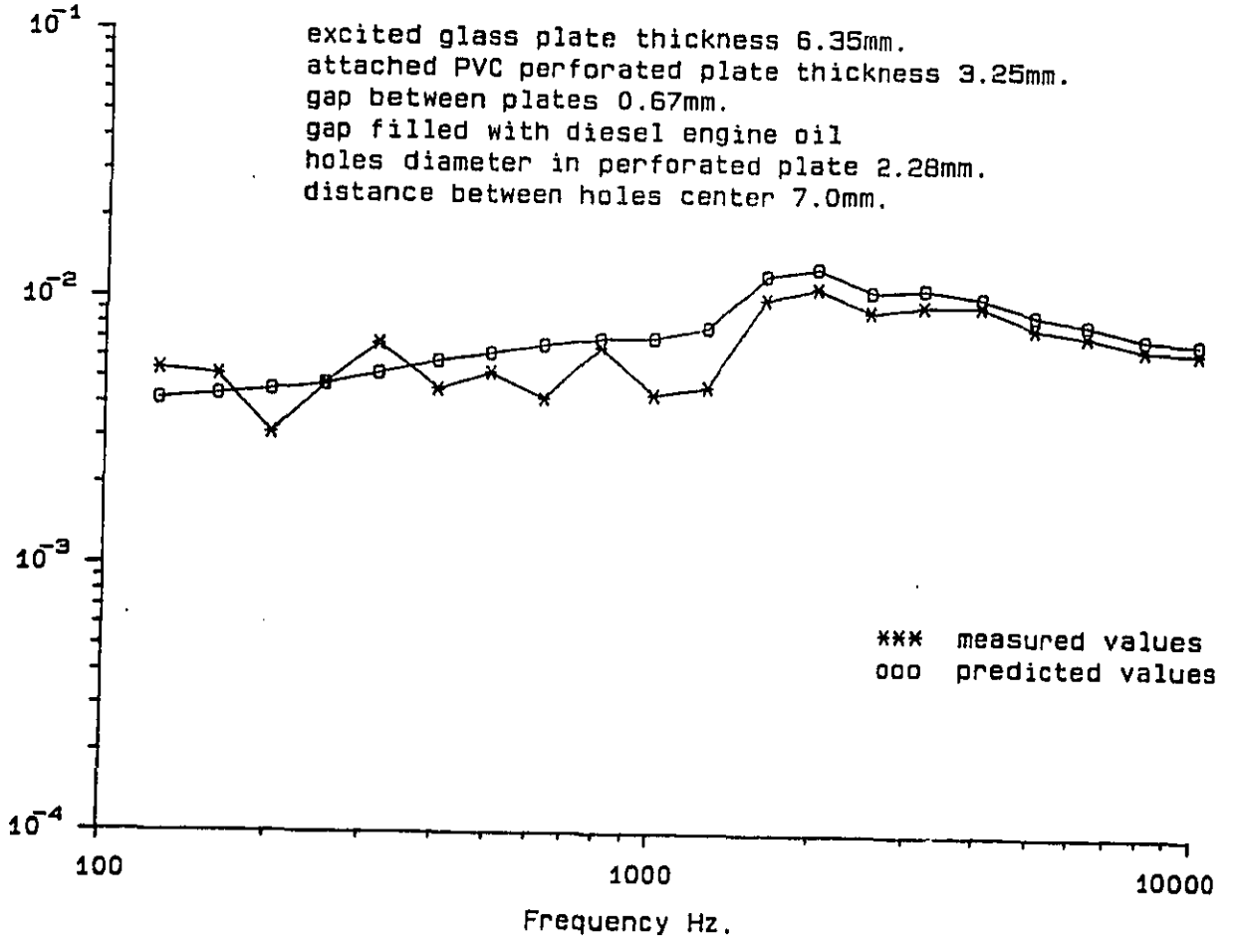

JRE 3.5b Comparison of the measured and predicted total loss factor on the glass-PVC plates.

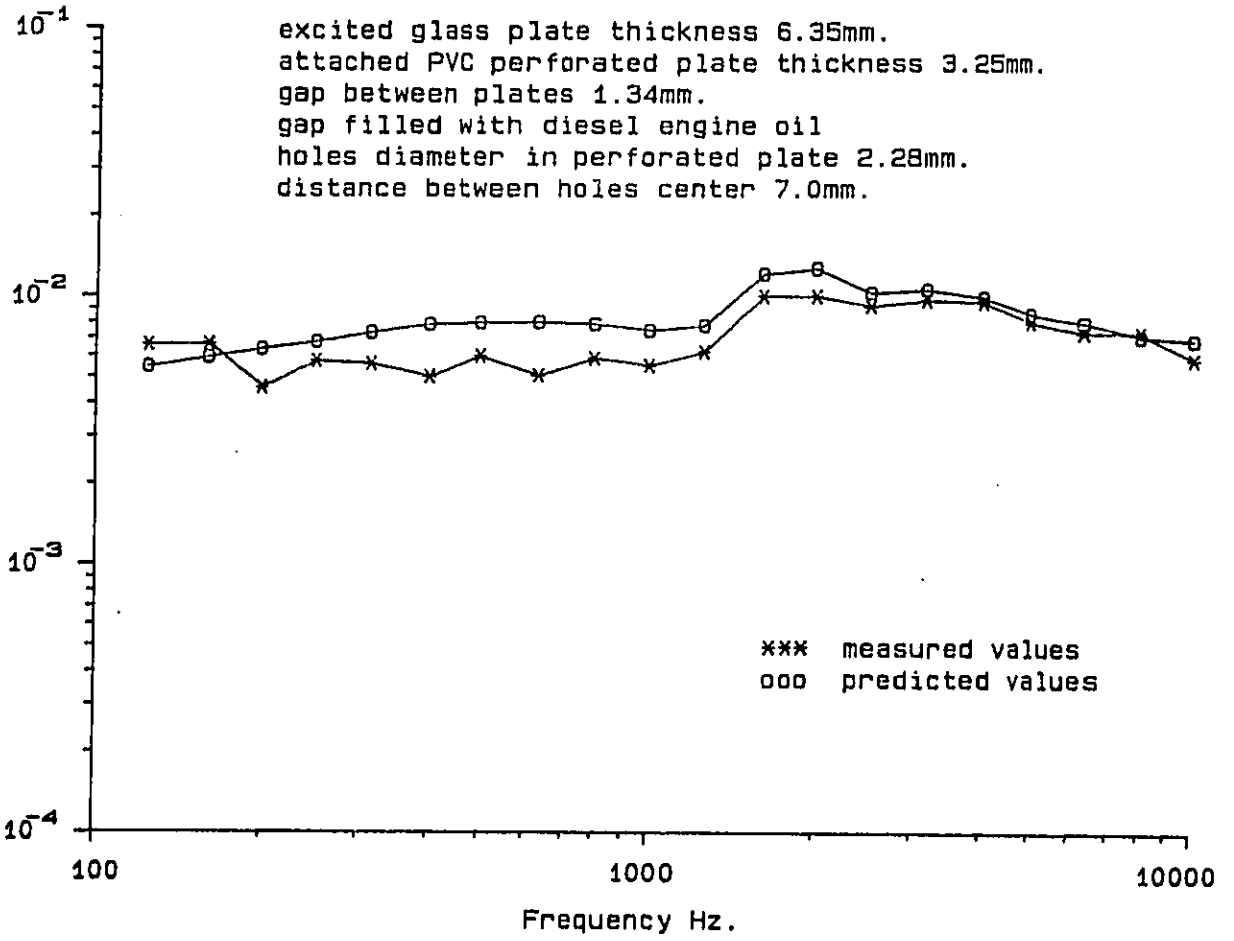

URE 3.5c Comparison of the measured and predicted total loss factor on the glass-PVC plates.

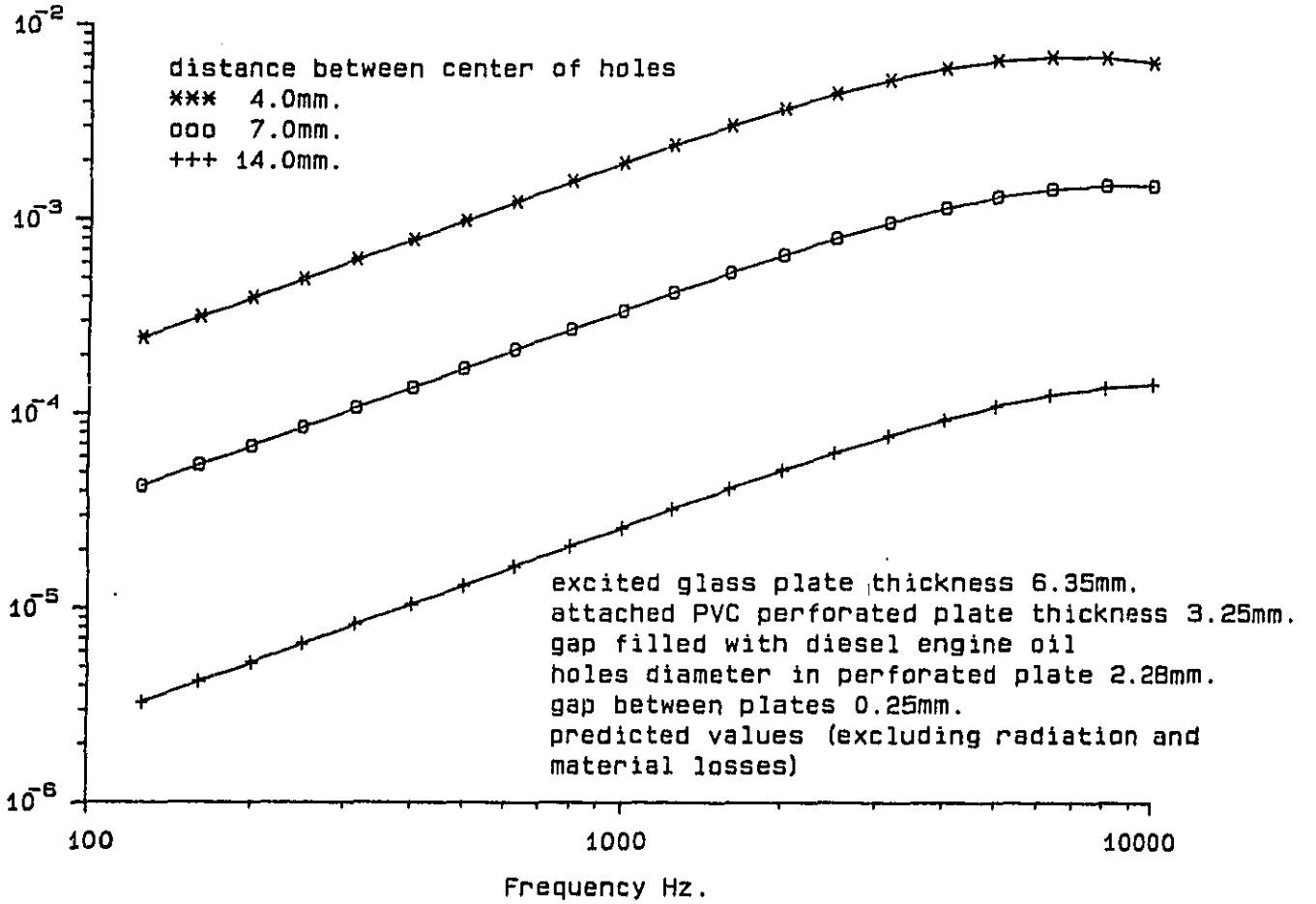

JRE 3.6a The estimated loss factor on glass-PVC plates by varying the distance between centre of holes on the perforated plate.

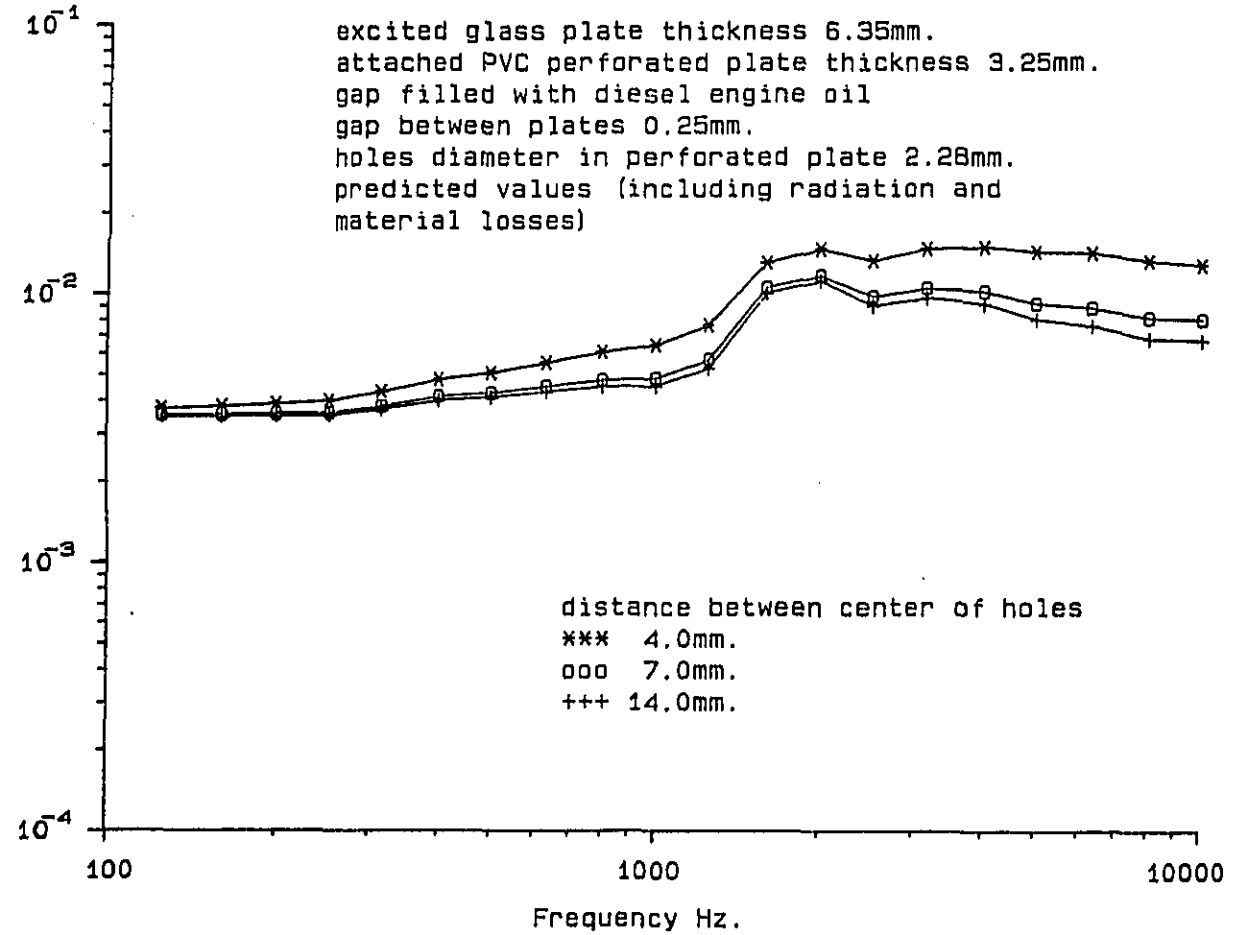

RE 3.6b The estimated total loss factor on glass-PVC plates by varying the distance between centre of holes on the perforated plate.

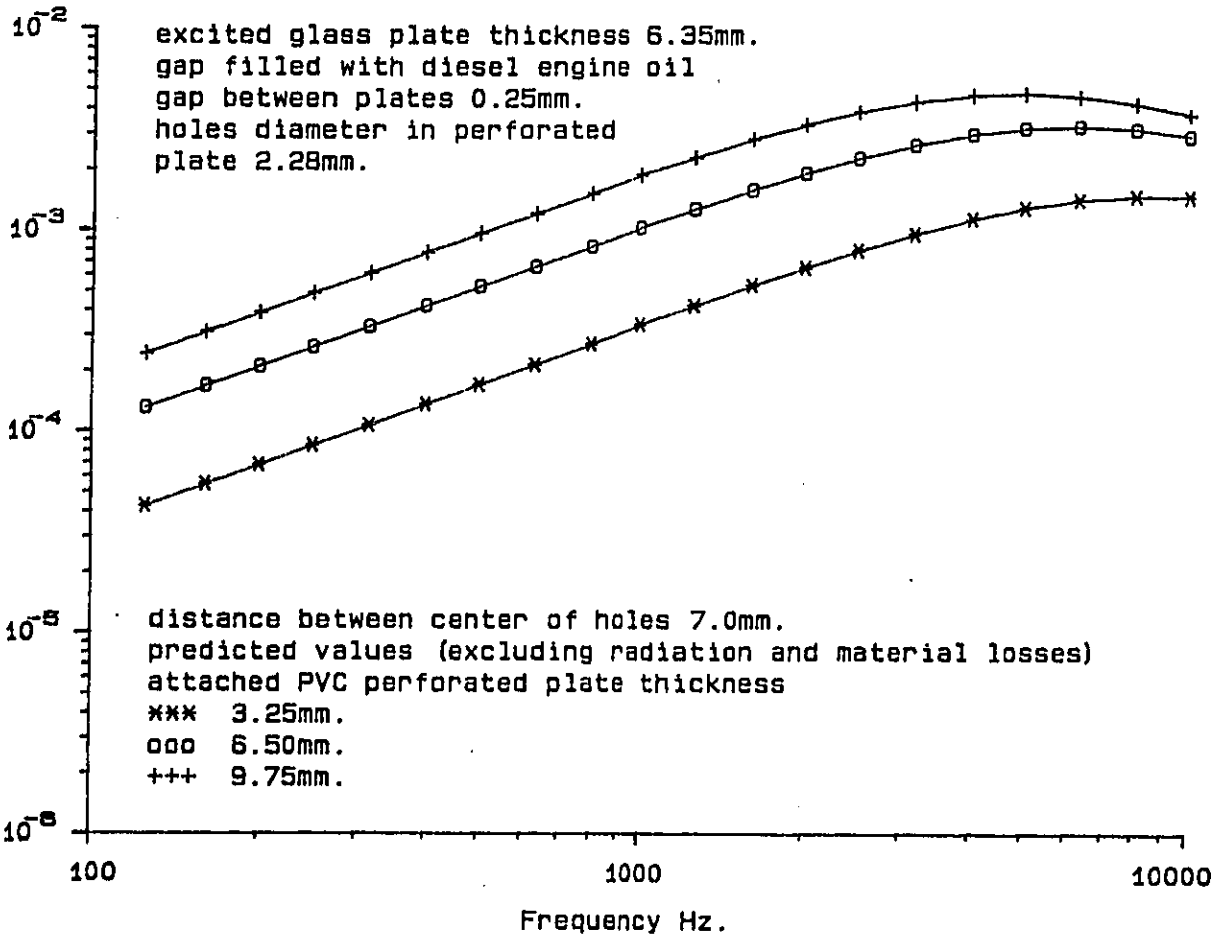

RE 3.7a The estimated loss factor on glass-PVC plates by varying the thickness of the attached plate.

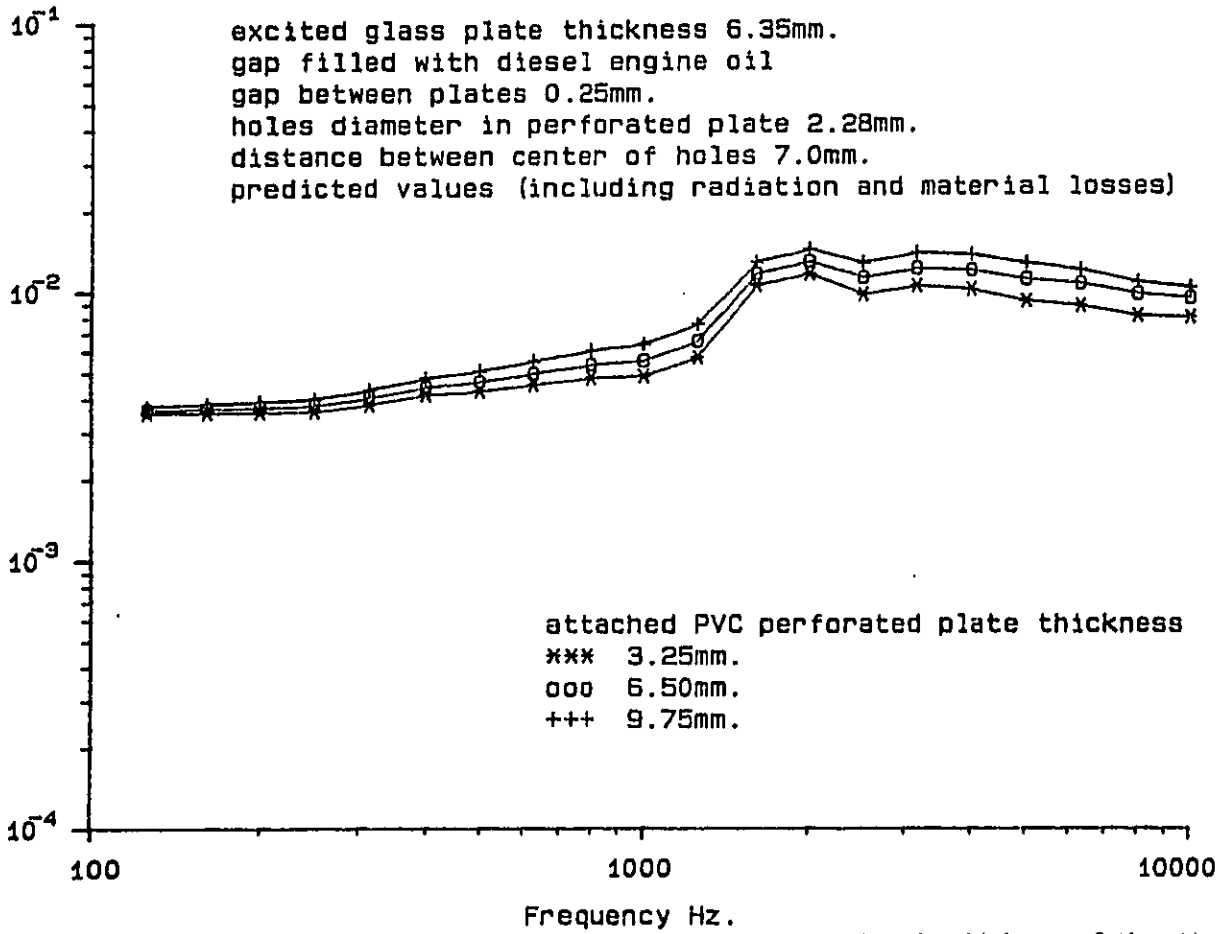

URE 3.7b The estimated total loss factor on glass-PVC plates by varying the thickness of the attached plate.

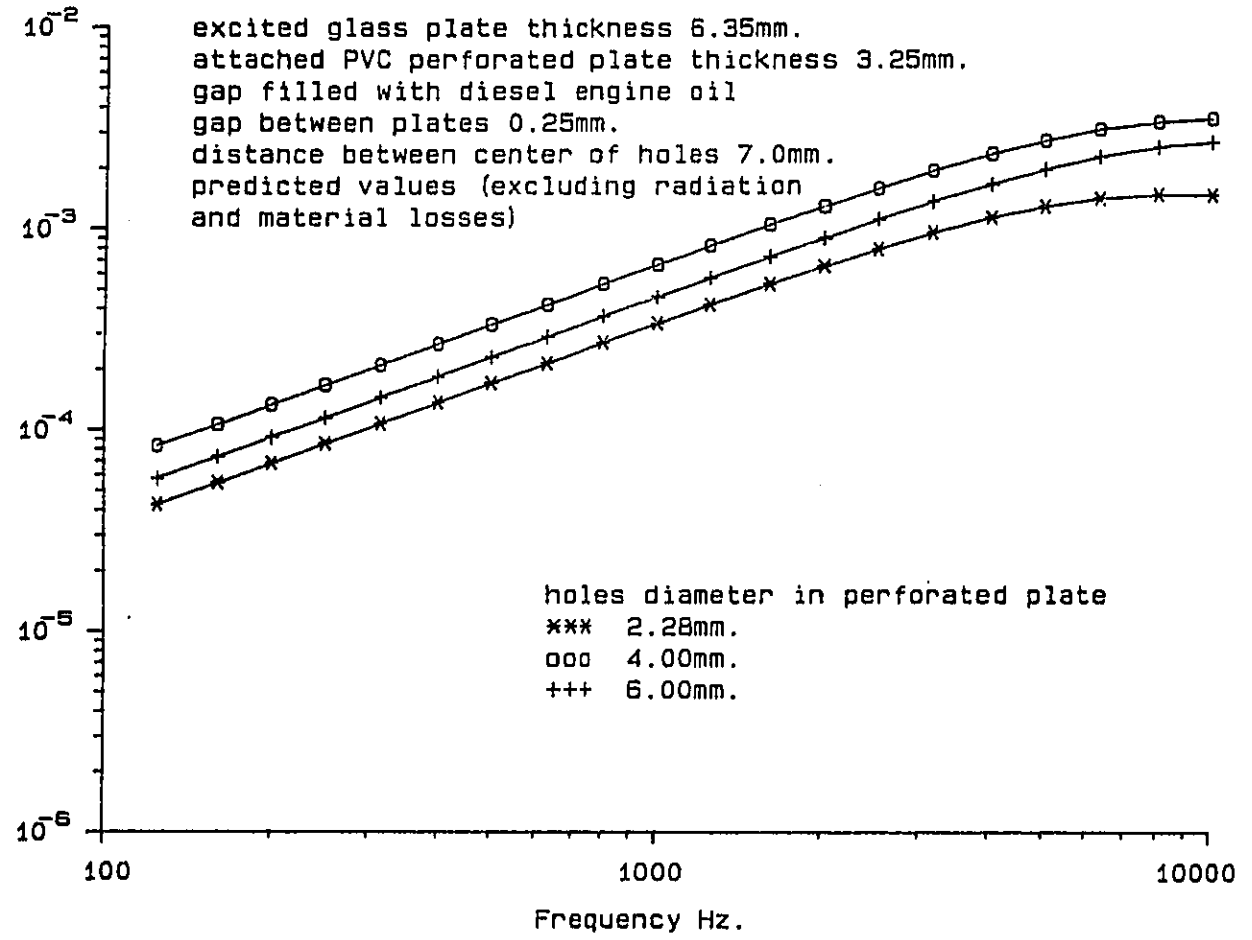

RE 3.8a The estimated loss factor on glass-PVC plates by varying the perforated plate holes diameter.

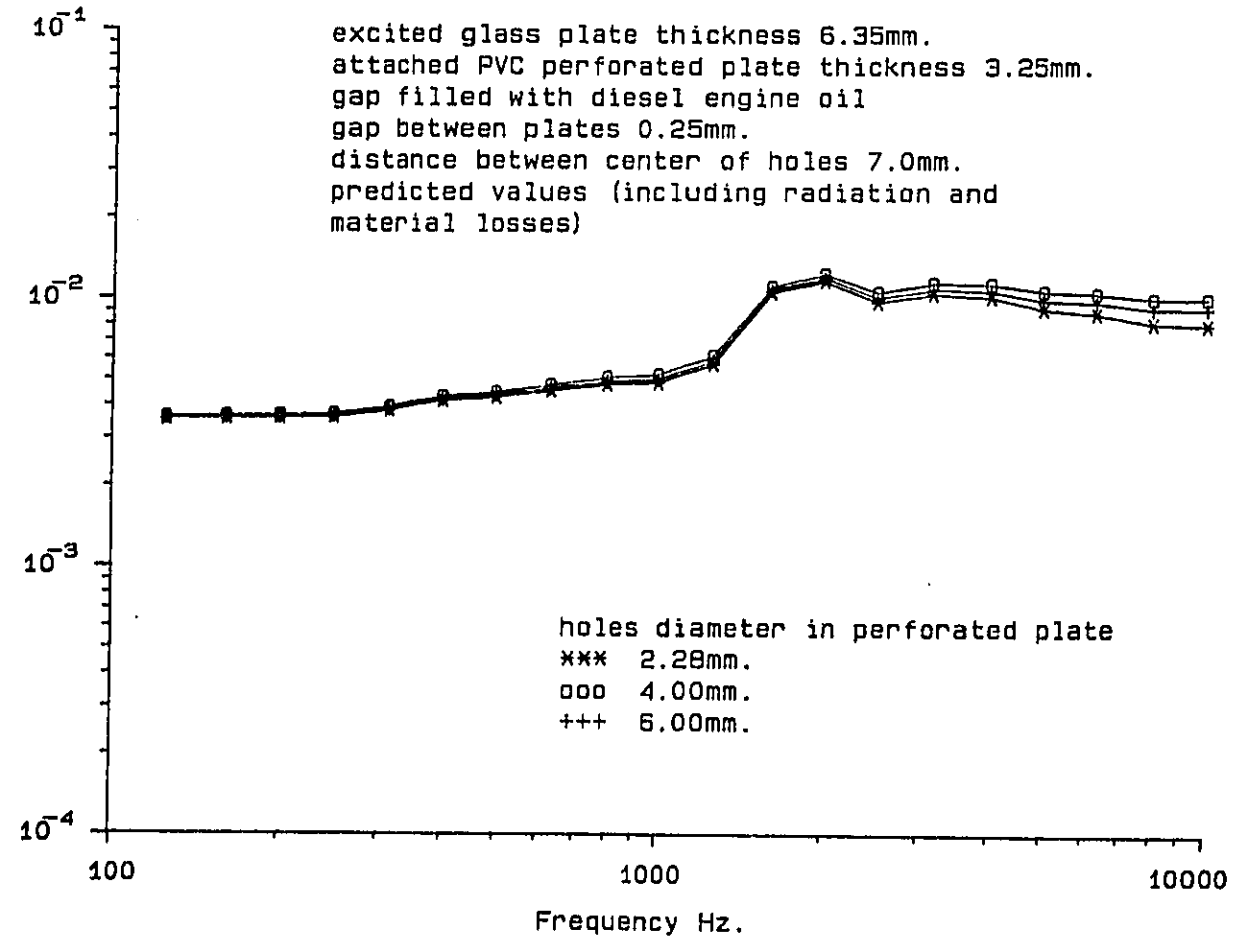

URE 3.8b The estimated total loss factor on glass-PVC plates by varying the perforated plate holes diameter.

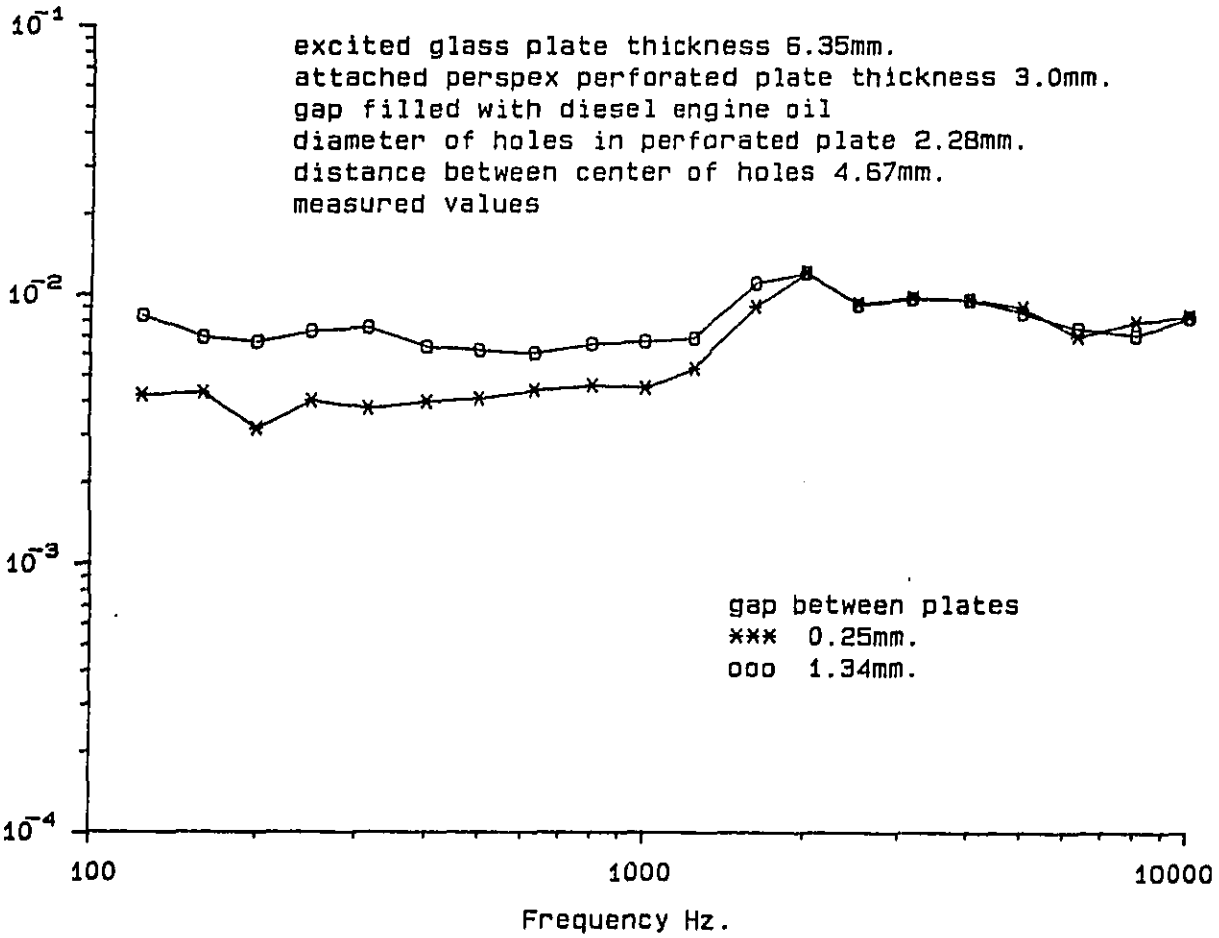

E 3.9 The measured loss factor on glass-perspex plates.

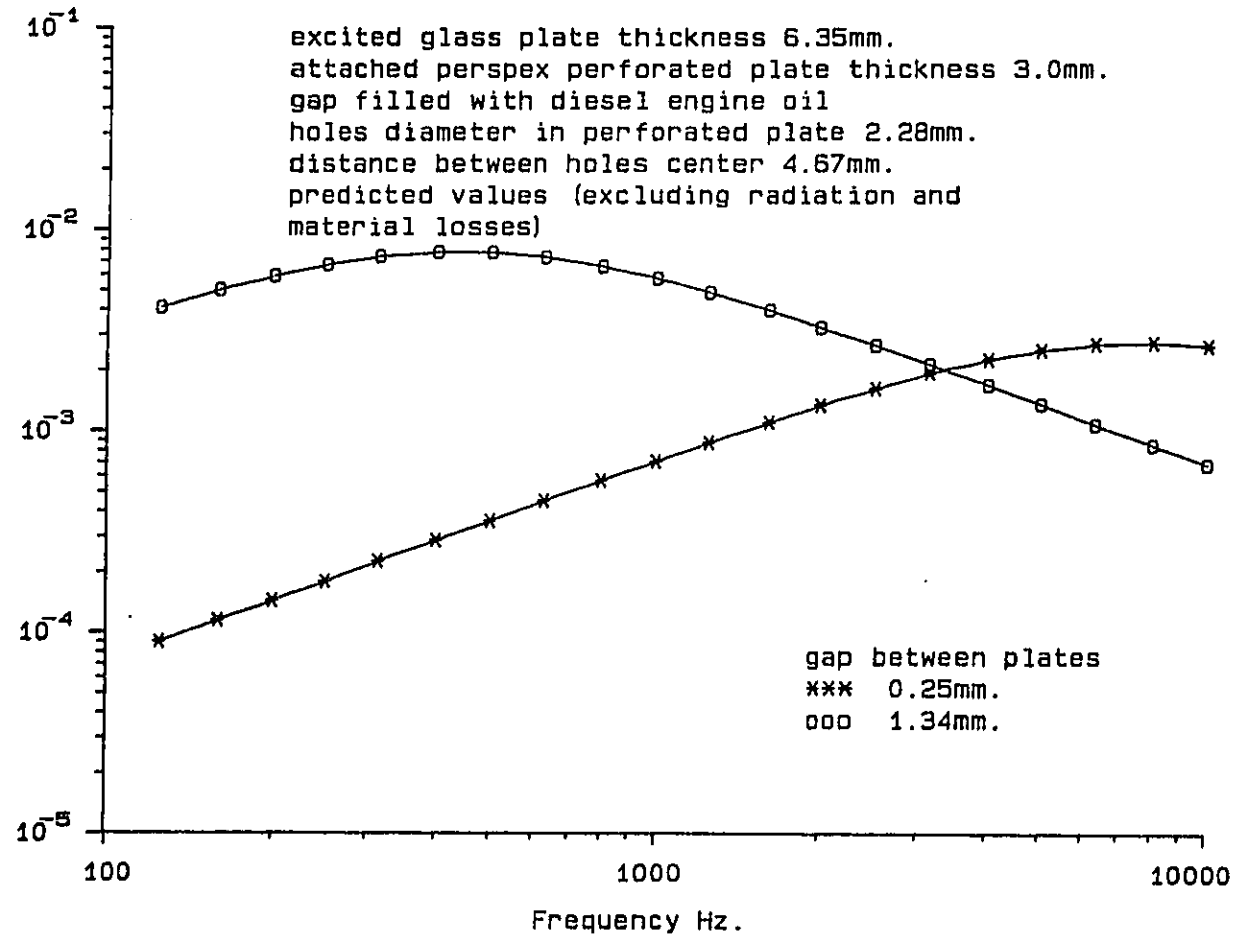

RE 3.10 The estimated loss factor of glass-perspex plates.

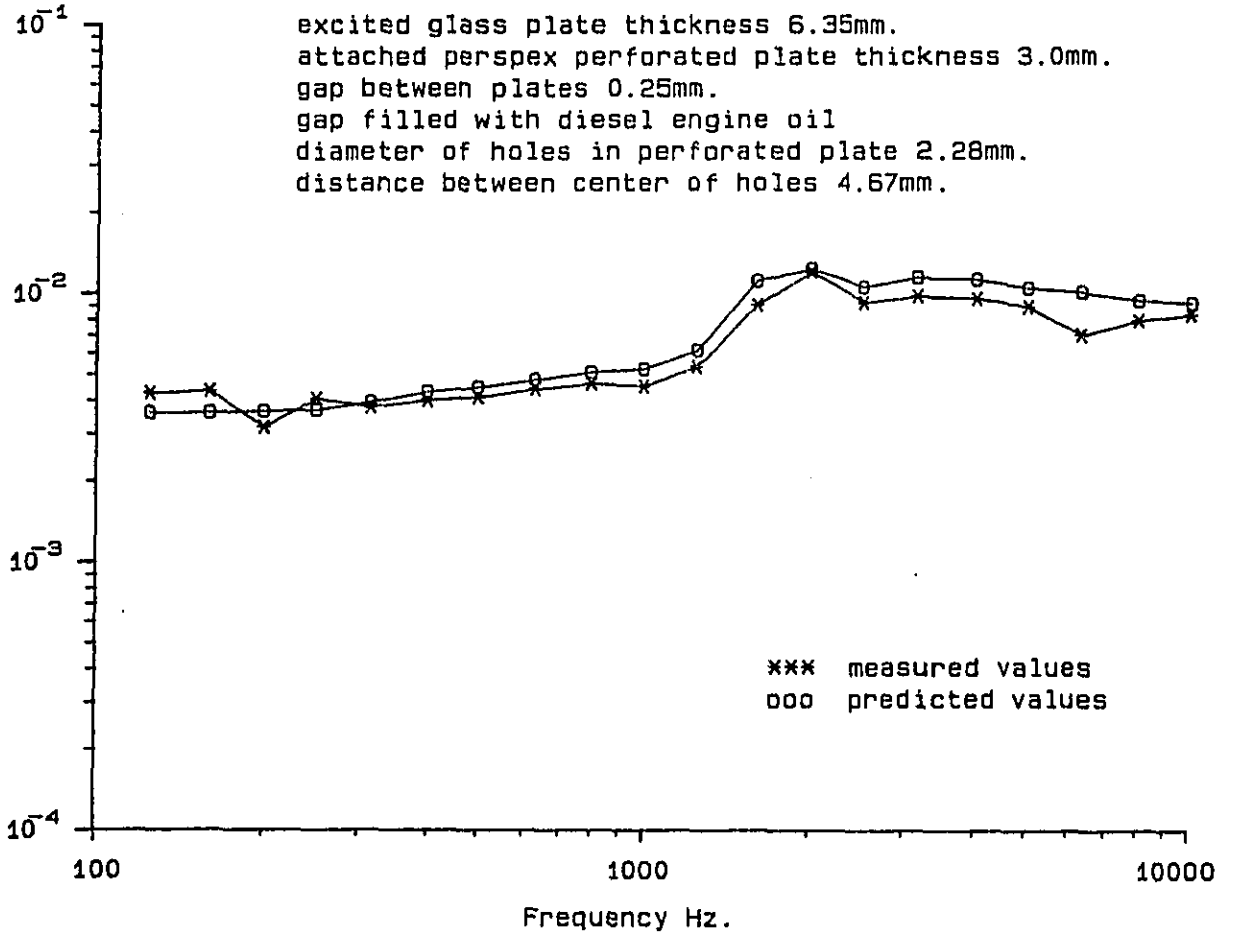

JRE 3.11a Comparison of the measured and predicted total loss factor on the glass-perspex plates.

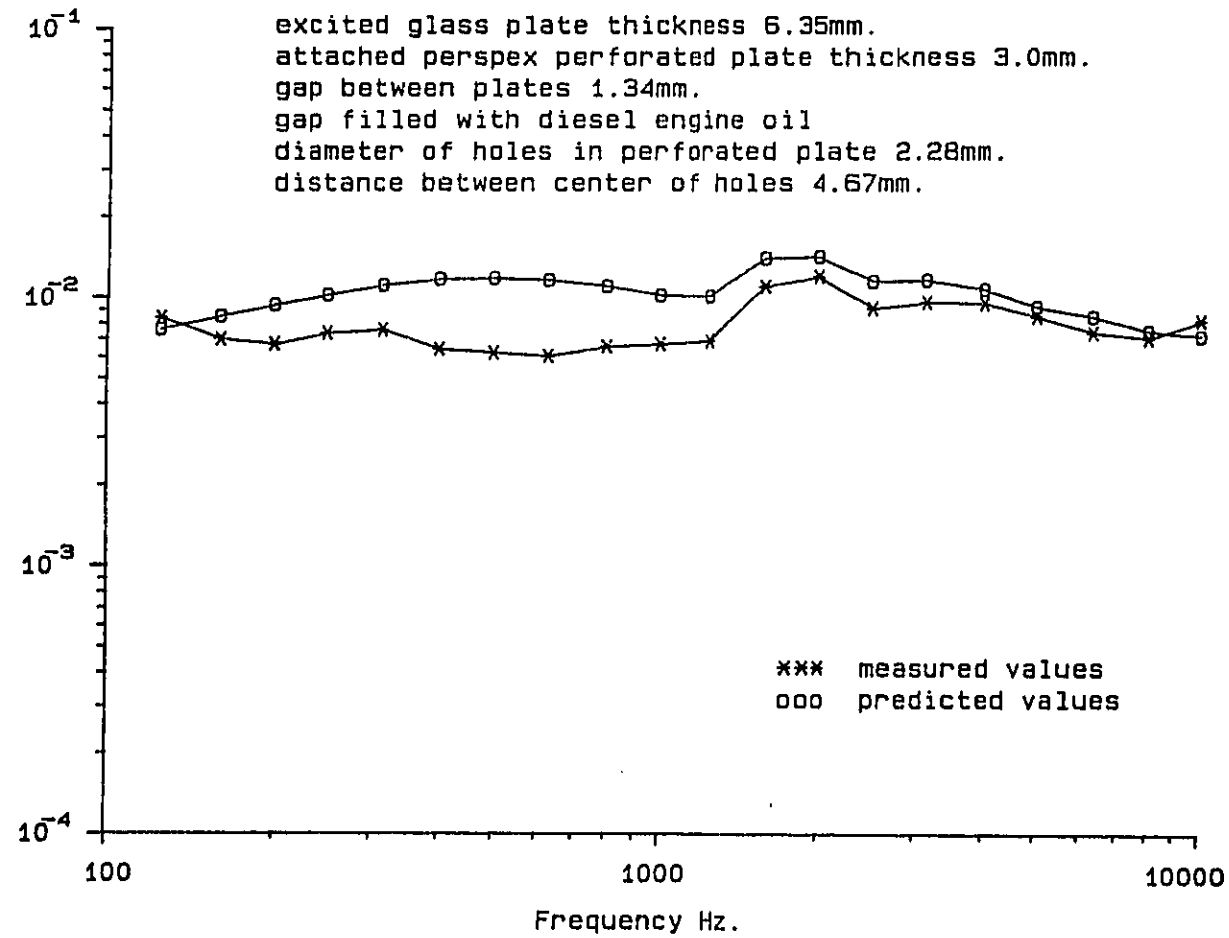

RE 3.11b Comparison of the measured and predicted total loss factor on the glass-perspex plates.

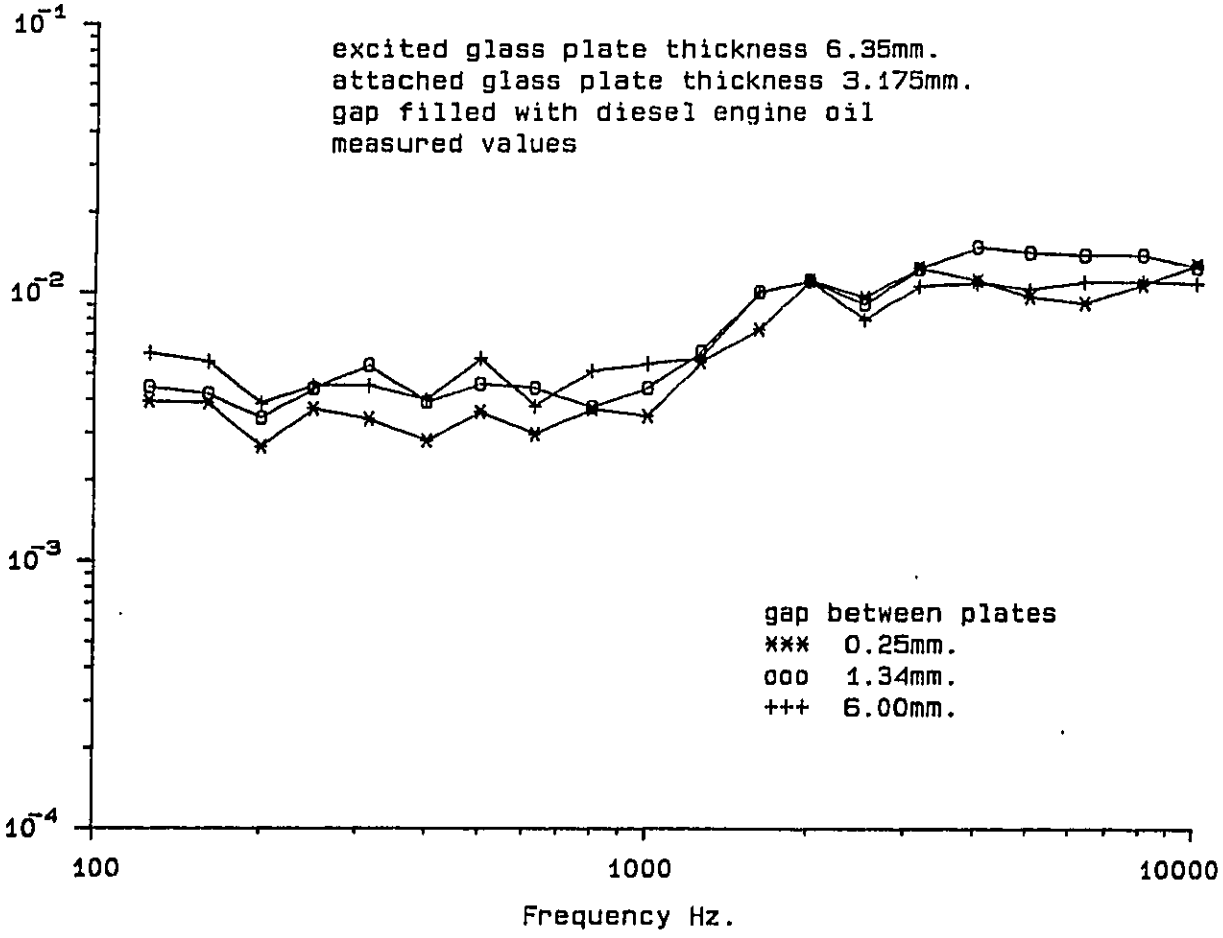

URE 3.12 The measured loss factor on glass-glass plates.

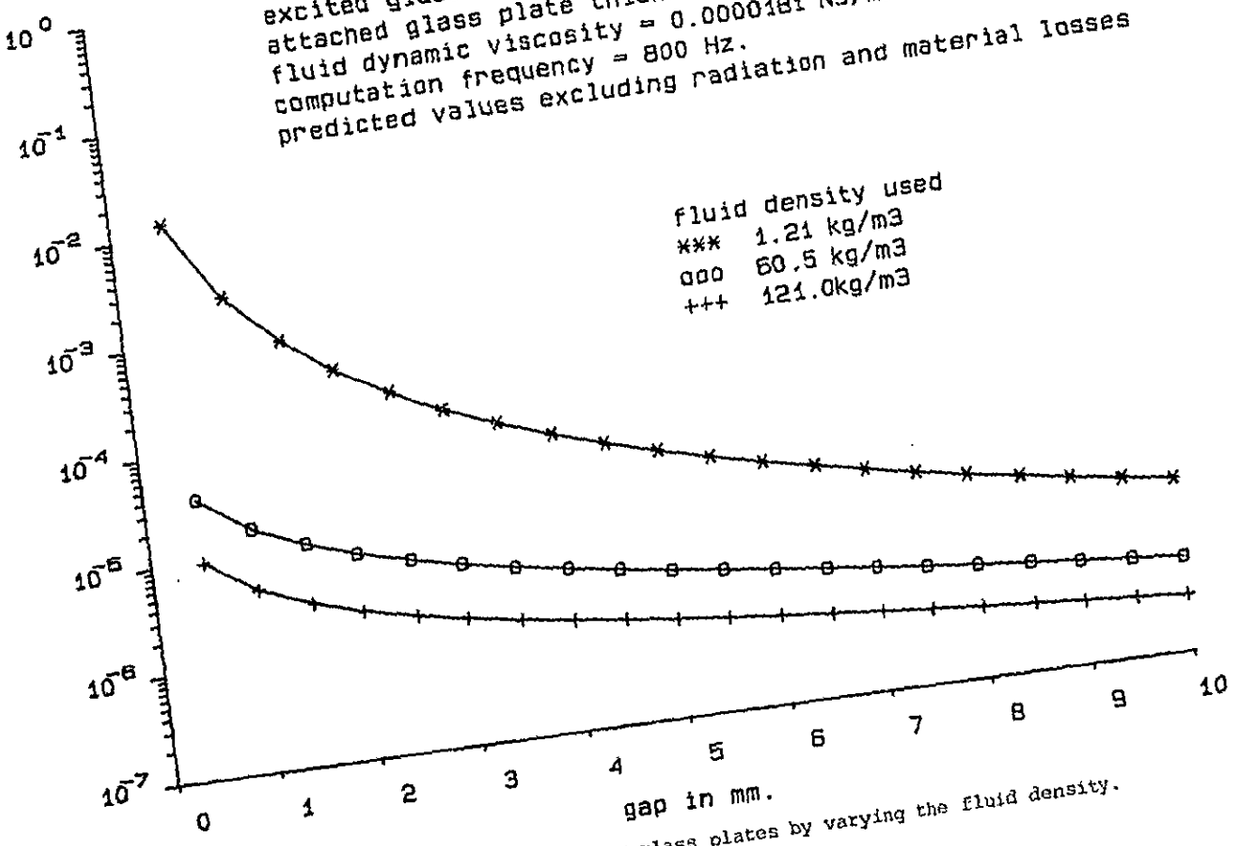

RE 3.13a The estimated loss factor on glass-glass plates by varying the fluid density.

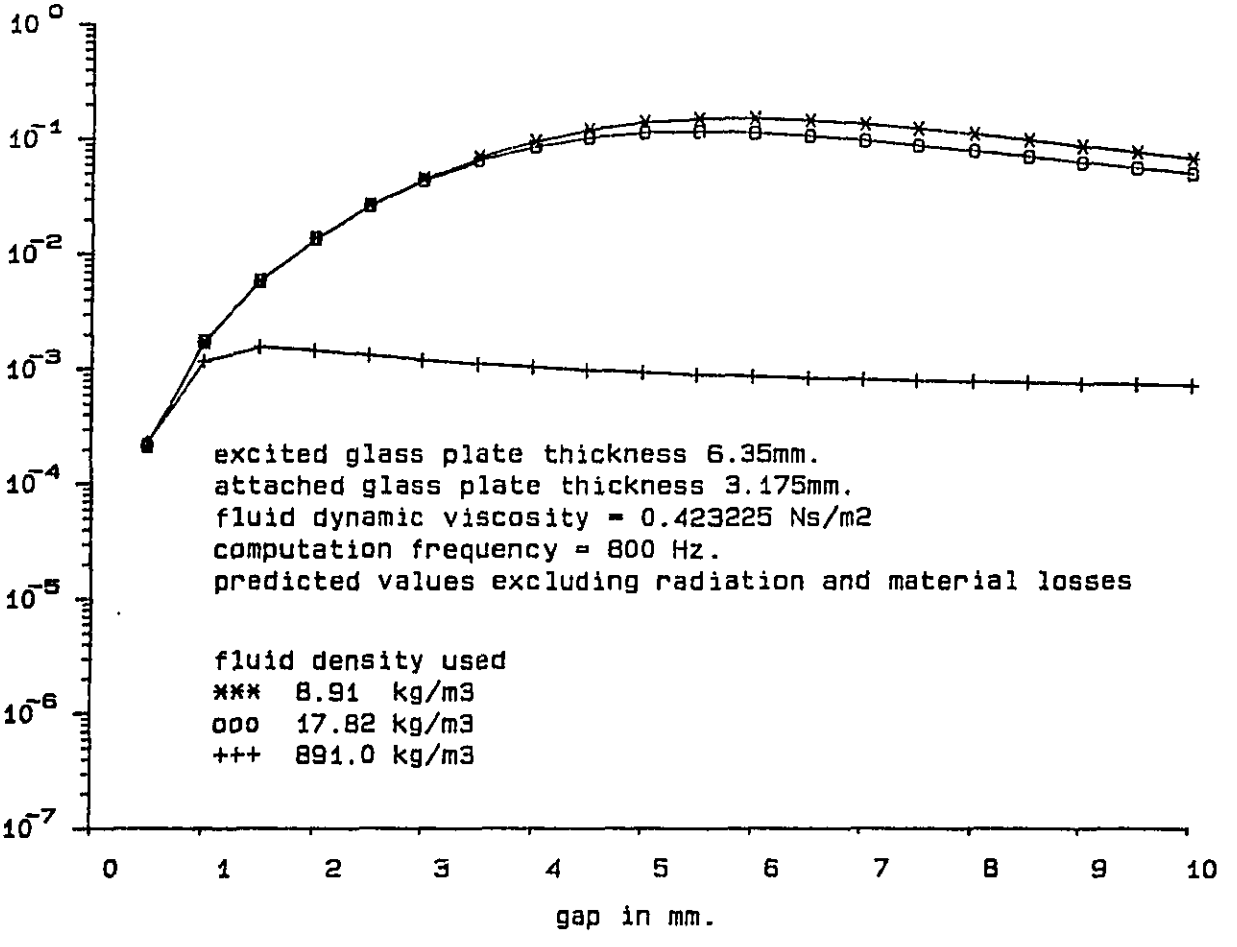

RE 3.13b The estimated loss factor on glass-glass plates by varying the fluid density.

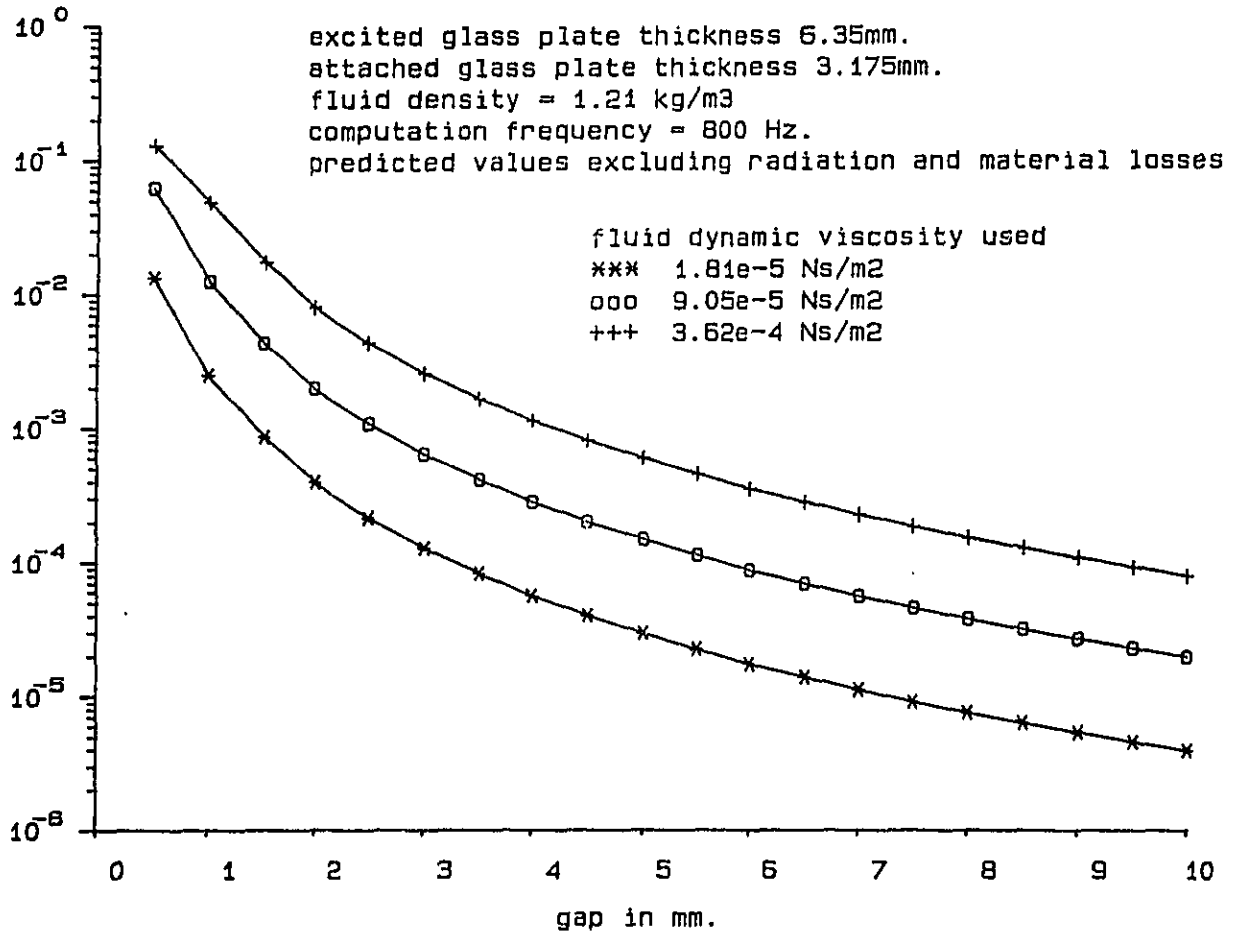

JRE 3.14a The estimated loss factor on glass-glass plates by varying the fluid dynamic viscosity.

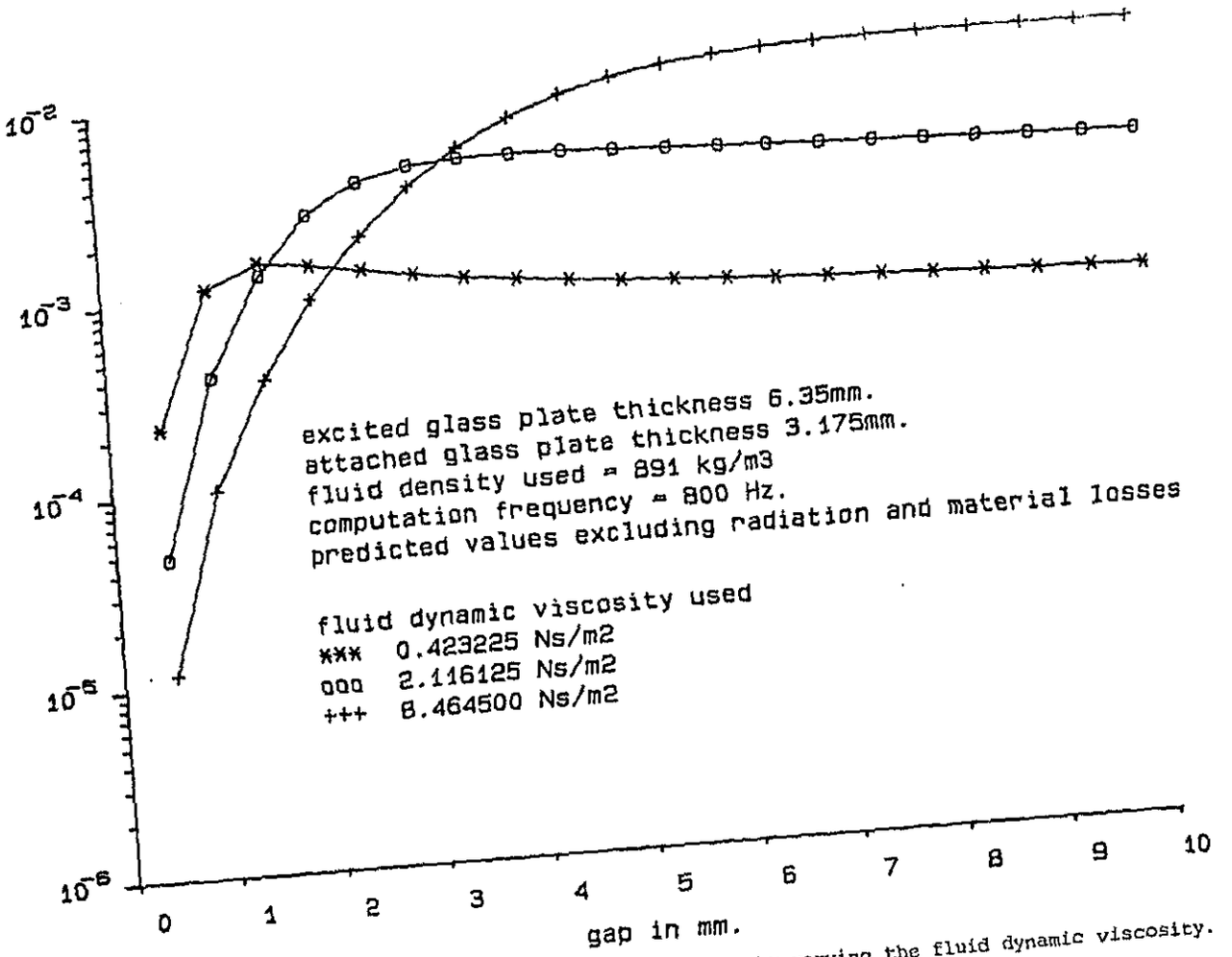

RE 3.14b The estimated loss factor on glass-glass plates by varying the fluid dynamic viscosity.

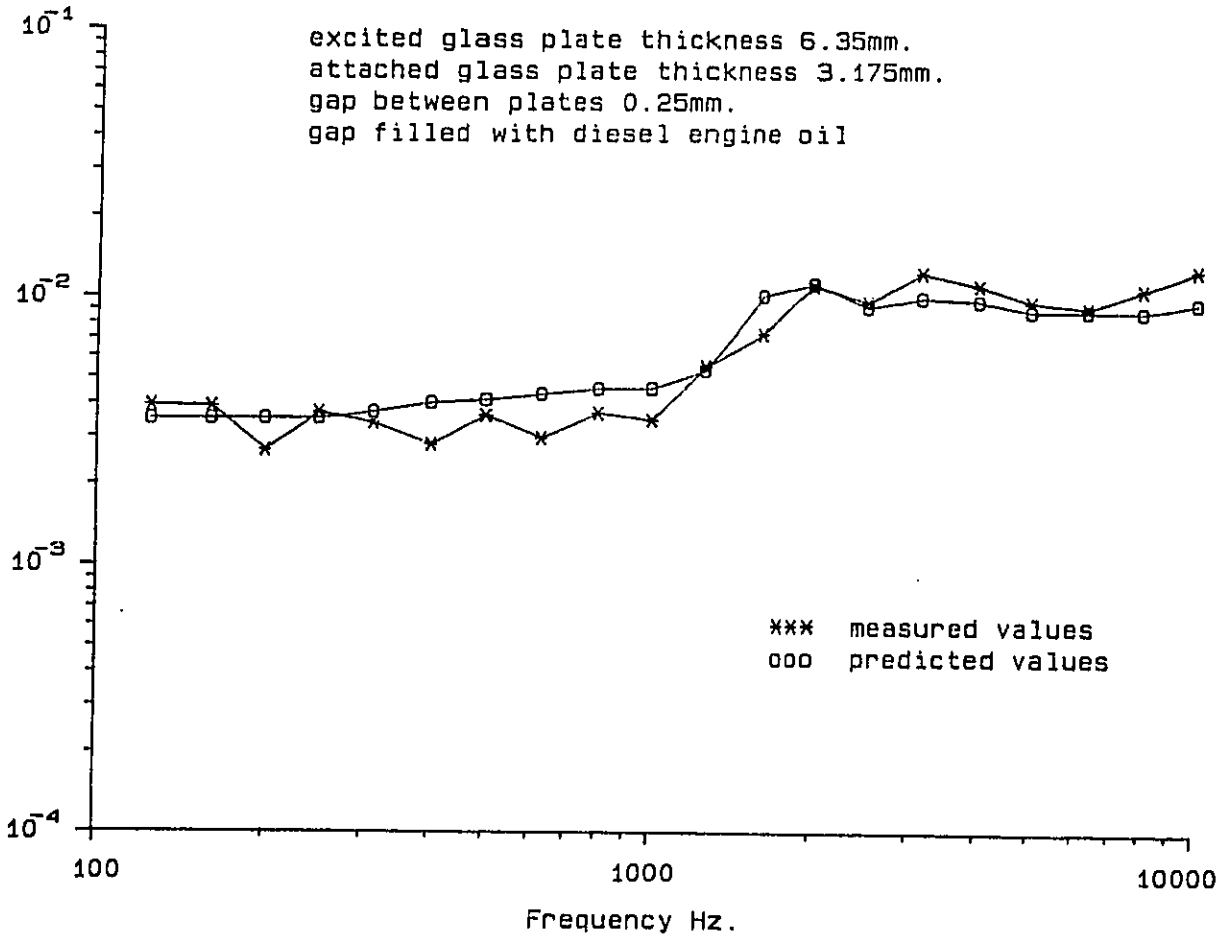

URE 3.15a Comparison of the measured and predicted total loss factor on glass-glass plates.

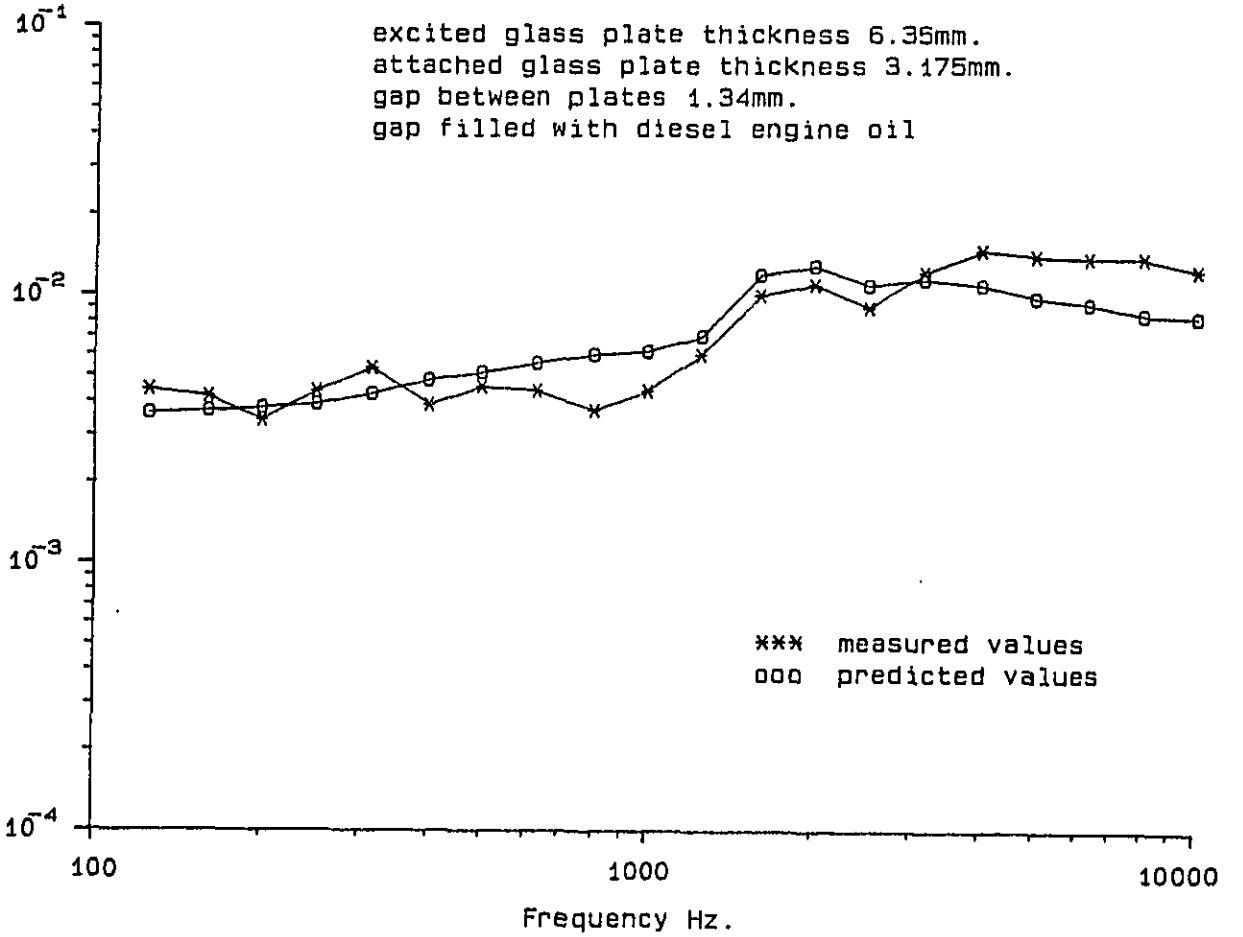

JRE 3.15b Comparison of the measured and predicted total loss factor on glass-glass plates.

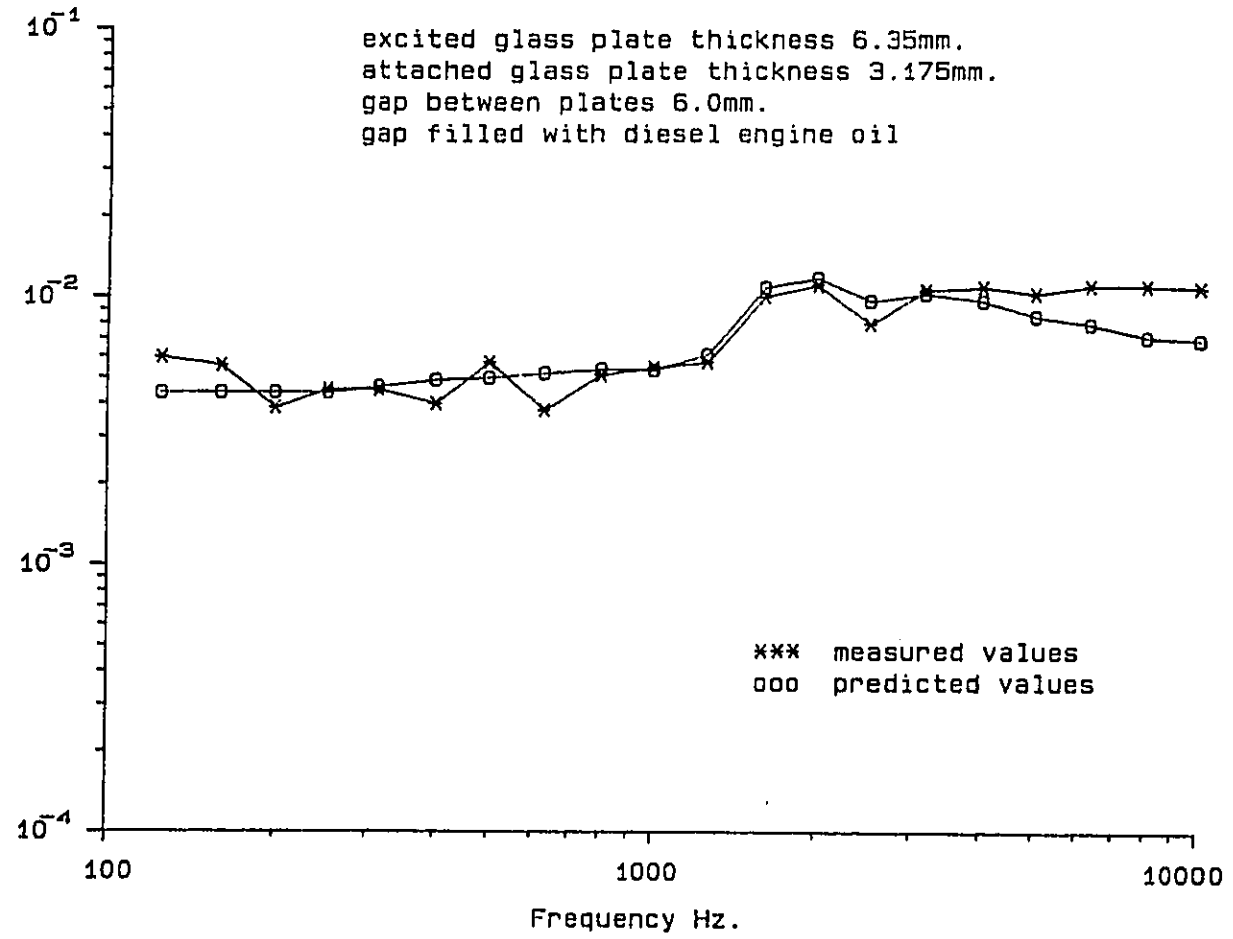

RE 3.15c Comparison of the measured and predicted total loss factor on glass-glass plates.

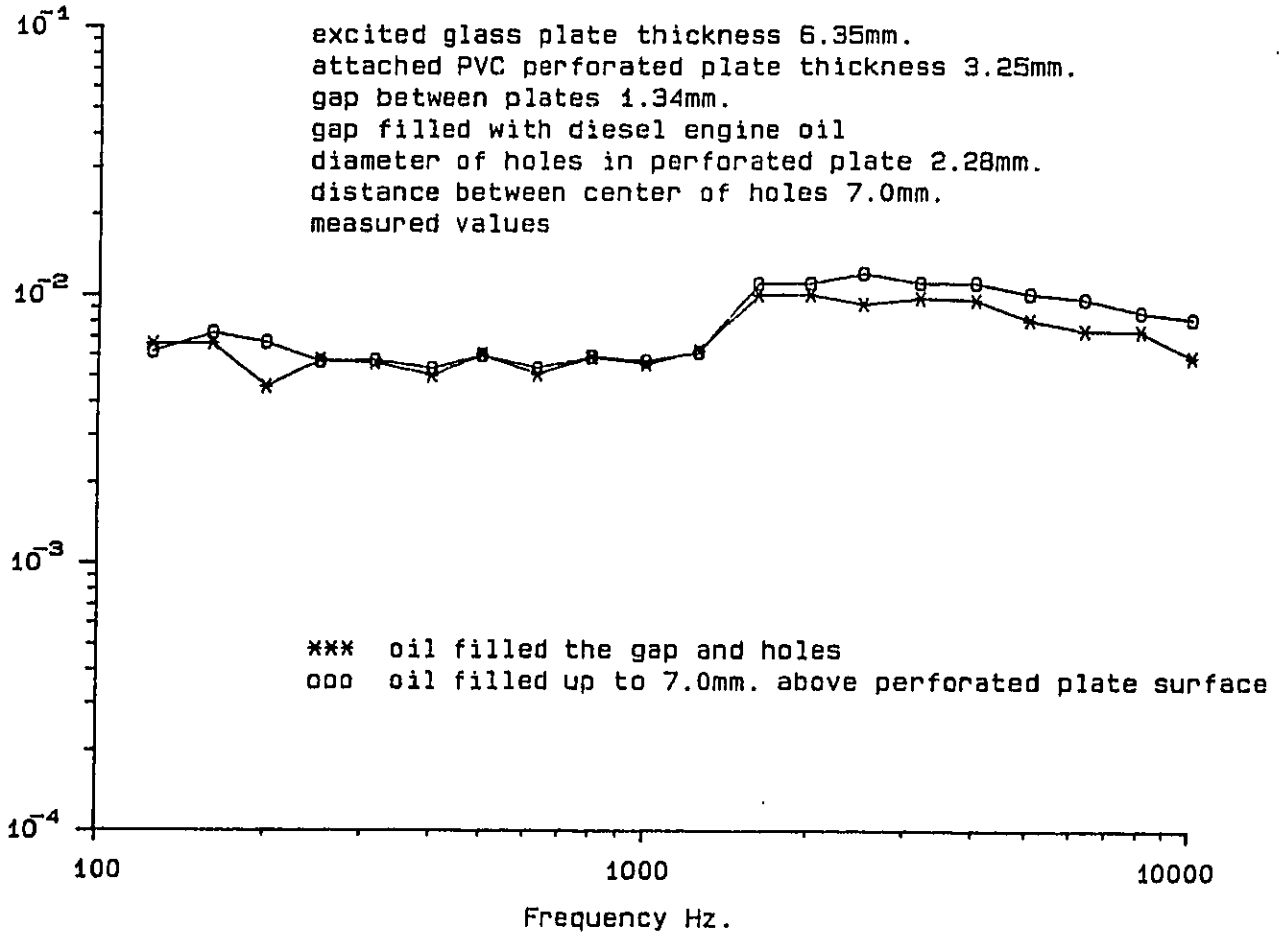

RE 3.16 Comparison of the measured loss factor with and without the oil above the PVC perforated plate.

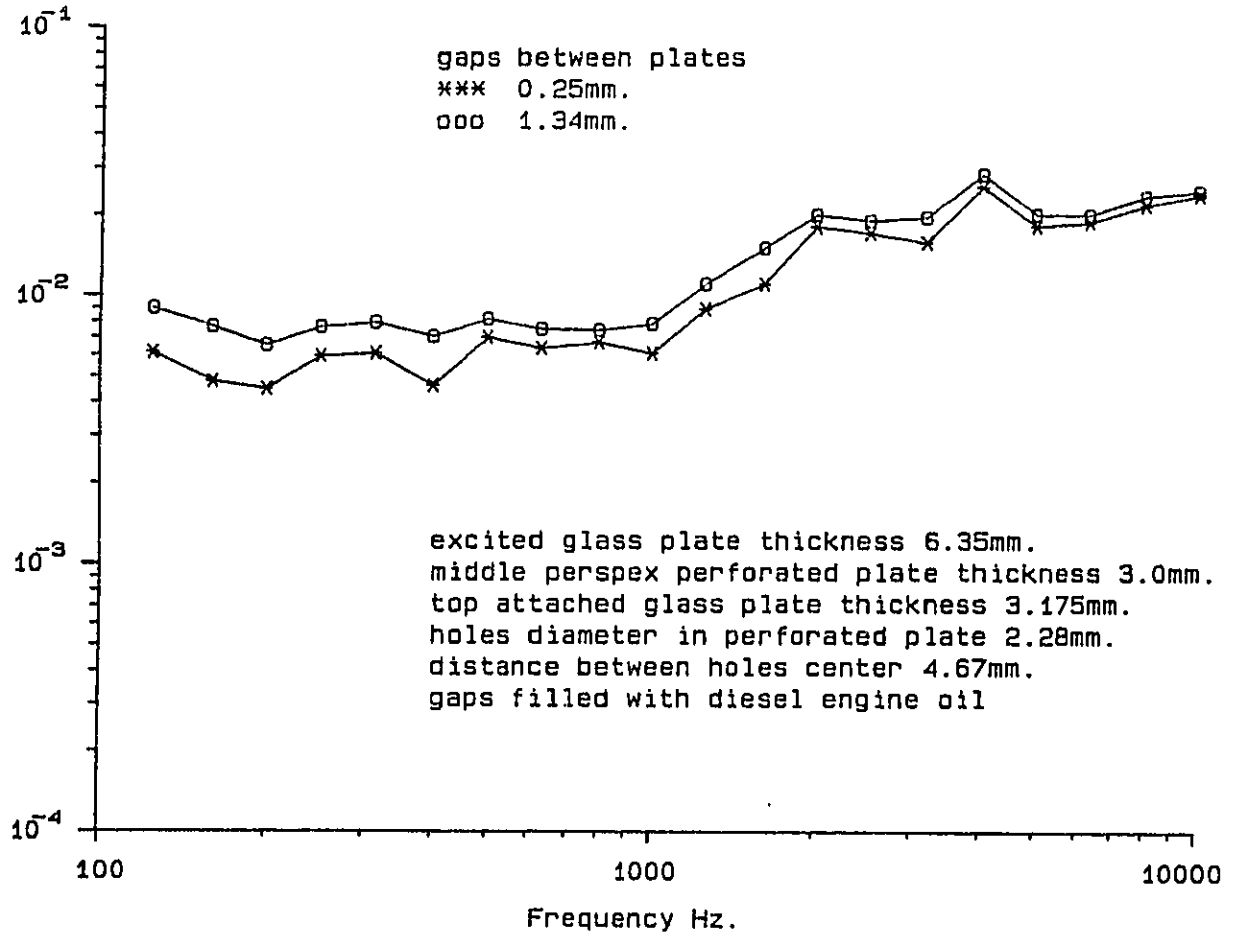

RE 3.17 The measured loss factor on glass-perspex-glass plates.

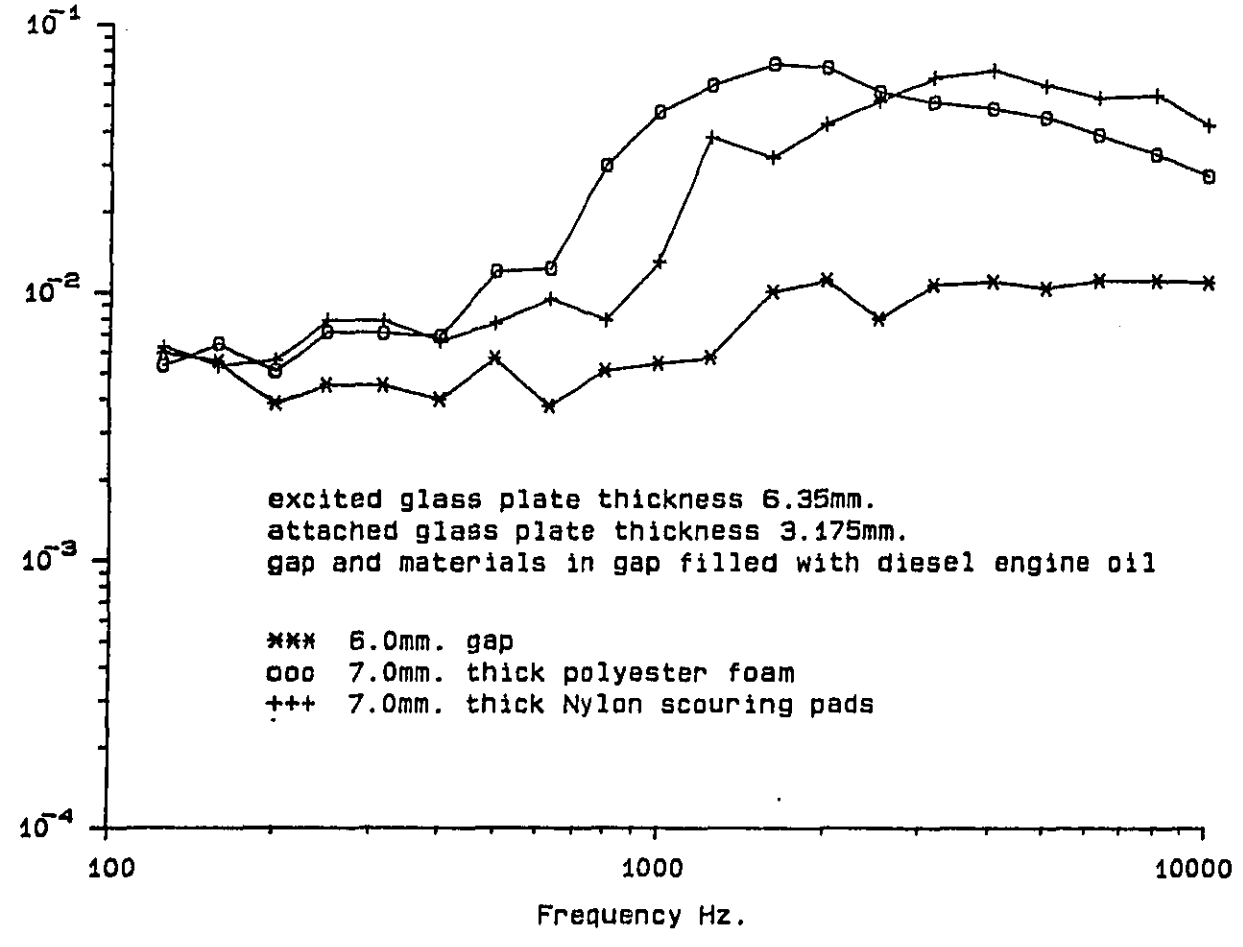

tE 3.18 The measured loss factor on glass-glass plates with different materials in the oil layer.

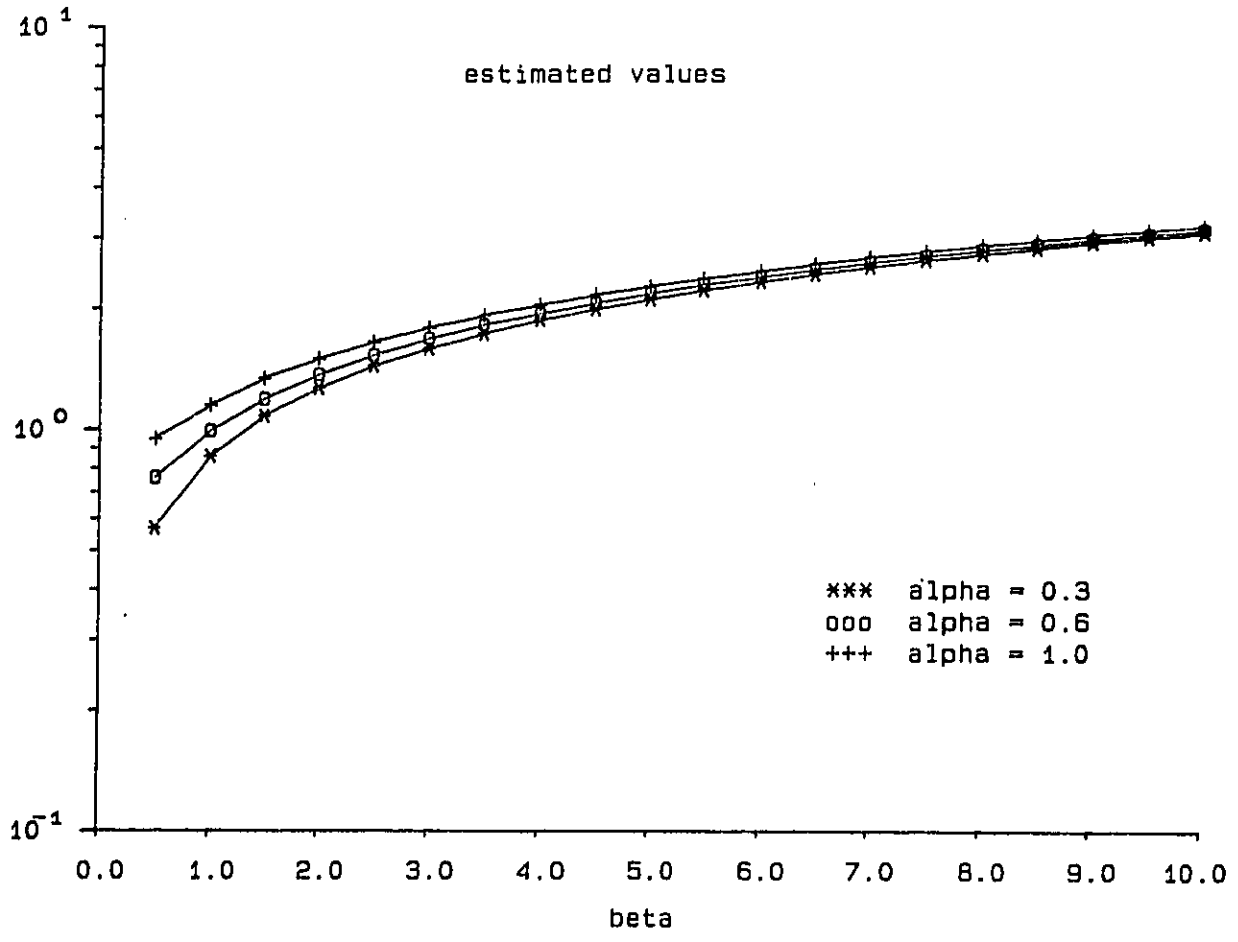

RE 4.1 The estimated maximum loss factor versus α by varying β.

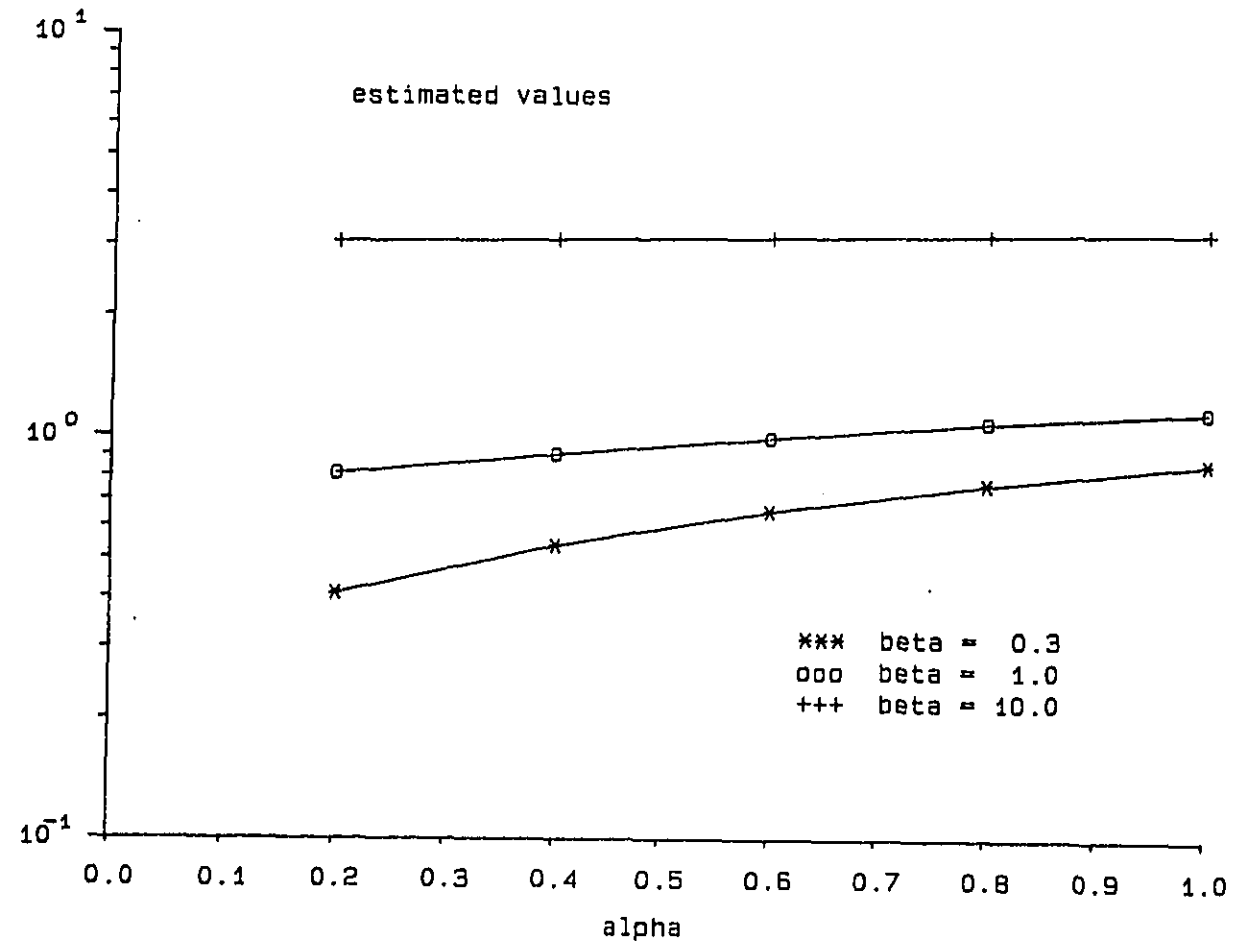

RE 4.2 The estimated maximum loss factor versus β by varying α.

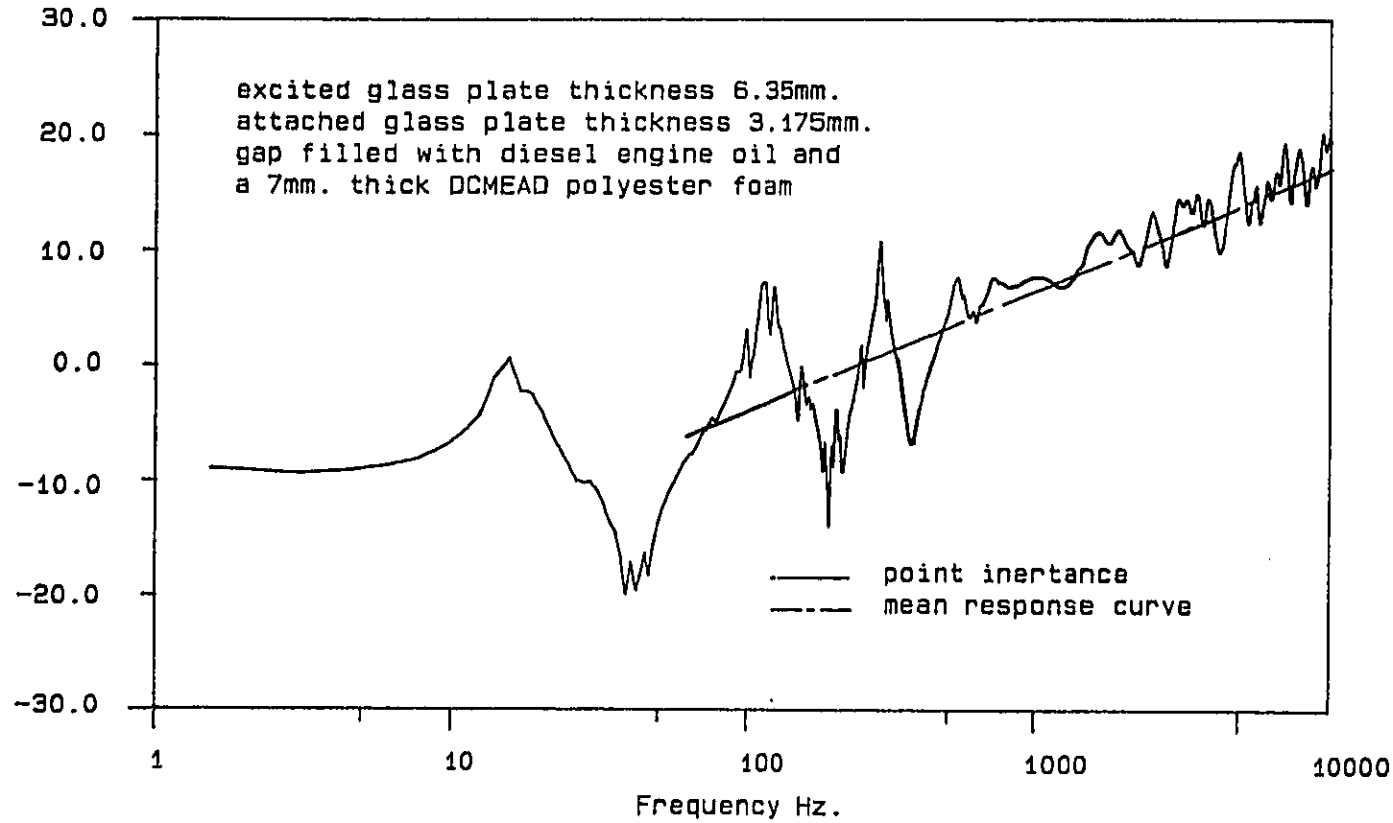

RE 5.1 The point inertance measurement on plates with foam layer.

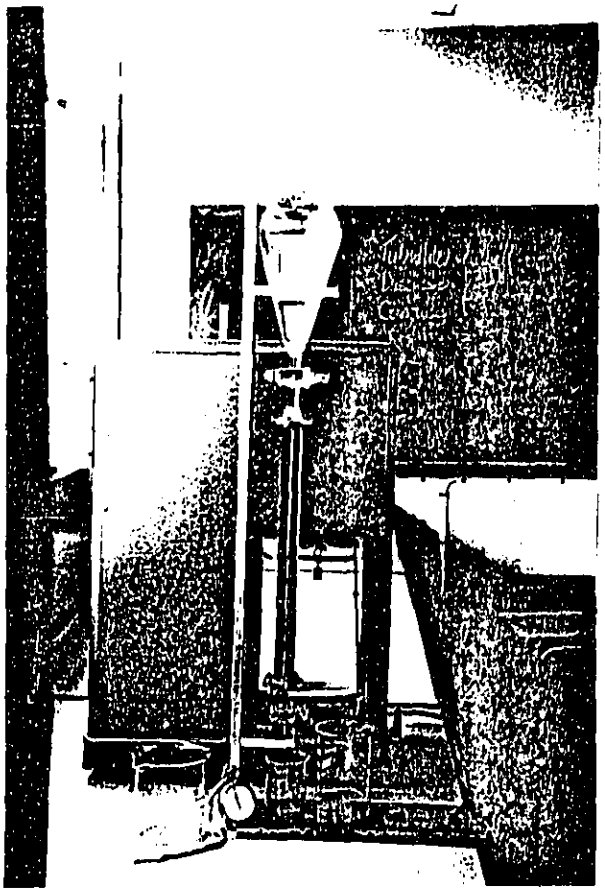

FIGURE 5.2 The apparatus for the flow resistance measurement.

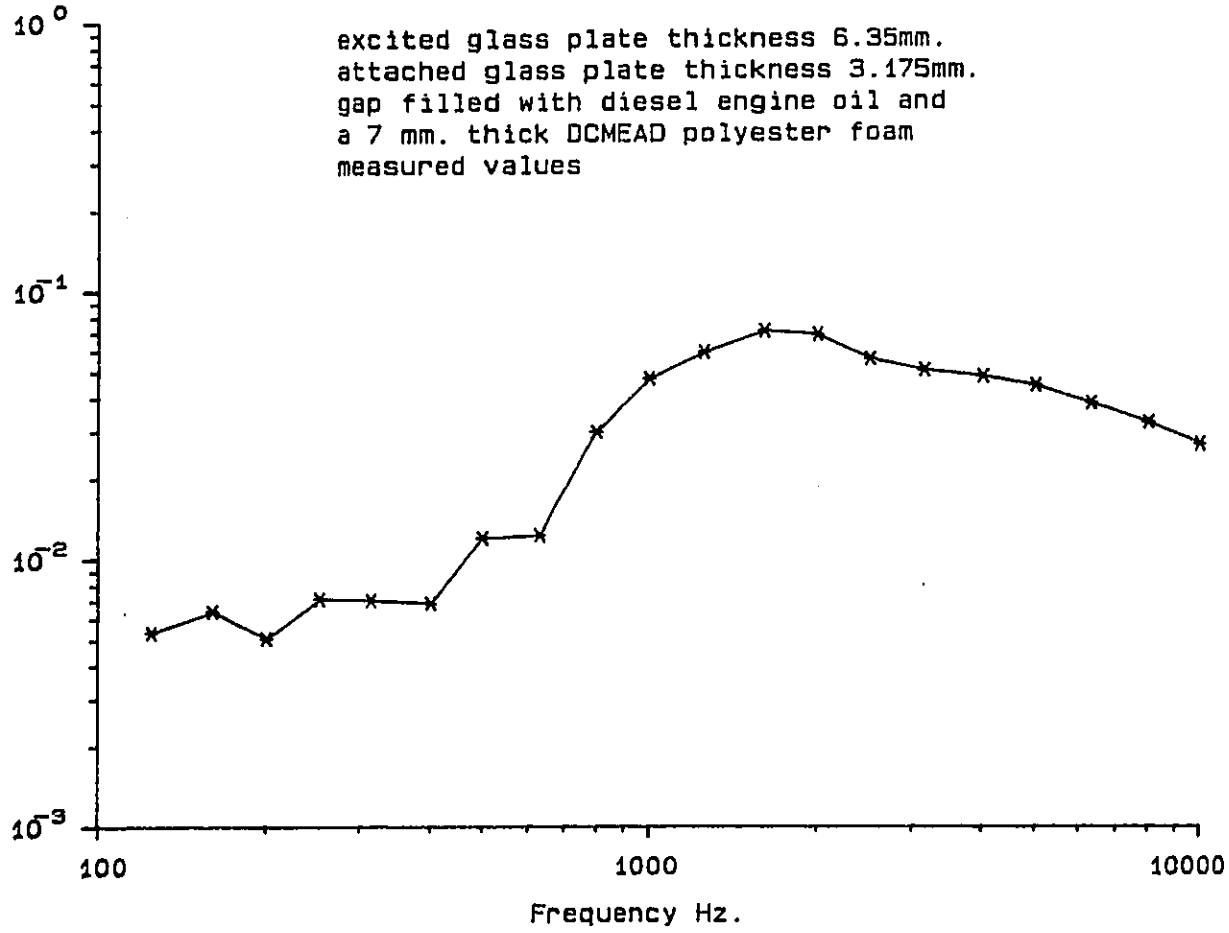

RE 5.3 The measured loss factor on the glass-polyester foam and oil-glass plates configuration.

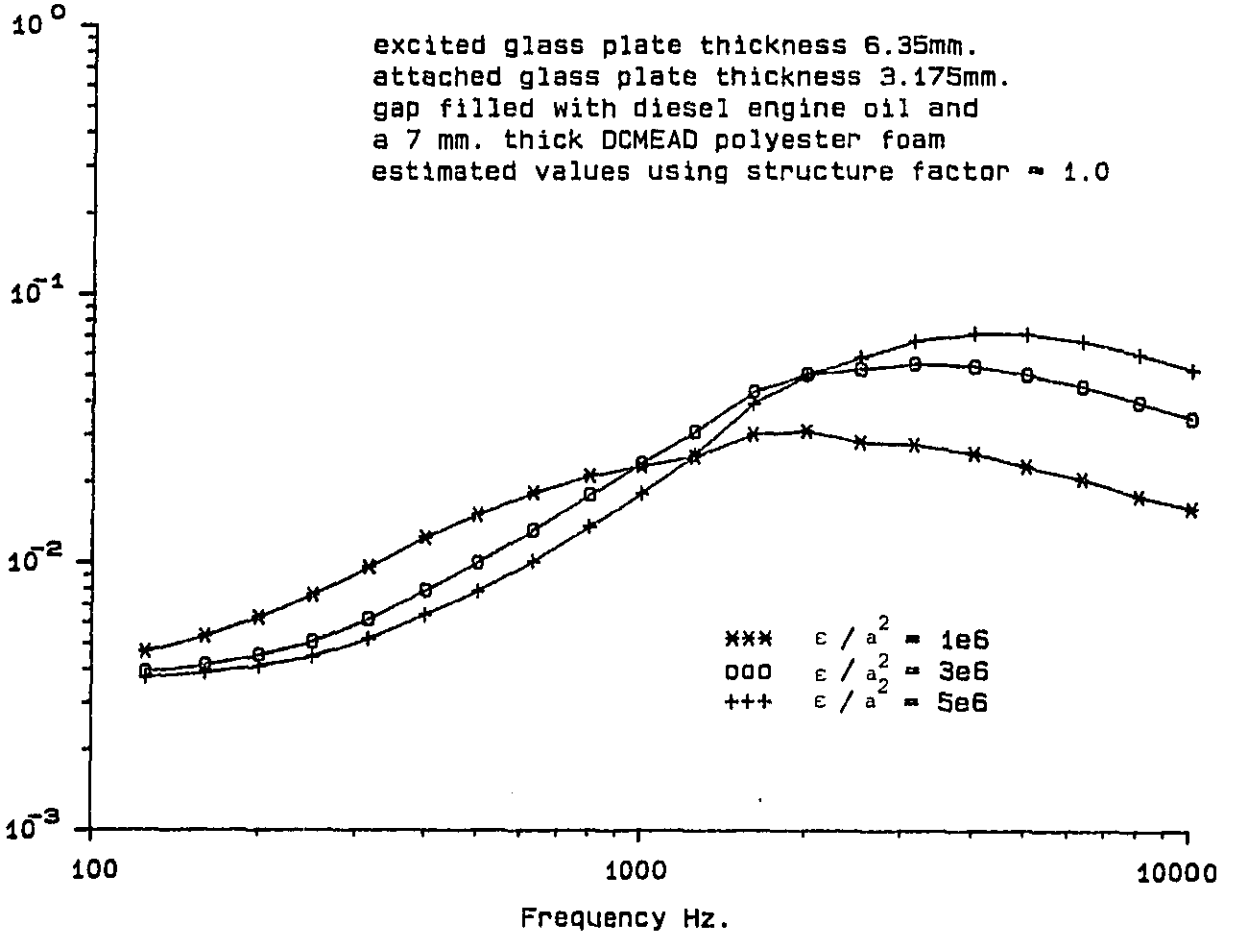

JRE 5.4 The estimated total loss factor on the glass-polyester foam and oil-glass plates configuration with varying ε/a^2.

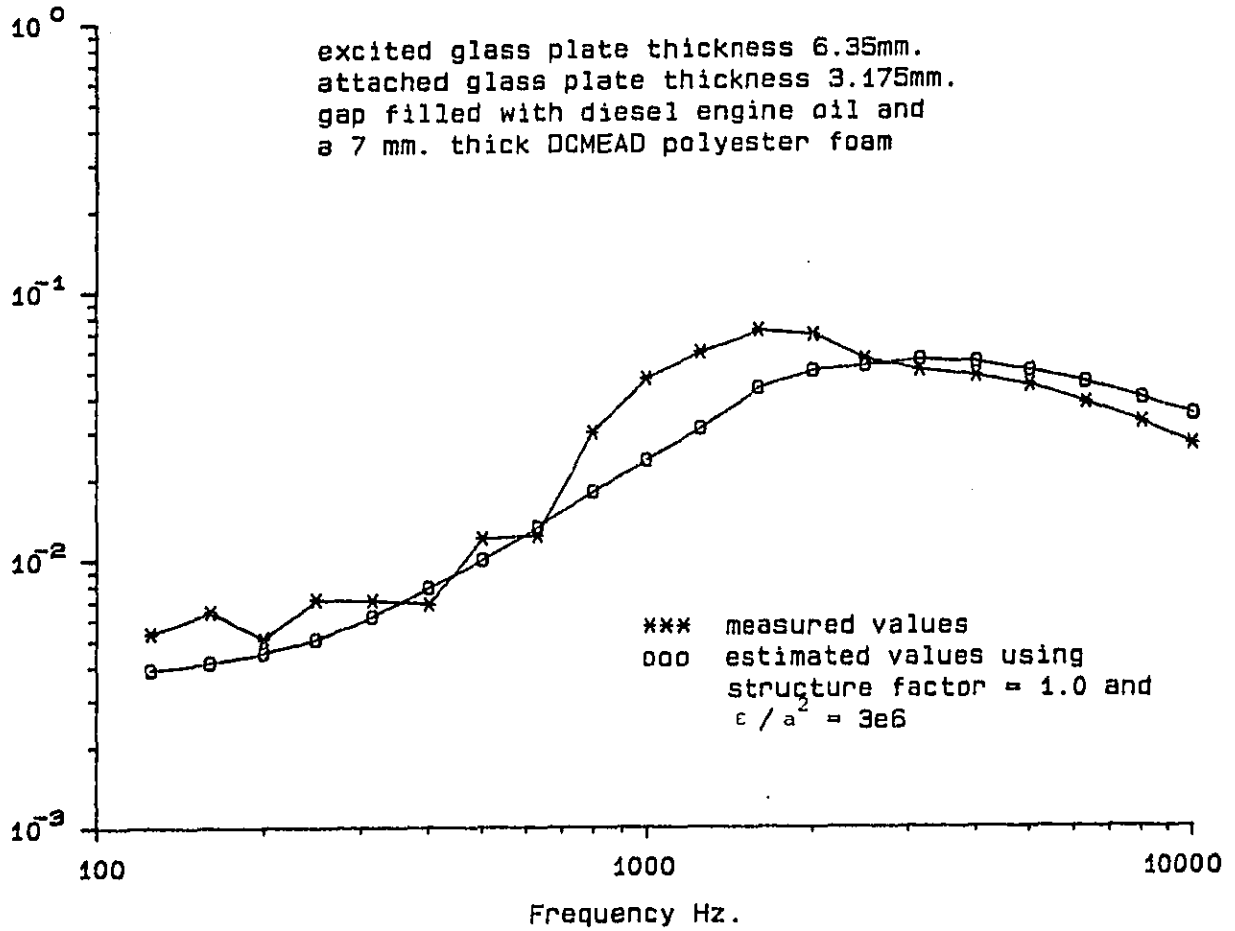

URE 5.5 The best fit curve on the glass-polyester foam and oil-glass paltes configuration.

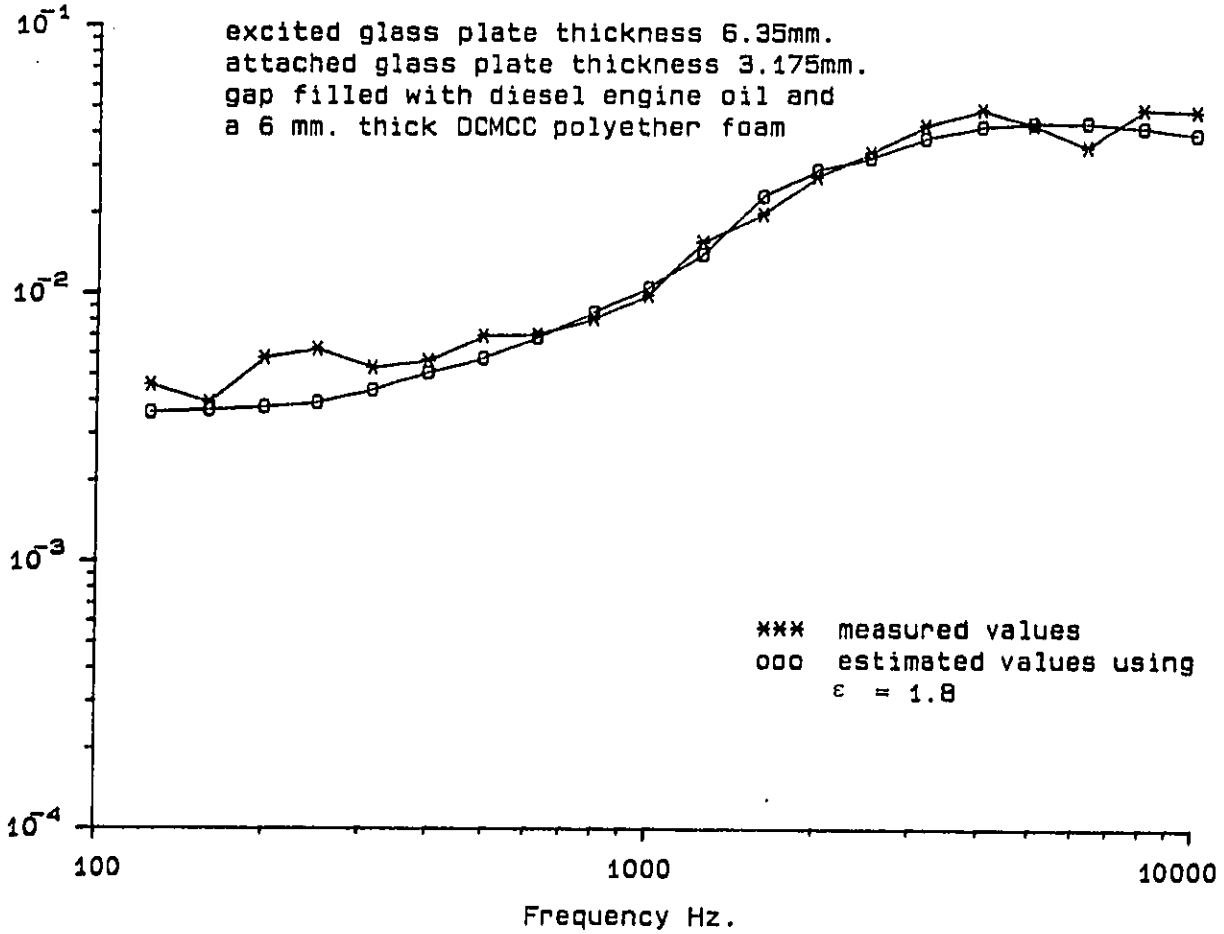

URE 5.6 Comparison of the measured and estimated total loss factor on the glass-polyether foam and oil-glass plates.

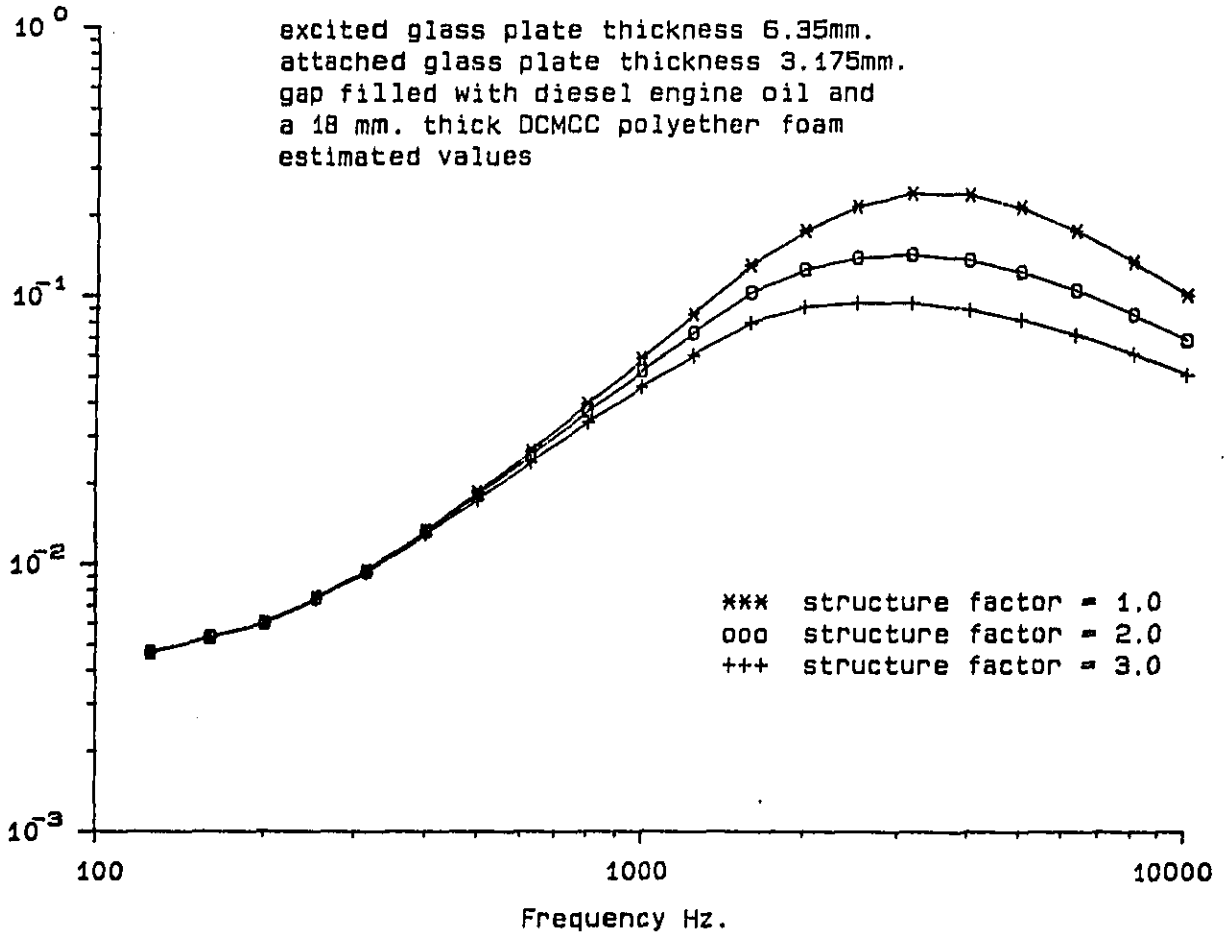

RE 5.7 The estimated total loss factor on glass-polyether foam and oil-glass plates configuration with varying structure factor.

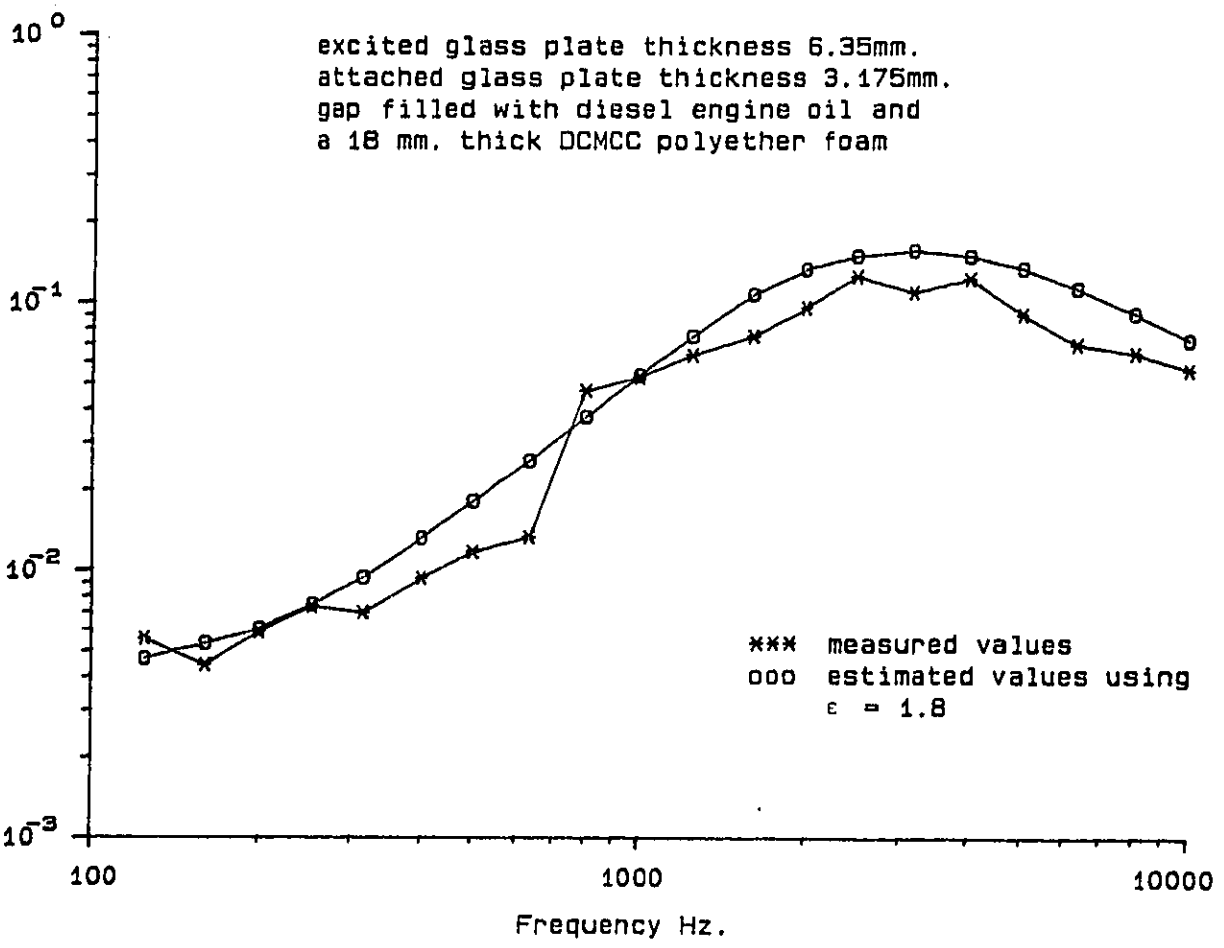

URE 5.8 Comparison of the measured and estimated total loss factor on the glass-polyether foam and oil-glass plates.

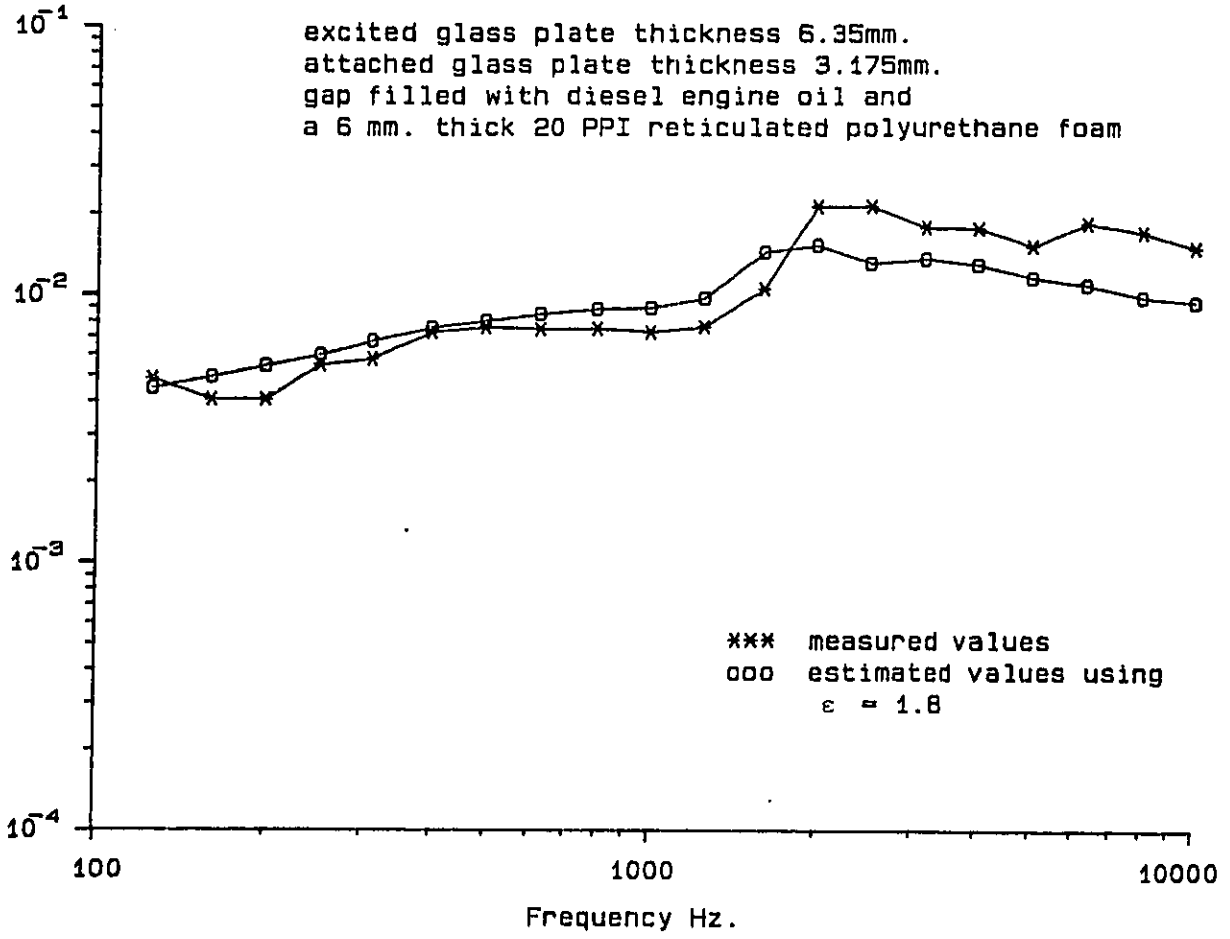

URE 5.9 Comparison of the measured and estimated total loss factor on the glass-polyurethane foam and oil-glass plates.

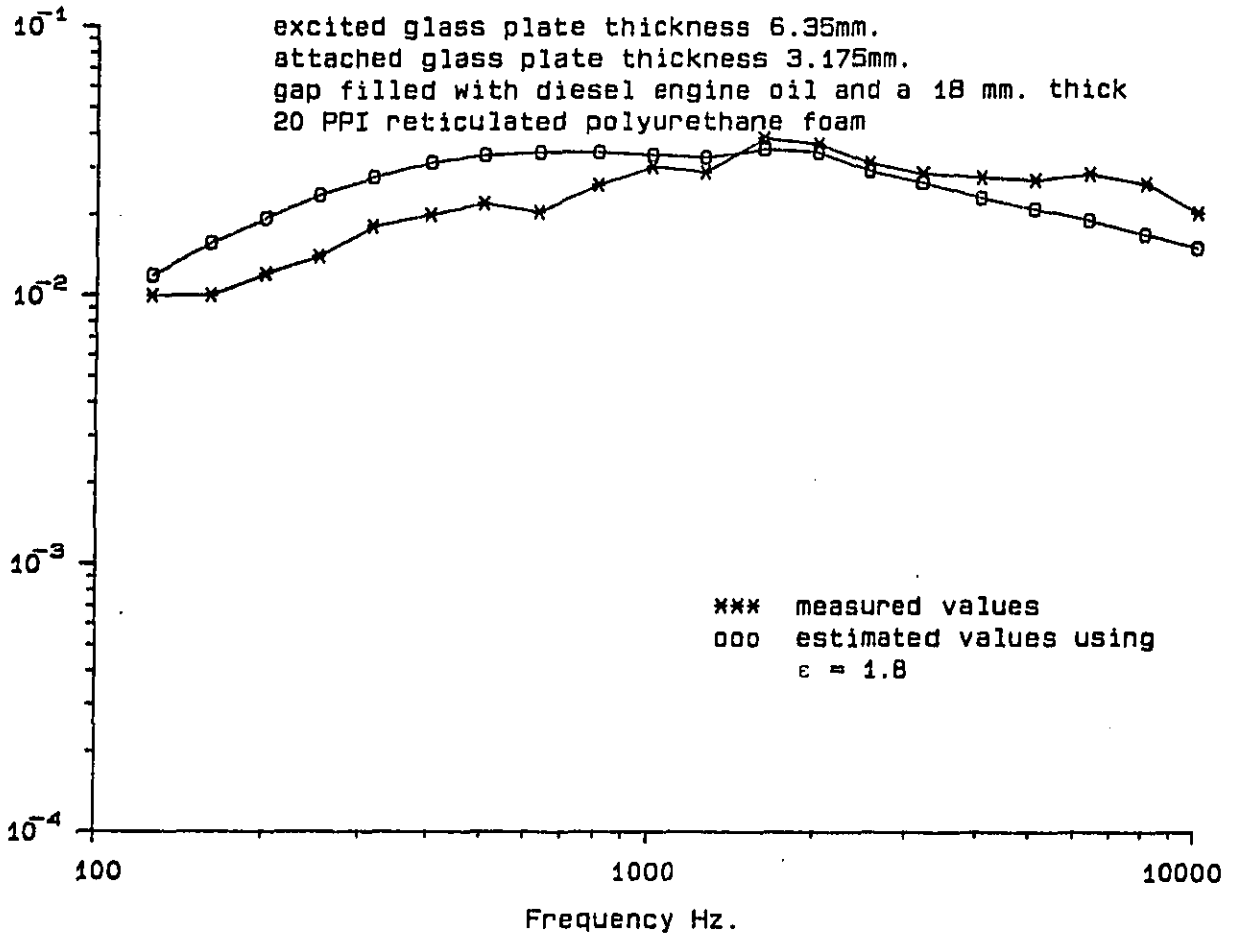

URE 5.10 Comparison of the measured and estimated total loss factor on the glass-polyurethane foam and oil-glass plates.

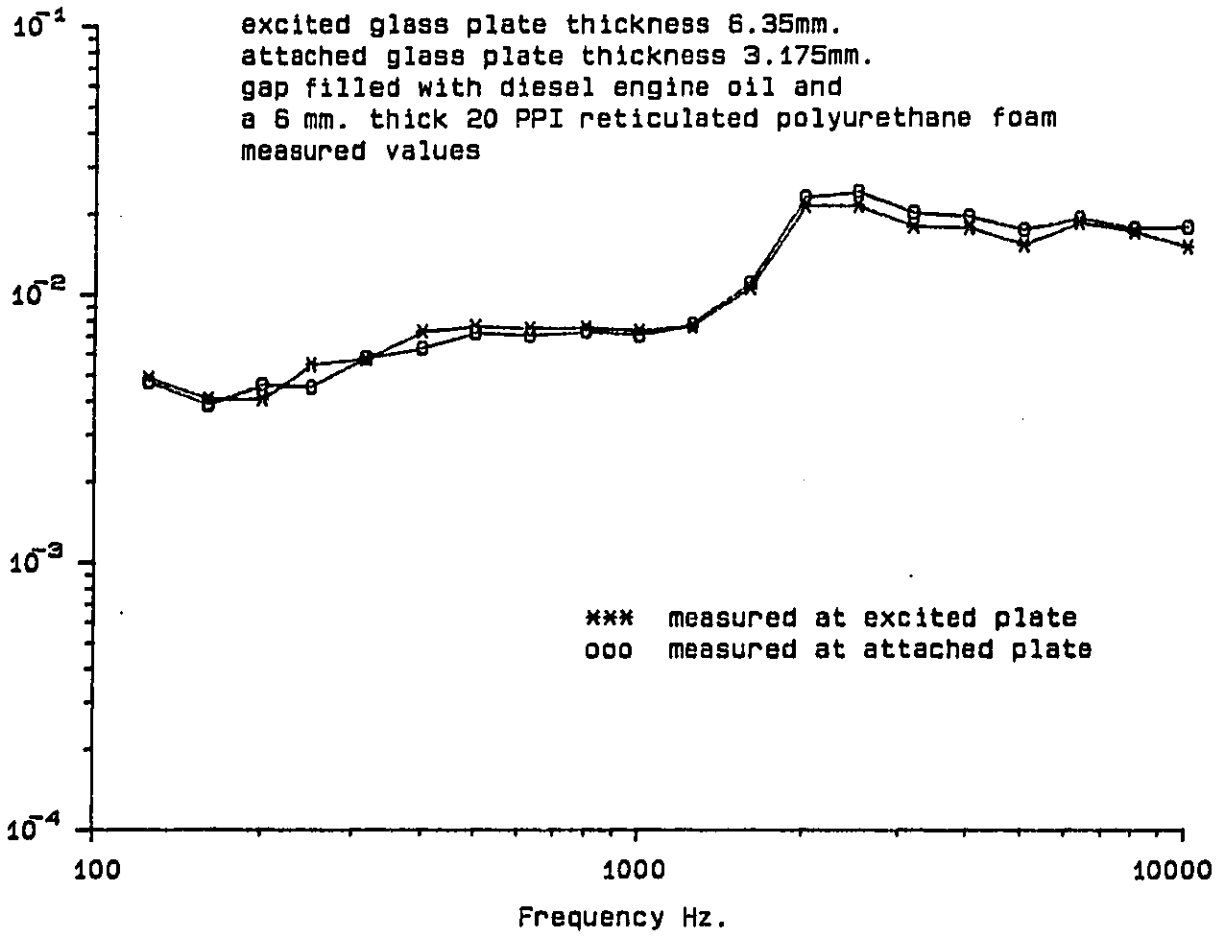

URE 5.11 The measured loss factor on both the excited and attached plates with polyurethane foam and oil layer.

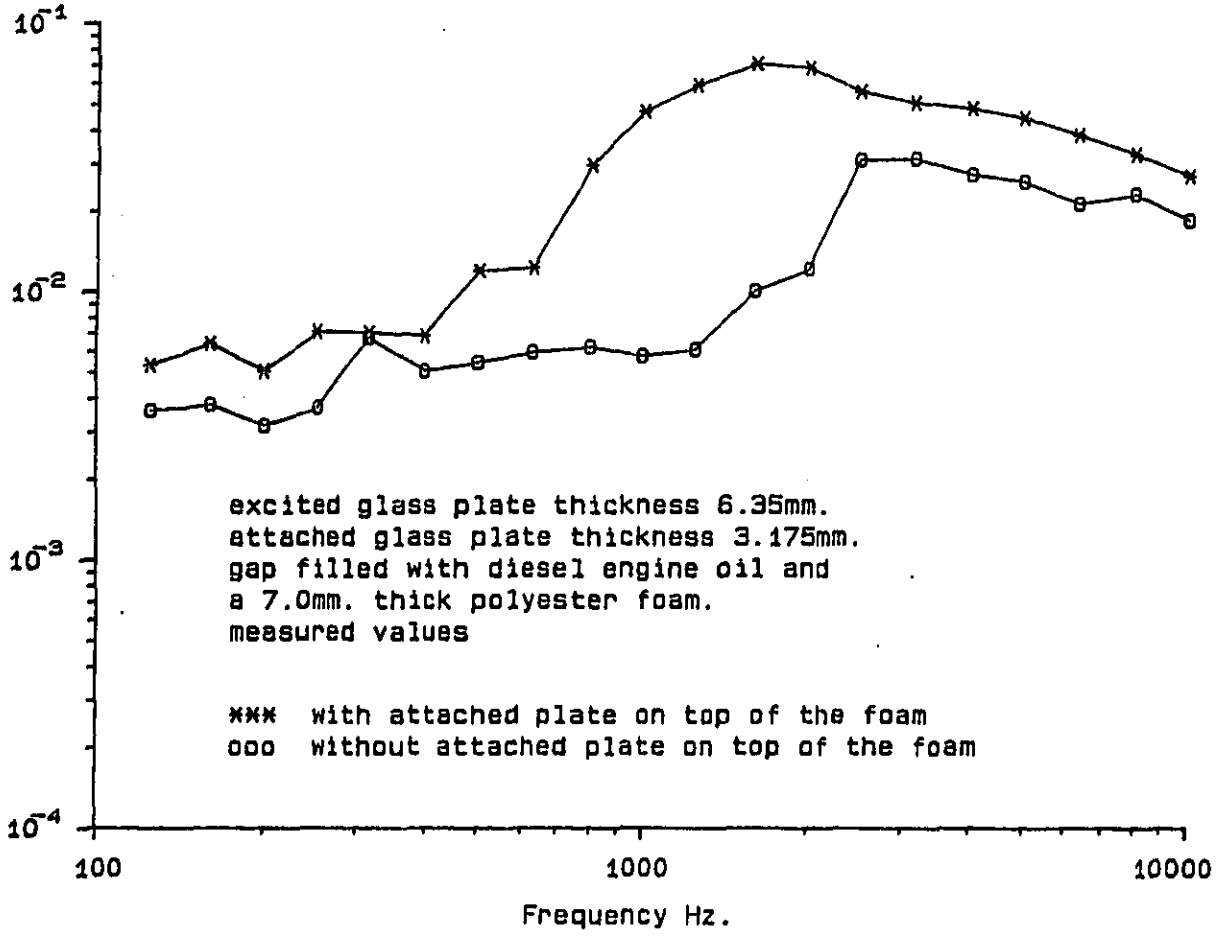

URE 5.12 Comparison of the measured loss factor with and without the attached plate on top of the polyester foam.

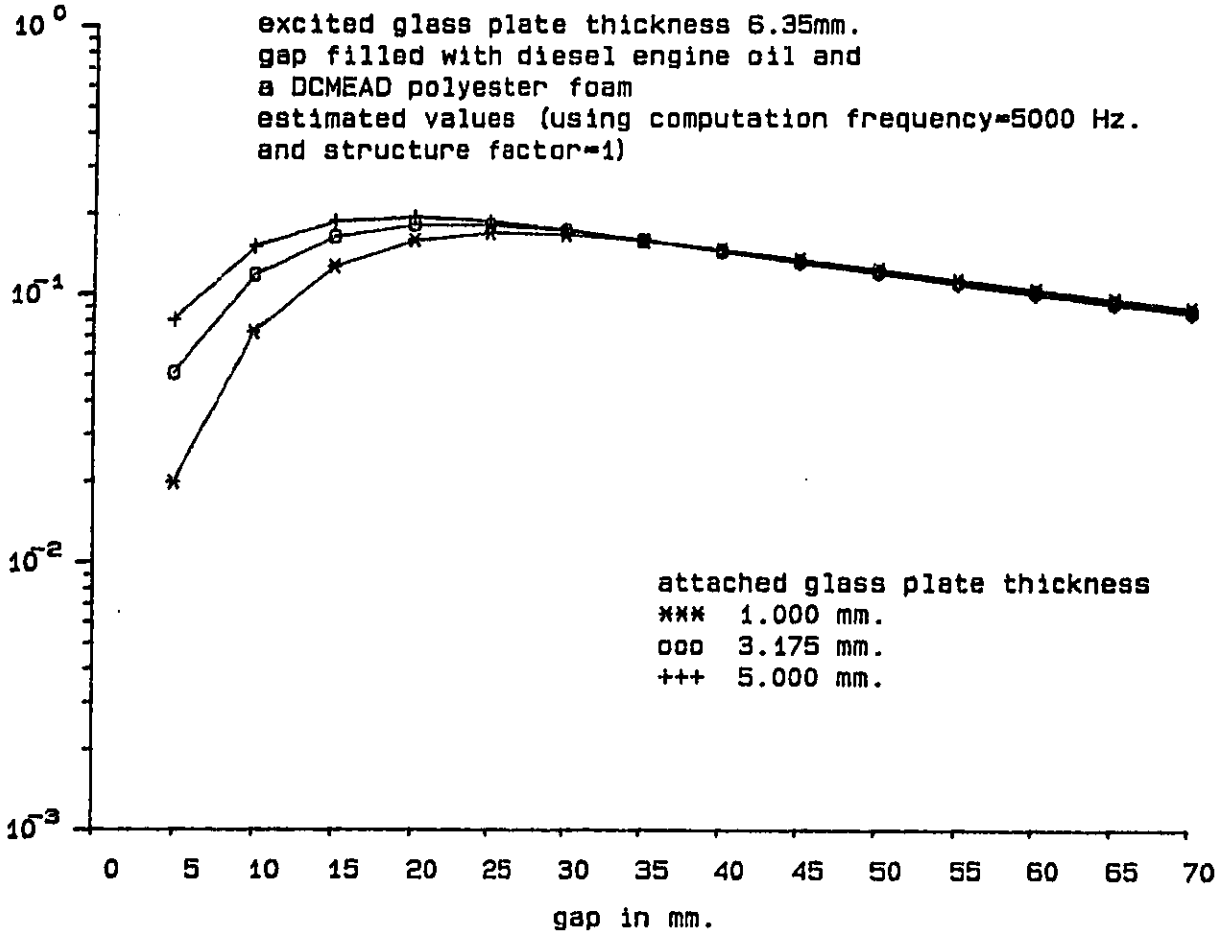

GURE 5.13 The estimated total loss factor on glass-polyester foam and oil-glass plates with varying attached plate thickness.

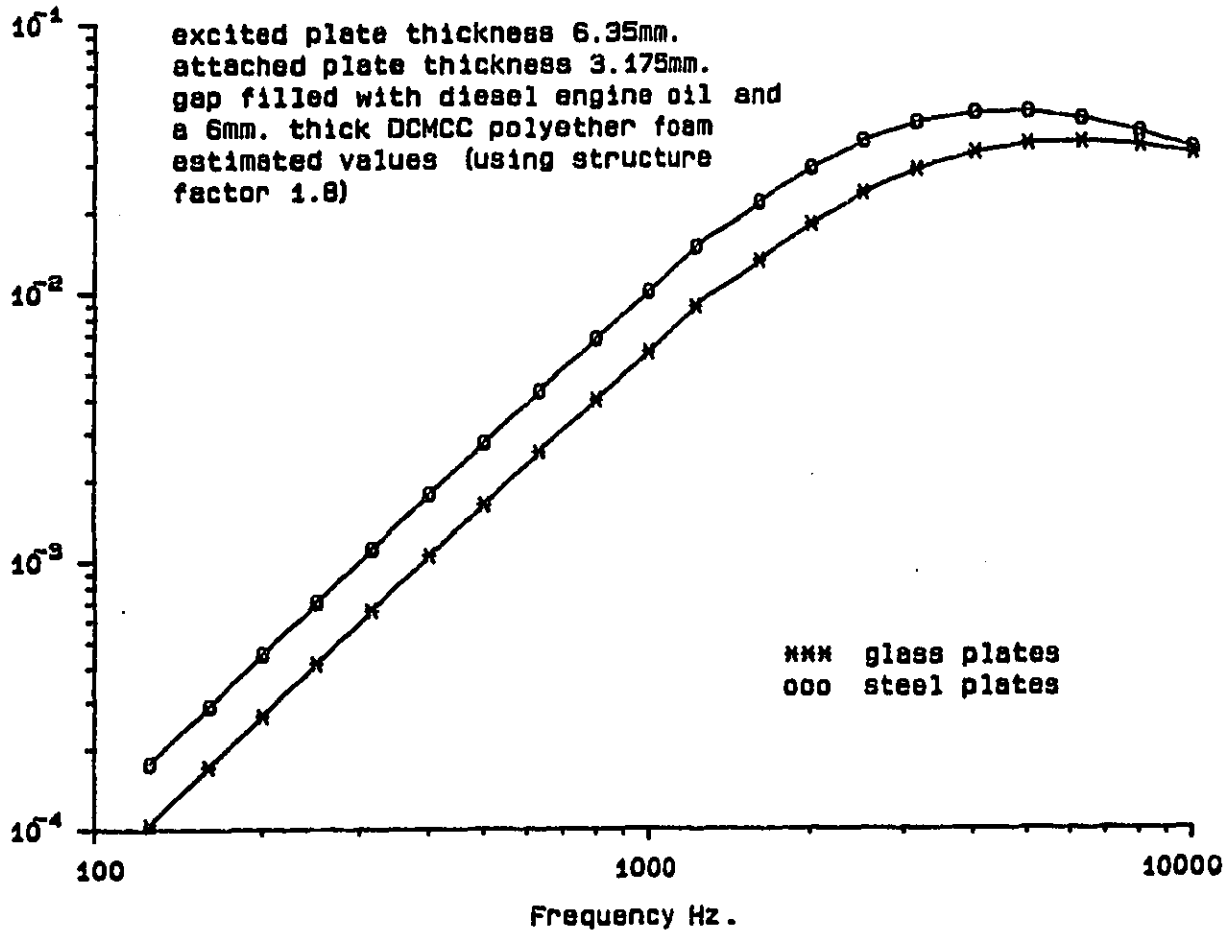

RE 5.14 Comparison of the estimated steel and glass plates total loss factor with a polyether foam and oil layer.

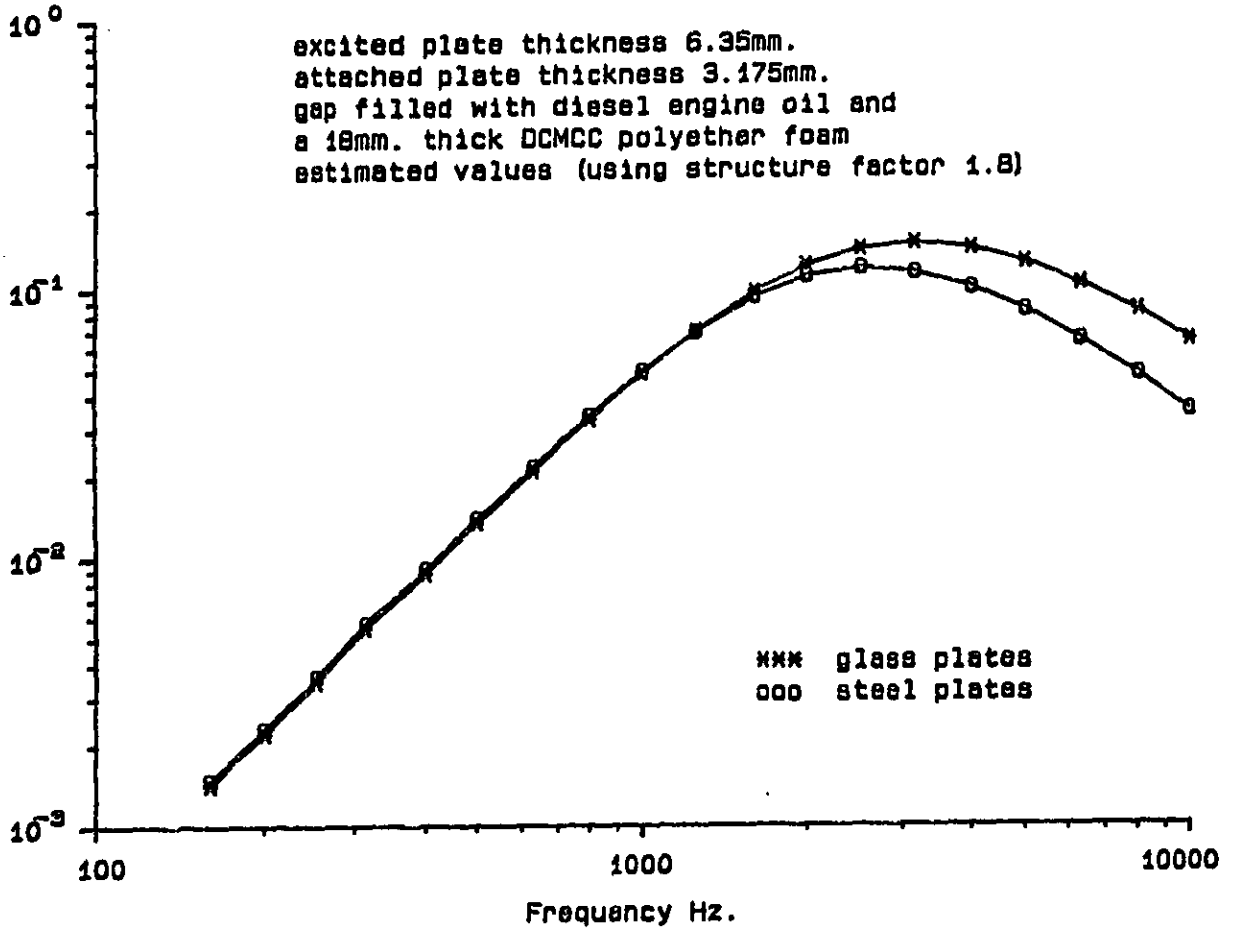

JRE 5.15 Comparison of the estimated steel and glass plates total loss factor with a polyether foam and oil layer.

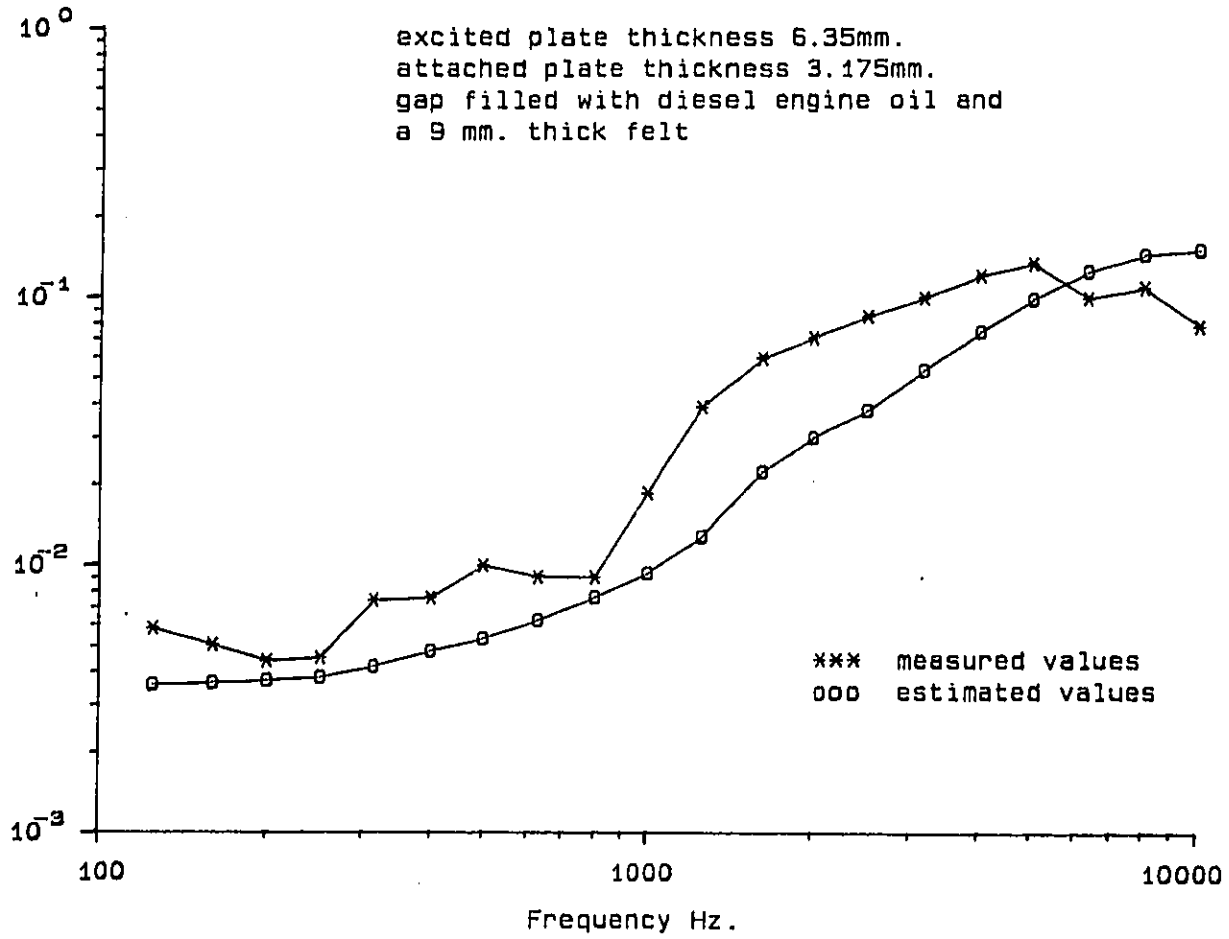

RE 5.16 Comparison of the measured and estimated total loss factor on the glass-felt and oil-glass plates.

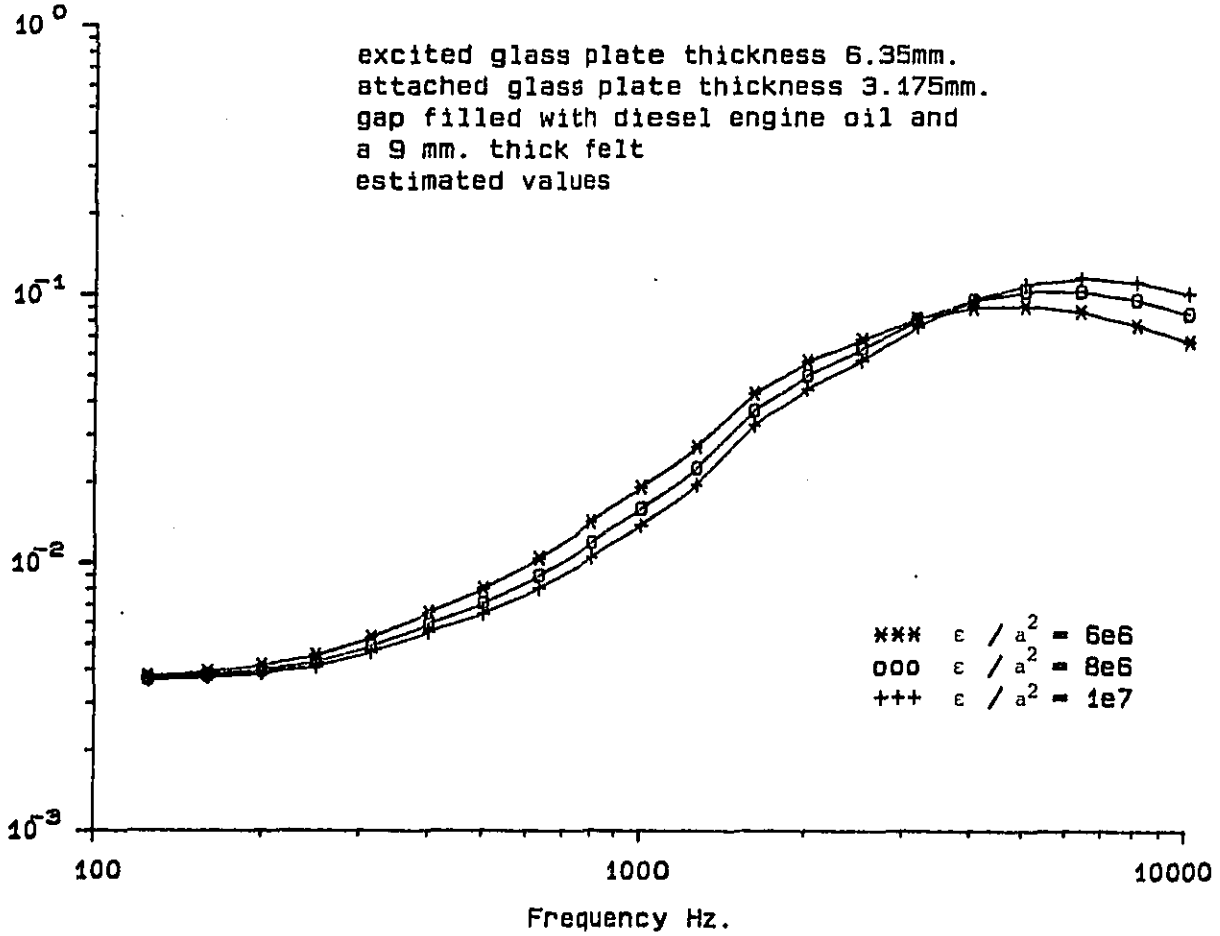

URE 5.17 The estimated total loss factor on the glass-felt and oil-glass plates with varying ε/a^2.

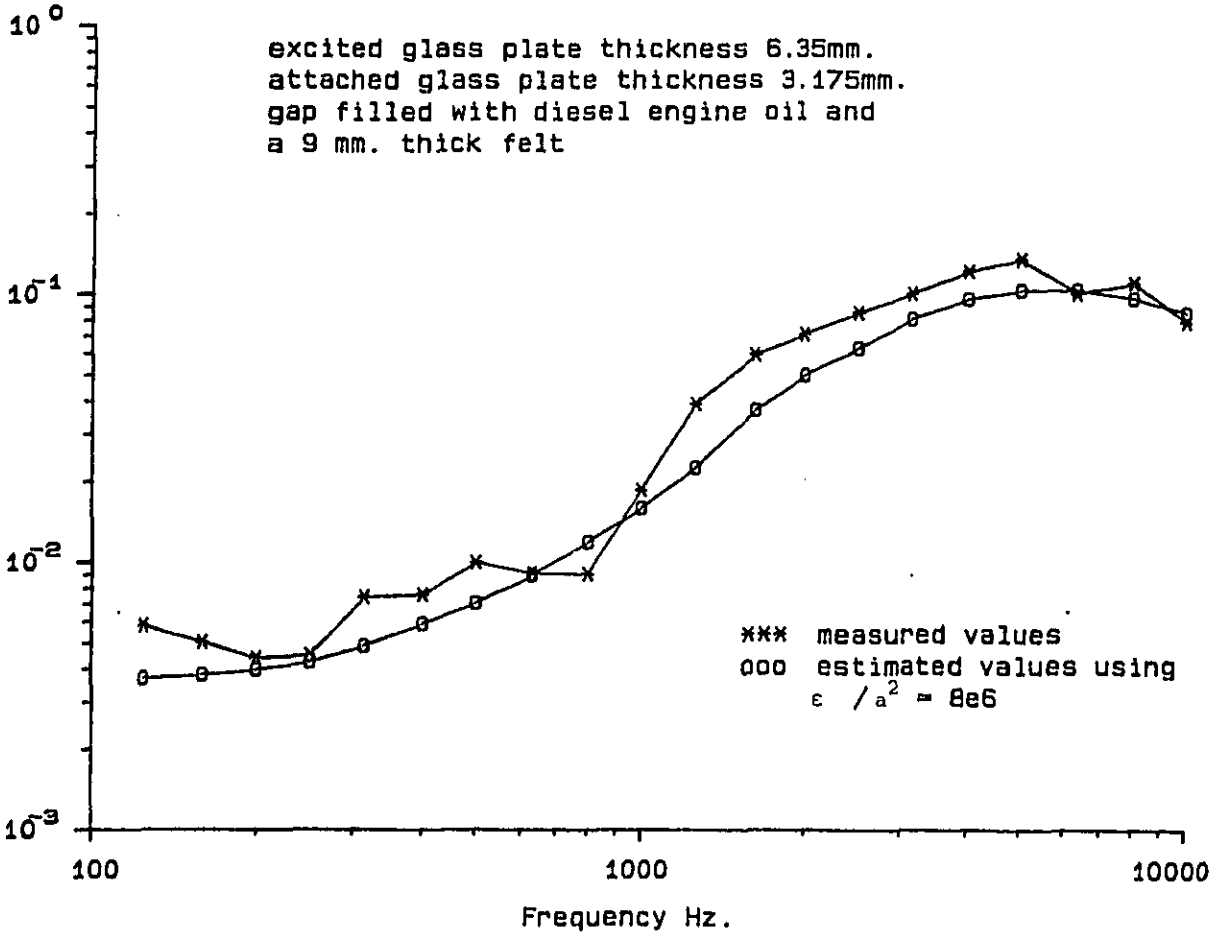

RE 5.18 The best fit curve on the glass-felt and oil-glass plates configuration.

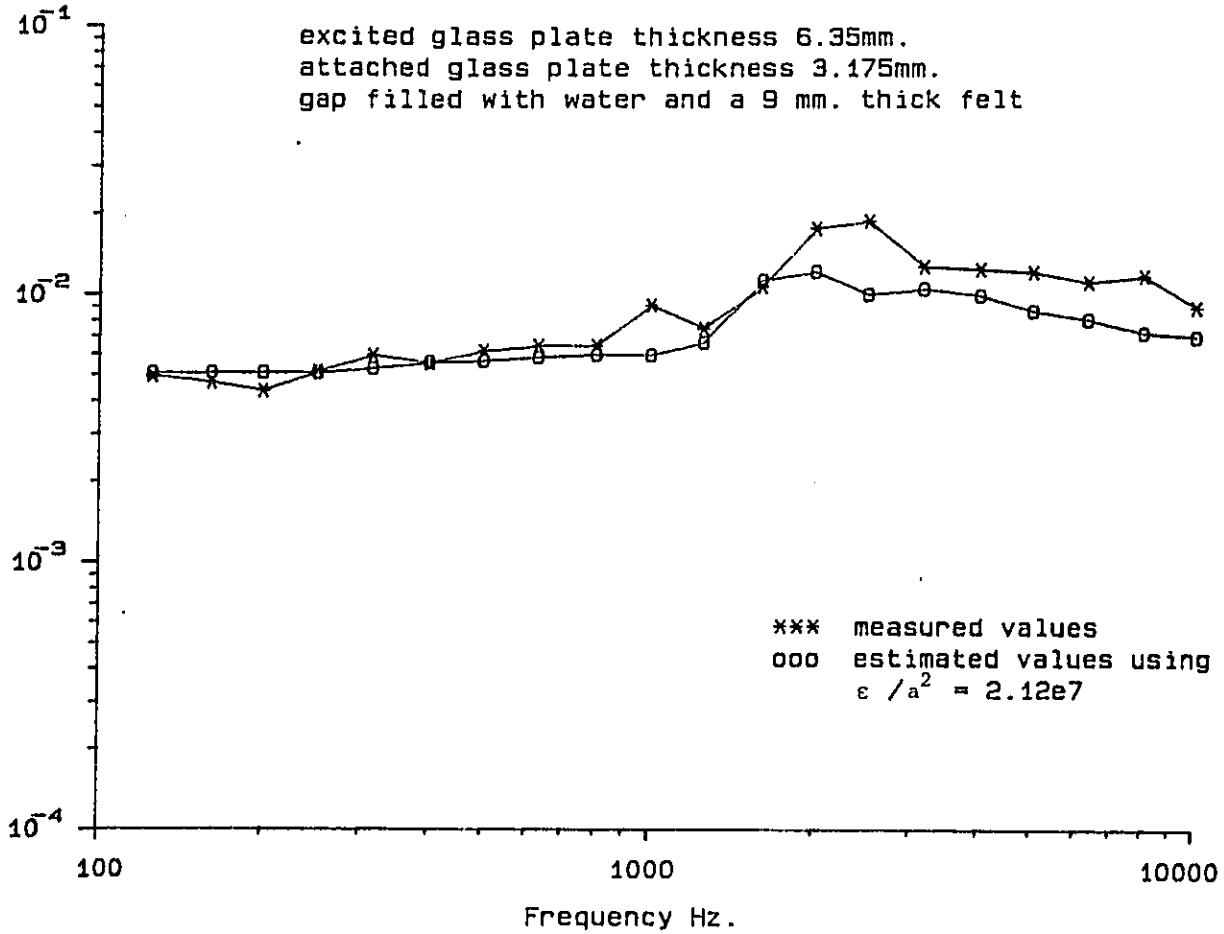

URE 5.19 Comparison of the measured and estimated total loss factor on the glass-felt and water-glass plates.